Stockholm University

Master Thesis

Degree Project in Geology 60 hp

Metal Mobility during metamorphism and formation of orogenic gold deposits: Insights from the Dalradian of Scotland

Adam Engström

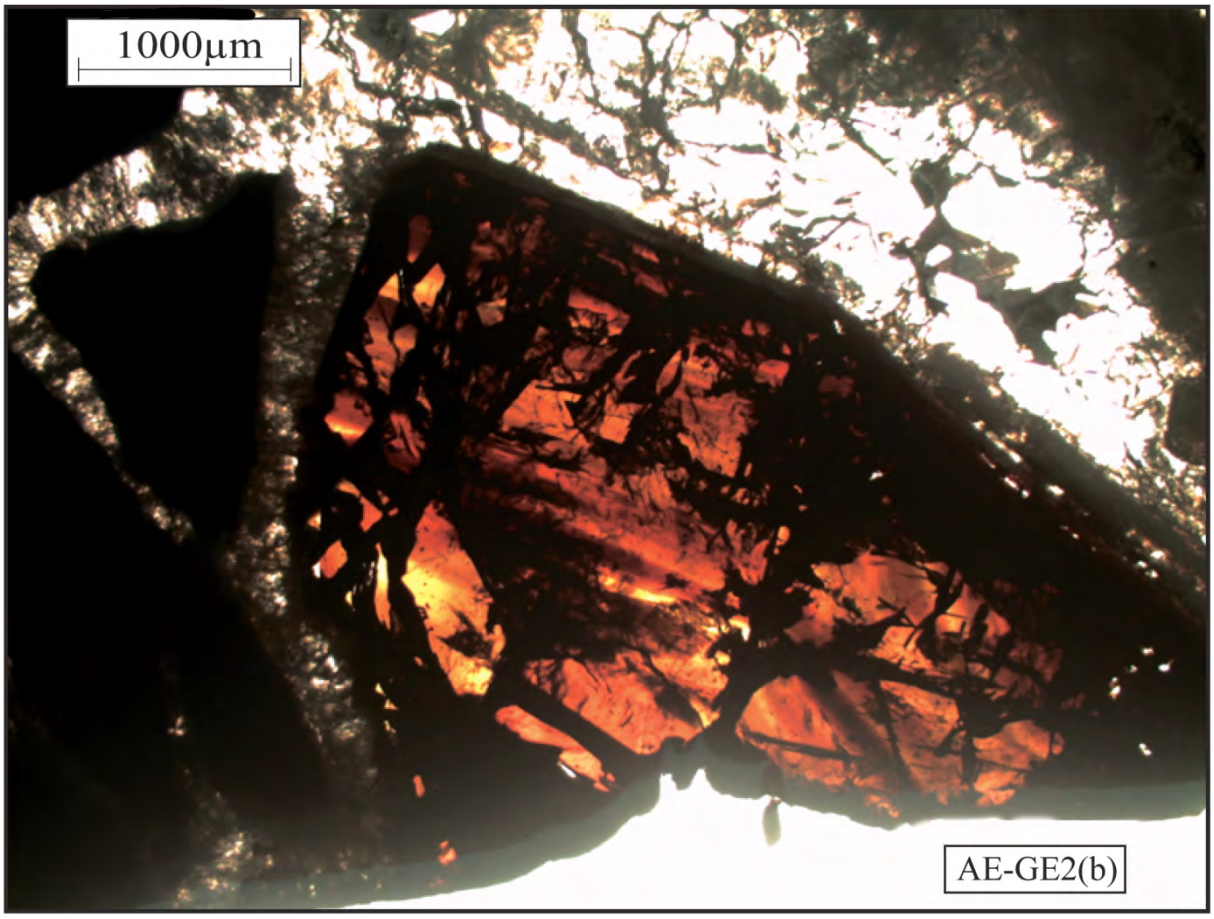

Stockholm 2013

Department of Geological Sciences
Stockholm University
SE-106 91 Stockholm

Abstract

Orogenic gold deposits occur within metamorphic belts throughout the world and have through time represented the source for over 25% of the world's gold production. Although orogenic gold deposits are of great economic importance, controversies exist on the subject of fluid and metal sources and there have been few studies of gold´s distribution and mobility outside of large economic deposits. Research made by Pitcairn et al. (2006), on the Mesozoic Otago and Alpine schists of New Zealand, observed systematic depletion of Au and a suite of 6 associated elements with increasing metamorphic grade. This depletion was identical to the suite of elements enriched in the Otago gold deposits and provided strong evidence that orogenic gold deposits form due to metamorphic processes. The mobilization of metals was attributed to the recrystallization of sulfide minerals during prograde metamorphism causing dehydration and release of metal-rich metamorphic fluids.

This thesis is part of a larger project aimed at testing the "Otago model" in a classic metamorphic terrain: The Dalradian metamorphic belt of Scotland. Rocks in the study are from the southern higlands group and the Appin and Argyll group which range in metamorphic grade from chlorite zone greenschist facies to sillimanite zone amphibolite facies. Three main aspects, which supplement earlier research, are addressed in this study: 1) Investigation of the sulfide paragenesis at Loch Lomond and Stonehaven was carried out to map the evolution of sulfides with metamorphic grade and the possible relations to the distribution of gold. Using SEM scanning to quantify the abundance of different sulfide minerals together with previous data on the Glen Esk region, a complex sulfide evolution pattern for the Dalradian Supergroup is identified. The sulfide evolution describes the same changes in texture and chemistry as observed in the Otago Schists but is made complex by the difference in geological evolution for the different regions. 2) Reinvestigation of the higher grade zones of Glen Esk (staurolite to sillimanite) was carried out as samples from the previous study were very weathered. Results from ultralow detection limit methods (HG-AFS and a gold detection method developed by Pitcairn et al. 2006) showed significant systematic depletion of Au and As with metamorphic grade. From chlorite to sillimanite zone average values of Au and As were showed to decrease by 65% and 88% respectively. Furthermore, a suite of 10 major and 12 trace elements were analyzed using ICP methods showing no trends of systematic depletion with increased metamorphic grade. 3) Investigation of Pb-Ag Veining and vein samples from each of the metamorphic index mineral zones in the Glen Esk area was carried out to identify fluid composition and ore mineralogy. Using microthermometry and Raman laser spectroscopy two distinct fluids were identified. The first type is a H_2O-CO_2-N_2-salt fluid of low salinity (0-15 weight percent NaCl equivalent) and medium temperature (150 to 250 °C) locally containing minor amounts of CH_4. It is found in the veins from the mineral index zones of Glen Esk and was formed in the ductile regime most likely related to late stage metamorphic devolatilization released during Caledonian uplift of the Dalradian. Pb-Ag veins from the locality of Hardhill host the second fluid type which was formed in the brittle regime accompanied by brecciation as a high salinity (15 to 20 weight percent NaCl equivalent) low temperature (70-140°C) H_2O-salt fluid with calcic composition was precipitated. This fluid bears much resemblance to Carboniferous calcic brines responsible for economic base-metal precipitation with widespread occurrence in southwest Scotland and Northern Ireland.

Results of this thesis show many similarities with the Otago study, with a connection between metal mobility and metamorphic grade, providing support for the dehydration model as a viable mechanism for the generation of orogenic gold deposits.

Key words: Gold mobility, ultralow detection limit, metamorphic devolatilization, Dalradian, Glen Esk, Loch Lomond, Stonehaven, fluid inclusions, HG-AFS

Acknowledgements

First of all, I would like to thank my supervisor Iain Pitcairn for his help and support in this project as well as for giving me access to his earlier research enabling me to put my work into a greater context. Alasdair Skelton, Alexander Lewerentz, Zhihong Zhao and Dan Zetterberg are thanked for their help during the field work. Finally Curt Broman is thanked for his help with the fluid inclusion part of the study and for supplying comments which helped to improve this thesis.

- Metal mobility during metamorphism and formation of orogenic gold deposits: Insights from the Dalradian of Scotland-

Table of Contents

I. Introduction

Orogenic gold deposits have historically contributed to over 25% of the global gold production and through erosion represent the origin for a considerable amount of the world's placer deposits. Commonly hosted in the form of gold-rich quartz veins or mineralized shear zones, orogenic gold deposits are a phenomenon that occurs in metamorphic belts throughout the world, with the vast majority being hosted in greenschist facies metamorphic rocks. Orogenic gold deposits are featured in the late Archean greenstone belts, Paleoproterozoic fold belts, late Neoproterozoic and younger orogens often associated with accretionary tectonics and major fault zones. The deposit-forming fluids in these metamorphic environments are uniquely CO_2 and ^{18}O rich with low to moderate salinities (Goldfarb et al. 2005). Ores from the Phanerozoic and Paleoproterozoic were generally formed at temperatures of 250 to 350°C with drastic pressure fluctuations with associated fluid unmixing and/or desulfidation during wallrock interaction as common precipitation mechanisms. Although orogenic gold deposits are of great economic significance uncertainties still remain in the understanding of their genesis.

The sources for fluids and metals of these deposits in particular remain ambiguous and several genetic models are proposed. These include 1) hydrous fluids released by metamorphic dehydration 2) CO_2-rich fluids originating from the mantle 3) deeply convecting meteoric water 4) magmatic-hydrothermal fluids and 5) fluids from an external source (like those generated during subduction). Much recent research has supported a metamorphic dehydration model where fluids produced during prograde mineral reactions act to mobilize, transport and deposit metals (Pitcairn et al 2006). In particular, this model has the advantage of providing a viable source of metals which can account for the regional-scale repeatable processes which are required to generate large gold fields worldwide.

Recent study was carried out to test the metamorphic dehydration model in the Otago and Alpine schists of New Zealand (Pitcairn et al. 2006a). These geological units host abundant orogenic gold deposits and belong to a Mesozoic (<200 Ma) metasedimentary belt formed during collision of the Torlesse and Caples terranes. They contain exposures of lithologically homogeneous rocks which ranges from unmetamorphosed greywackes to amphibolite facies rocks. The study used analytical methods with ultra low detection limit to enable the observation of metal depletion (Pitcairn et al. 2006a; Pitcairn et al. 2006b). This analysis showed systematic depletion of Au, Ag, As, Sb, Hg, Mo and W from upper greenschist to amphibolite facies rocks. The depletion of these elements was attributed to evolution of the sulfide assemblage during metamorphism and with the use of an electron microprobe, gold and its associated elements were shown to mobilize from recrystallization of pyrite into pyrrhotite. In unmetamorphosed samples gold was hosted in pyrite which in the subgreenschist-facies recrystallized to pyrrhotite. This recrystallization led to the remobilization of gold into cobaltite, sphalerite and galena which grew in abundance along with the transition of pyrite into pyrrhotite. In greenschist-facies these minerals decreased significantly in abundance to disappear completely in amphibolite-facies rocks. As the suite of depleted elements were identical to those enriched in nearby ore deposits, metamorphosed samples were inferred to represent the source for metals via pervasive grain-boundary fluid flow active on a regional scale.

This project aims to test "the Otago model" for the formation of orogenic gold deposits in a classic metamorphic terrain: The Dalradian metamorphic belt of Scotland. The Dalradian host few orogenic gold deposits and as such provide an opportunity for comparison to more well-endowed metasedimentary belts like the Otago schists. This comparison will aid in the understanding of the regional distribution of gold deposits and provide insights into the question why some metamorphic belts are mineralized and others are not. Prior to my involvement a lot of work had already been carried out by Dr. Iain Pitcairn using similar methods to those in the Otago study to investigate gold mobility using whole rock and mineral analyses. The project involved approximately 100 metasedimentary samples from three main regions located in the Dalradian and were collected both from the Appin and Argyll group and the Southern Highland group. The regions were Glen Esk, Stonehaven and Loch Lomond, and represents parts of the metmamorphic belt which have experienced different geological evolution in terms of temperature and pressure (Vorhies and Ague 2011).

Although a lot of data was already collected three main areas were in need of further investigation and these form the main aims of this thesis. These are **1)** Investigation of sulfide paragenesis from Loch Lomond and Stonehaven. Analysis of sulfide paragenesis had not been carried out for these two regions and was needed, with comparison to Glen Esk, for a complete understanding of the sulfide evolution with metamorphic grade within the Dalradian metamorphic belt. **2)** Investigation of the higher grade zones of Glen Esk. Earlier Glen Esk analysis included a limited number of samples from the staurolite to sillimanite zones. The previous suite of samples was weathered and sulphide-poor. To increase the data from these higher grade zones, 12 samples were collected in the field and 14 samples from Dr. Iain Pitcairn's collection which had not yet been analyzed were processed. In addition some elements such as As, Sb, Se and Te required reanalysis with better analytical methods **3)** Investigation of post-metamorphic Pb-Ag veining. Pb-Ag veins had been mapped in Glen Esk which were believed to be similar to veins of economic importance found on Islay and in SW highlands of Scotland. 2 samples were collected to identify ore mineralogy and fluid composition. In addition vein samples from each index mineral zone of the existing Glen Esk collection were made into doubly polished 150 µm wafers and also analyzed.

These aims were pursued using a selection of methods similar to those used in the Otago study. To analyze depletions in gold and its associated elements from the higher metamorphic grade samples two methods of ultralow detection limit, HG-AFS (Hydride-Generation Atomic Fluorescence Spectrometry) and gold analysis by ICP-MS, were used (Pitcairn et al. 2006b). This data was supplemented by ICP analysis covering a suite of 10 major and 12 trace elements. For analysis of the Loch Lomond and Stonehaven samples, optical microscopy and SEM scanning were used to identify and quantify the sulfide abundance and its evolution with metamorphic grade. Finally microthermobarometry and Raman Laser Spectroscopy was used to identify fluid composition and ore mineralogy of the vein samples from Glen Esk.

i. Sulfide evolution during metamorphism

Sulfide minerals are widely distributed in nature where pyrite (FeS_2) is considered the most abundant sulfide in marine sediments and sedimentary rocks while pyrrhotite ($Fe_{1-x}S$) is the most abundant sulfide in rocks of higher metamorphic grade. During prograde metamorphism pyrite is inferred to undergo a transition into pyrrhotite by means of a desulfidation reaction. This reaction has been observed to occur in close relation to the chlorite and biotite mineral isograds between the sub-greenschist and greenschist facies (Pitcairn et al 2006;2010 and Carpenter 1974). Thermodynamic modeling has shown that the main release of sulphur occurs over a narrow range of preassure and temperature conditions coinciding with the breakdown of chlorite in the lower amphibolite facies. The stability of pyrite is believed to partly be controlled by temperature and pressure but also by the amount of H_2O present. A number of different reactions can be envisaged to alter pyrite to pyrrhotite depending on what minerals and fluids are present. An example of this would be local mobilization of sulphur where pyrrhotite grows at the expense of pyrite and iron oxides. However, a reaction more likely to be of importance for the large scale mobilization of gold is given in a simplified form below (Ferry 1981):

$$2\ FeS_2 + 2\ H_2O + C \rightarrow 2\ FeS + 2\ H_2S + CO_2$$

Here large volumes of fluids generated by prograde metamorphic devolatilization react with carbon to, via removal of sulphur from the rock, produce pyrrhotite. Reversal of this reaction where sulfidation of pyrrhotite leads to crystallization of pyrite is a common retrograde reaction in high-grade metamorphic rocks. In the study from Otago, recrystallization of pyrite into pyrrhotite was shown to release Au, Ag, As, Hg, Mo, Sb and trace elements from the mineral structure and remobilize it into minerals such as cobaltite, sphalerite and galena. In amphibolite-facies rocks cobaltite, sphalerite and galena decreased dramatically in abundance and the elements they contained were leached by pervasive metamorphic fluids.

ii. The mobility of gold

The enrichment of gold in ore deposits around the world represents geochemical anomalies to the background levels of gold concentrations in Earth's crust. Average abundances of most rock types typically range from 1-4 ppb while ore deposits display an enrichment of 10 000 times that background level (Phillips and Powell 2010). The spatial distribution and size of gold fields worldwide suggests that the underlying formational process of these deposits operates simultaneously in many places over thousands of kilometers, but only at places is able

to successfully generate major gold fields. This relationship provides strong support for the metamorphic devolatilization model for the formation of orogenic gold deposits.

In nature gold exist in three common oxidation states Au^0, Au^{1+} and Au^{3+}, the first of which is the dominant mineralogical form and the other two which are present when gold is transported in solution (Phillips and Powell 2010). The oxidation state of gold affects its electronegativity and ionic radii which in turn influence the bonding character and complexing behavior. Gold deposits can be classified into three different types 1) Gold-only deposits (where gold is the dominant or only ore) 2) Gold-plus deposits (where gold is accompanied by a variation of elements such as Ag, Cu, Pb, Zn, and Bi and commonly uneconomic in its own right) and 3) placer/alluvial deposits. Elevated gold concentrations in metamorphic fluids responsible for the formation of gold-only deposits are believed to be attained through complexing of Au^{1+} with reduced sulphur which along with CO_2 and H_2O is brought into solution by dehydration (a H_2O-CO_2-H_2S, low salinity fluid). Au^{1+} is a soft cation with preference for covalent bonding and a high electronegativity making sulphur a suitable candidate for bonding (Phillips and Powell 2010). The elements As, Sb, B, Se, Te, Hg, Bi, Mo and W share a similar chemical behavior to both Au and S and are as such often mobile alongside gold.

Base metals have lower electronegativity than that of Au^{1+} and as such are generally not mobile together leading to a geochemical segregation of gold deposits from base metal ore deposits. However, Au^{3+} has considerably lower electronegativity and is harder than Au^{1+} making it stable in ionic bonds where it preferentially bonds to moderate-to-hard anions such as Cl^-. In contrast to Au^{1+}, the Au^{3+} oxidation state is mobile with base metals and provides means for gold to be transported to form gold-plus deposits (which commonly are of high salinity).

The generation of giant gold fields require several factors to work together to facilitate the mobilization, transport and precipitation of ore deposits. Redox conditions play an important role in the formation of large gold deposits as it is vital that gold is mobilized but not prematurely precipitated.

For mobilization, the availability of the right ligands is important. During transport CO_2, one of the key components of metamorphic fluids which is assumed to always be present, is believed to help retaining favorable solubility conditions for gold. Evidence points towards weak acid buffering of H_2CO_3 derived from CO_2 which act to negate fluctuations of pH thus keeping gold in solution and at its maximum solubility (Phillips and Powell 2010). Two important precipitation mechanisms are the presence of Fe and reduced C in the surrounding wallrock. Reduced carbon affects pH of the fluid and by reducing it precipitates gold. Fe in the wallrock can react with the reduced sulphur in solution to precipitate for example pyrite and in turn gold.

iii. Geological Setting

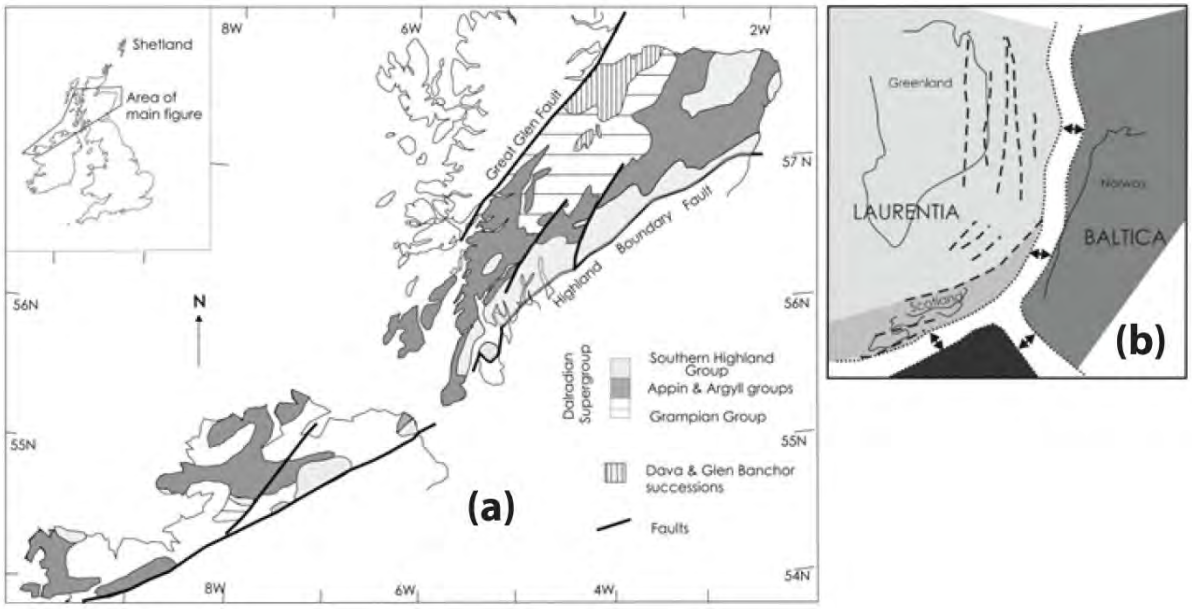

Figure 1. ***a)*** *Map of the different units in the Dalradian Supergroup of Scotland, an overturned and folded sequence with relatively intact stratigraphy (Fettes et al. 2011 and Craw 1990).* ***b)*** *Tectonic reconstruction of the breakup of the Rodinia supercontinent upon the opening of the Iapetus Ocean (Fettes et al. 2011)*

The Dalradian Supergroup (Figure 1-a), central Scotland, is composed of a subset of Neoproterozoic-Cambrian rocks located in between the Great Glen Fault and the Highland Boundary Fault (Fettes et al. 2011). It is situated in the Central Highland Terrane with Precambrian to Cambrian metasediments bordering the Devonian sediments of the Midland Valley Terrane below the Highland Boundary Fault (SE) and the Precambrian sediments of the Moine above the Great Glen Fault (NW). The sequence extends down into the north western part of Ireland, Connemara, where much of the tectonic history is the same (Vorhies and Ague 2011). In Scotland, the rocks of the Dalradian Supergroup are dominantly of metasedimentary origin but also include metavolcanic rocks along with several generations of granitoids.

The original tectonic setting of the Dalradian Supergroup began on the margin of Laurentia where deposition of marine successions record a rifting environment associated with the break-up of Rodinia (Figure 1-b, Figure 2). This rifting eventually led to the opening of the Iapetus Ocean around 600 Ma (Vorhies and Ague 2011, Fettes et al. 2011) where the Dalradian rocks were deposited on a passive margin. Upon the closure of the Iapetus around 500 Ma the sedimentation ended and at approximately 480 Ma the Dalradian sequence was subjected to the Grampian Event of the Caledonian Orogeny. During this event peak metamorphism was reached in the Supergroup as Laurentia started to converge with the Midland Valley Arc, outboard microcontinents and the Highland Border Ophiolite (Vorhies and Ague 2011, Masters and Ague 2005, Breeding et al. 2004). Modern day exposures range from greenschist to upper amphibolite facies.

As a consequence of the orogeny the rocks of the Dalradian metamorphic belt were deformed, forming and refolded nappe structures at a regional scale during the four Grampian deformation events (D_1-D_4). These events represent several generations of syn- to post-metamorphic folding with peak temperatures of Barrovian metamorphism occurring at D_3 (Craw 1990, Masters and Ague 2005).

iv. Age and stratigraphy of the Dalradian Supergroup

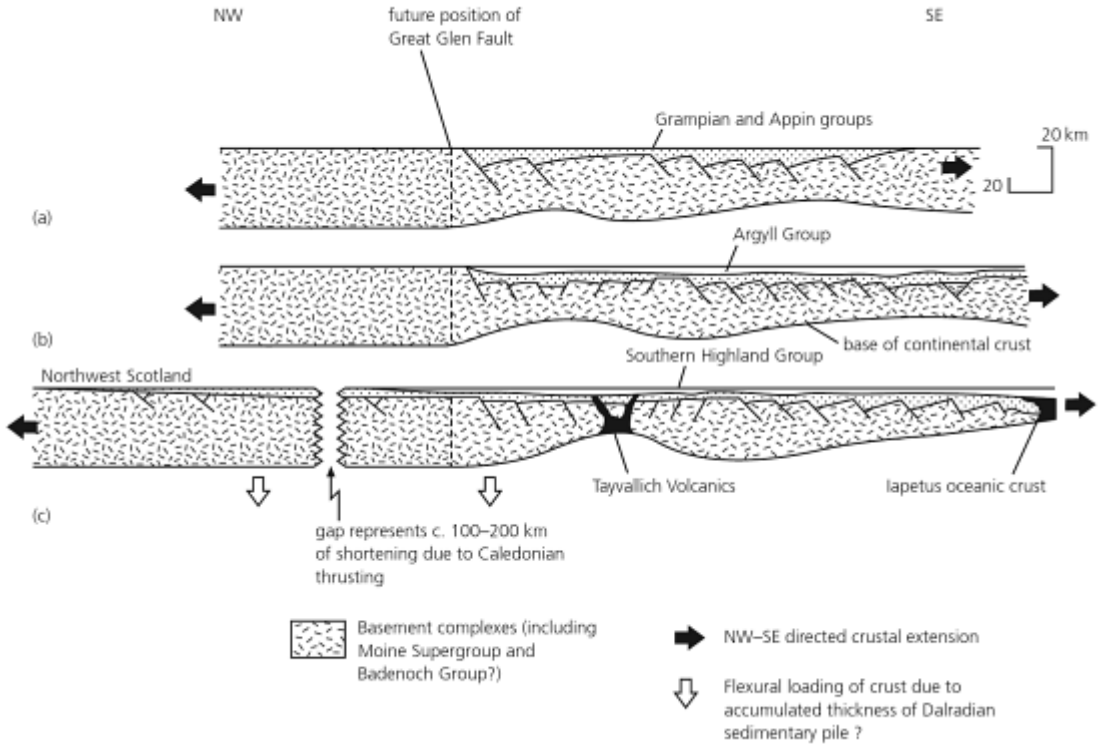

Figure 2. *Model for the tectonic evolution of the Dalradian Supergroup (The Geology of Scotland 2010, Geological History of Britain and Ireland 2012).*

The Dalradian Supergroup is subdivided into the Grampian, Appin, Argyll and Southern Highland group as listed in ascending stratigraphic order (Figure 2, Figure 3). The initial sediments were deposited as marine sands, silts, muds and limestones providing records of the tectonic history of the Supergroup in the form of sedimentary structures. Although these lithological units and their relations are well documented the age determination is poorly constrained for the initiation of the rifting related to the opening of the Iapetus Ocean (Fettes et al. 2011, Vorhies and Ague 2011, The Geology of Scotland 2010, Geological History of Britain and Ireland 2012). Age estimates from radiometric U-Pb zircon dating of granitoids provide reliable data from the late Neoproterozoic rifting (600 Ma) to Palaeozoic orogeny (420-400 Ma) but conflicting data from rocks older than 600 Ma makes dating problematic for a large part of the Dalradian Supergroup (Figure 3. Oliver et al. 2008 Fettes et al 2011, The Geology of Scotland 2010, Geological History of Britain and Ireland 2012).

Notable age determinations that have been made below the Tayvallich subgroup (a volcanic succession from the upper part of the Argyll group coinciding with Neoproterozoic rifting) include 1) Port Askeig tillite (713 Ma) which is inferred to correlate to major environmental events during the Neoproterozoic (snowball earth) 2) Pegmatites of Glen Banchor and Dava successions which are interpreted to constrain the beginning of the Grampian to younger than 800 Ma and 3) Carbon isotopic dating of Ballachulish limestone to 800 Ma. The last two measurements in particular are indicating the problem with conflicting data and represent an example of the uncertainty related to the total time span of the Dalradian Supergroup (Figure 3).

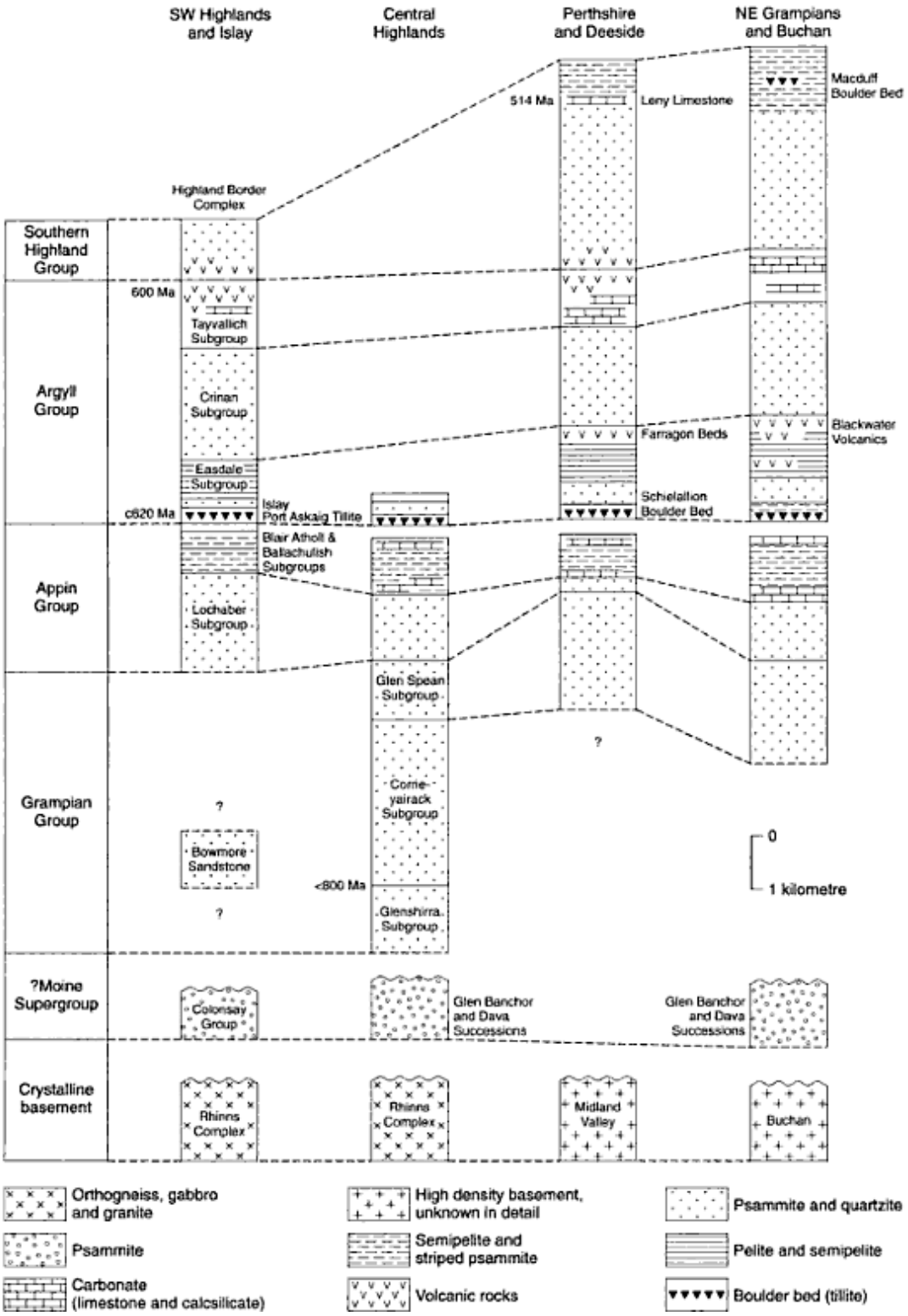

Figure 3. *Stratigraphy of the Dalradian Supergroup and its occurrence across Scotland. The sedimentary structures and lithology have lead to the following broad interpretation of the sub groups:* ***1)*** *Grampian, representing early basin development* ***2)*** *Appin, shelf sedimentation* ***3)*** *Argyll, sedimentation during tectonic instability* ***4)*** *Southern Highland Group, continuing marine sediments in the form of turbidites mixed with volcanic strata (Masters and Ague 2005, Fettes et al. 2011, The Geology of Scotland 2010, Geological History of Britain and Ireland 2012).*

v. Metamorphic history, tectonics and mineralization of the Dalradian Supergroup

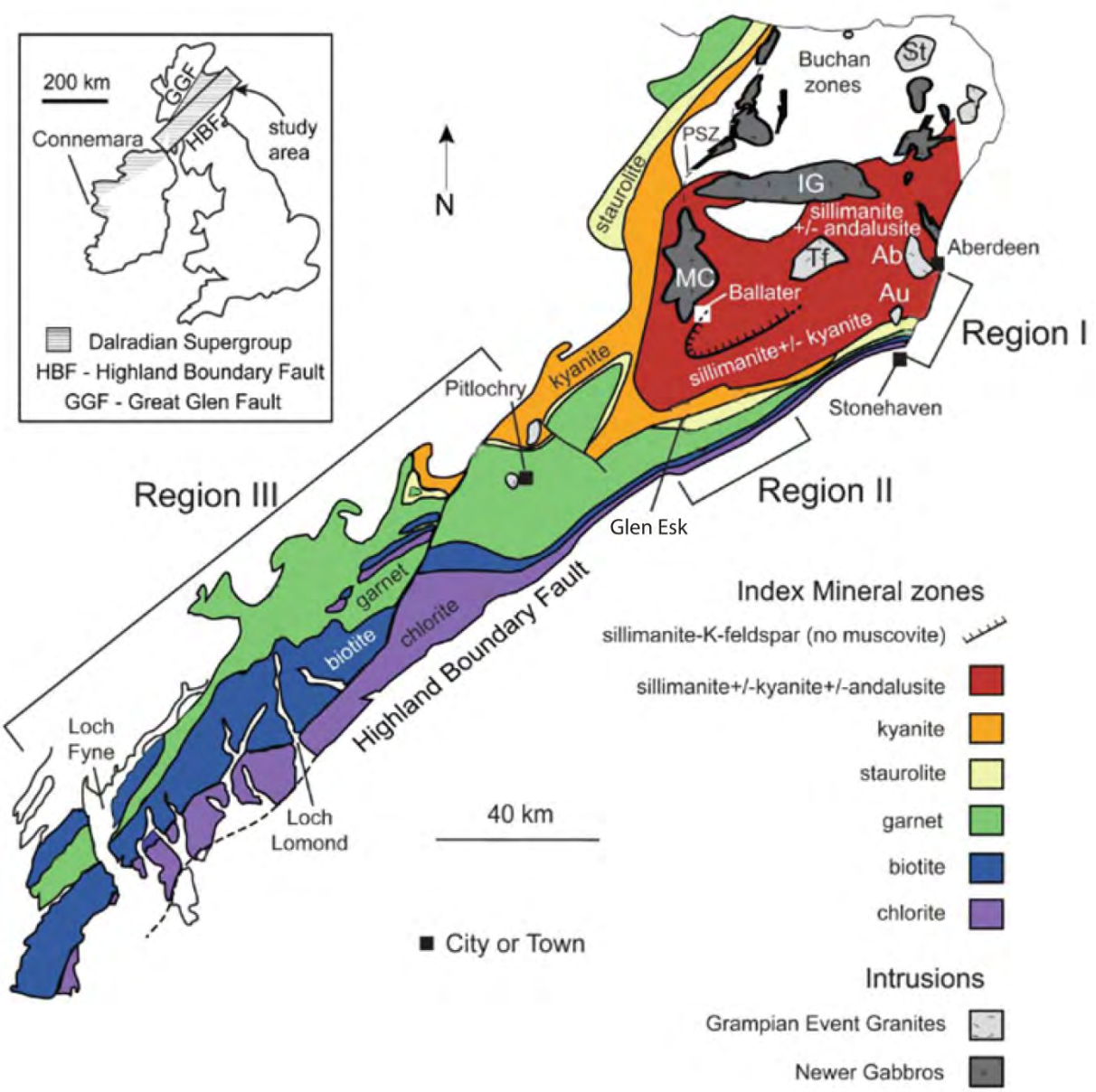

Figure 4. *Map of the distribution of metamorphic zones and igneous intrusions in the Central Highlands terrane (Vorhies and Ague 2011). Also marked are the three major metamorphic regions of I), Stonehaven II) Glen Esk and III) Loch Lomond.*

Previous studies with focus on geothermobarometry recognize three regions within the Dalradian which record different Pressure-Temperature evolutions (Figure 4). This thesis represents these regions by the localities of Stonehaven (I), Glen Esk (II) and Loch Lomond (III). In region III towards the SW the index mineral isograds are broad while in region I and II they are notably thinner close to the Highland Boundary Fault. Furthermore the staurolite, kyanite and sillimanite zones of higher-grade metamorphism are highly restricted to regions I and II in the NE. In their paper from 2011, Vorhies and Ague summarized earlier work on the P-T conditions of the Dalradian and with addition of their own data concluded that peak metamorphism of the Barrovian and Buchan zones was reached as a result of Ordovician synorogenic magmatism (region I and II). The magmatism varied greatly across the terrane and is likely to have occurred during rapid exhumation, contributing to peak thermal conditions through pulses of advective heat transfer (Vorhies and Ague 2011, Oliver et al. 2008). This is consistent with mineralogical evidence supporting multiple phases of metamorphism in parts of the sequence and coincides with the spatial distribution of igneous intrusions. Moreover, observations describing similar effects on metamorphism by

heat input from magmatic activity have been made in the Connemara region of NW Ireland and other metamorphic core complexes across the world. Although heat transfer away from emplaced magmas is believed to be the main cause of heating, textural evidence and geochronology suggest that fluid flow is likely to have contributed to this (Masters and Ague 2005, Vorhies and Ague 2011).

Published thermobarometric data focus on the classic Barrovian localities at region II and fewer investigations have been carried out for region III and I. The relative P and T conditions from each region are: region III at a high pressure, low temperature regime (up to 600 °C and 1.0 GPa), region II to high pressure, high temperature (up to 700 °C and 0.85 GPa) and region I at low pressure, mid temperature (around 600 °C and 0.55 GPa). Regions I and II record higher temperature conditions interpreted as a result of advective heating from intruding magmas during collisional thickening while region III was not superimposed by magmatism. Magmas affecting the regions in the NE were likely intruded at different depths and time. Evidence for this can be seen by the comparison between P-T estimates of Glen Muick and Glen Clova (both located in region II) where the former records intrusion at depth (peak T at 0.9-1.0 GPa) and the latter intrusion after extensive exhumation (peak T at 0.6 GPa). Region I records a maximum pressure of 0.5-0.6 GPa and thus was not as loaded region II and III. This is probably a result of region I being a shallower section of the crust and may explain the absence of the kyanite zone at this region.

Correlation between various estimates from data on fluid alteration of zircon, garnet growth Sm-Nd dating and radiometric dating of intrusions suggest that Barrovian peak metamorphism occurred somewhere around 475-465 Ma (Vorhies and Ague 2011, Oliver et al. 2008, Fettes et al. 2011 and Breeding et al. 2004).

Although the Dalradian Supergroup in Northern Ireland is believed to have experienced similar metamorphic evolution it has interestingly have become considerably more mineralized in terms of gold and base-metal deposits. At several locations in Ireland the Dalradian Supergroup host significant gold and base-metal sulphide-bearing vein deposits of orogenic origin closely related to major fracture systems and fault zones (Lusty et al. 2007, Baron and Parnell 2005, Parnell et al 2000, Anderson et al. 2004). By comparison, the Scottish Dalradian is nearly devoid of economic mineralization with a few notable exceptions located in the south west such as gold mining at the Tyndrum Fault zone which is in the time of writing undergoing exploration.

II. Methods

This study aims to investigate different aspects of large-scale metal mobility during the formation of the Dalradian Supergroup in Scotland. For this purpose a large number of samples are required and my project is part of a larger project being carried out by Dr. Iain Pitcairn who has previously collected and analyzed approximately 100 samples from the Glen Esk, Stonehaven and Loch Lomond (with the prefixes GE, ST and LL respectively) sections in the Dalradian (Figure 4). Although this earlier sampling was extensive, the number of unweathered samples from the staurolite to the sillimanite zones in Glen Esk was limited. Exposures of these higher grade zones in the classic localities at Glen Esk are commonly very weathered causing oxidation of sulfide minerals and possible leaching of the primary contents of gold and related element that are the focus of this study.

One of the main aims of my MSc thesis was to collect and analyze a suite of unweathered samples from the staurolite, kyanite and sillimanite zones in Glen Esk. To do this I selected a suite of 14 samples (new GE) from the existing collection of Dr. Iain Pitcairn that had not previously been analyzed and also collected a suite of my own samples (AE-GE) from Glen Esk during fieldwork carried out between 04/10/12 and 11/10/12 (Table 1, Figure 5). The aim of this trip was to investigate and sample new the staurolite, kyanite and sillimanite zone localities in the hills to the west of the road in Glen Esk in the hope of finding unweathered samples. A secondary aspect of my thesis is to investigate the fluid inclusions from vein samples in the Glen Esk section. A suite of 6 vein samples from the different isograds of Glen Esk were chosen from the existing collection to be used for this fluid inclusion investigation along with 2 samples collected by myself from Hardhill, a locality within the sillimanite zone at Glen Esk where Pb-Ag mineralization has been marked on the geological map.

A third aspect of the study was to carry out SEM scanning to quantify the proportions of sulfide minerals in the existing collections from Stonehaven and Loch Lomond. Such SEM scanning had already been carried out for the existing Glen Esk samples but not for these other section. For this project all thin sections from each suite were scanned digitally to act as maps for SEM scanning and the fluid inclusion study.

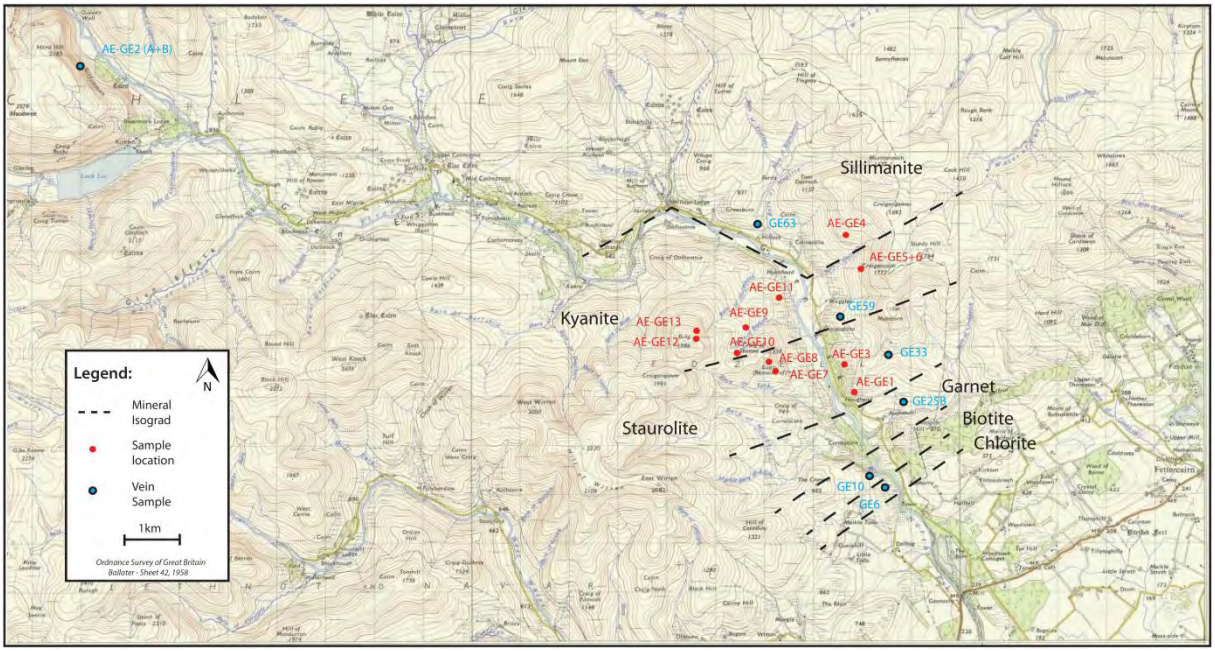

Figure 5. *Map of the Glen Esk area with mineral isograds (Ordnance Survey of Great Britain. Ballater – Sheet 42, 1958. Isograds marked from Harte and Hudson, 1979). Also marked are sample locations for the AE-GE collection and the fluid inclusion samples (both AE-GE and GE).*

AE-GE1*	Craig of Weston	Semi-pelite	Staurolite	GE1	Craig of Weston	Psammite	Staurolite	GE6	Dalbog	Chlorite
AE-GE3	Craigoshina	Psammite	St/Ky	GE31*	Ladder Burn	Pelite	Sillimanite	GE10	Burn of Mooran Gorge	Biotite
AE-GE4*	Road to Craigangowan	Semi-pelite	Sillimanite	GE34*	Maolearn	Pelite	Staurolite	GE25b	The Long Pool	Garnet
AE-GE5*	Craigancash	Semi-pelite	Kyanite	GE39*	Maolearn	Semi-pelite	Kyanite	GE33	Maolearn	Staurolite
AE-GE6	Craigancash	Semi-pelite	Kyanite	GE41	Craigancash	Semi-pelite	Kyanite	GE59	Craigoshina	Kyanite
AE-GE7*	Craig of Shanno	Psammite	Staurolite	GE54*	Craig of Weston	Semi-pelite	Staurolite	GE63	Hillock	Sillimanite
AE-GE8*	Craig of Shanno	Semipelite	Staurolite	GE58*	Craigoshina	Pelite	Kyanite	AE-GE2	Hardhill	Post-meta
AE-GE9	Craig of Shanno	Psammite	Kyanite	GE60	Burn of Dalforth	Pelite	Kyanite	(A+B)		
AE-GE10	Craig of Shanno	Semi-pelite	Kyanite	GE61	Burn of Dalforth	Psammite	Kyanite			
AE-GE11*	Bulg	Semi-pelite	Kyanite	GE66	Hillock	Pelite	Sillimanite			
AE-GE12*	Bulg	Semi-pelite	Kyanite	GE68	Auld Craig	Semi-pelite	Sillimanite			
AE-GE13*	Bulg	Semi-pelite	Kyanite	GE71	Auld Craig	Semi-pelite	Sillimanite			
				GE74*	Auld Craig	Pelite	Sillimanite			
				GE76*	Glen Effock	Psammite	Sillimanite			

Table 1. *List of the samples of AE-GE and new GE. The samples marked with an asterisk were analyzed with gold and HG-AFS analysis in addition to WRA.*

i. Polished thin sections and microscopy

11 samples from the AE-GE collection and 14 samples from the new GE collection were made into thin sections. The preparation for this was made at Stockholm University where the samples were cut into pieces of approximately 20 mm width, 35 mm length and 10 mm thickness with a diamond edge saw. These thin chips were then sent to Vancouver Petrographics Ltd in Canada for the making of the thin sections themselves.

Upon their return to Stockholm University each thin section was described in terms of textural relationships and mineralogy using a conventional petrographic microscope. Also documented in this way were the existing Stonehaven and Loch Lomond collections.

ii. SEM (scanning electron microscopy)

In this study a scanning electron microscope (SEM) was used for the purpose of assessing the sulfide paragenesis of the samples in terms of chemistry. This assessment was made as a continuation of the observations made in the microscopy stage to chemically determine what types of sulfides were present. In addition this analysis provided the data necessary to define the chemical composition of the sulfides and, with the use of the scanning function of the instrument, map their relative abundance. Before being placed in the SEM the samples were carbon coated in a vacuum in order to increase electrical conductivity and prevent the accumulation of electrostatic charge.

"Point and ID"

The first step of analysis was to identify the different sulfides present in the thin section by the "Point and ID" function in the INCA data processing program. This function allows for point analysis of mineral grains and quick assessment of the larger features of the thin section. After the general sulfide paragenesis had been determined pictures were taken of different parts of the thin section with representative sulfide assemblages and characteristic textures.

"Feature" - Thin section scanning

The most abundant sulfides could be identified using "Point and ID" but smaller, more isolated grains were only picked up by thin section scanning. For mapping of the sulfides and calculation of relative abundances, scanning of 8 samples from the Stonehaven region (I) and 6 from the Loch Lomond region (III) was carried out. This was made in order to provide a comparison to the more well-documented region of Glen Esk (II) and see if the same changes in sulfide paragenesis could be observed over the whole Dalradian Supergroup section. Two samples from each metamorphic zone were chosen for analysis (with the exception of the biotite and sillimanite zone from Stonehaven for which the sample collection proved insufficient) and where possible both psammitic and pelitic samples were analyzed to search for differences between lithologies. After the thin section had been surveyed using "Point and ID" a representative area containing several types of sulfides were chosen and scanned using the "Feature" function in INCA. For each run an individual setting of the SEM grey scale (related to the chemistry of the mineral grains with heavier elements appearing brighter) was applied using brightness and contrast to help the program distinguish between different grains. These settings were then tested on locations where different sulfides were in contact or close to one another (such as composite grains) in order to see if the program treated them as separate grains.

The type of SEM used was a FEI Quanta™ 650 FEG (field emission gun) ESEM operating at 20kV at a working distance of 10 mm with a spot size of 4. Analysis was made at Stockholm University with calibration being made with a cobalt standard and the data gathered by the Oxford EDS was processed using INCA system from Oxford instruments.

iii. WRA (Whole Rock Analysis)

12 samples from the AE-GE collection and 14 samples from the new GE collection were sent to Actlabs, Vancouver for whole rock major and trace element analysis. Preparations for the analysis were made at Stockholm University where the samples were cut into smaller sections of approximately 50 mm width, 90 mm length and 30 mm thickness using a diamond edged saw (avoiding any potentially weathered surfaces). At the Museum of Natural History these sections were broken into smaller pieces using a jaw crusher and then finally grinded to a powder using a Steel TEMA. Approximately 10 g per sample were sent to Actlabs and analyzed using two different methods for two suites of elements. The analytical methods at Actlabs were:

"Total Digestion - ICP"
0.25 g sample was digested using four acids. In the first stage hydrofluoric acid was added followed by a mixture of nitric and perchloric acids. This was accompanied with heating of the sample in several ramping and holding cycles eventually leading to sample dryness. In the final stage samples were brought back into solution using hydrochloric acid. The samples were then analyzed by inductively coupled plasma mass spectrometry (ICP-MS) using a Varian Vista 735 with in-lab standards (traceable to certified reference materials) or certified reference materials being used for quality control. Elements analyzed this way included Ag, Cd, Cu, Ni and Pb.

"Lithium Metaborate/Tetraborate Fusion – ICP"
For this analysis samples were prepared and analyzed in a batch system. Included in each batch were a method reagent blank, certified reference materials and replicates. The samples were mixed with a flux of lithium metaborate and lithium tetraborate before being fused in an induction furnance. The melt produced were then immediately poured into a solution of 5% nitric acid (containing an internal standard) and mixed to complete dissolution. The samples were then run on a combination of simultaneous/sequential Thermo Jarrell-Ash ENVIRO II ICP or a Varian Vista 735 ICP using calibration from prepared USGS and CANMET certified reference materials. Elements analyzed this way included Si, Al, Fe, Mn, Mg, Ca, Na, K, Ti, P, Ba, Sr, Y, Sc, Zr, Be and V.

iv. Gold analysis

Preparation

Gold concentrations were analyzed using a method with ultralow detection limit (10 ppt) that involves a 5-stage digestion using hydrofluoric acid and aqua regia, followed by chromatographic separation of Au from other elements before being analyzed using ICP-MS (Pitcairn et al. 2006b). An even mixture of samples (with the same preparation as WRA rock powder) from AE-GE and the new GE suites were chosen for this analysis (see Table 2).

Prior to analysis a number of samples containers were pre-cleaned using different cleaning methods. These differing cleaning methods were used due to difference in tolerance of acids of the container material and with regard to what material they contained during analysis. 100 ml plastic bottles and 50 ml centrifuge tubes were pre-cleaned using a 50% HCl cleaning solution (1:1 12 M HCl and ultrapure water) which they were filled with for the duration of one week. 15 ml columns were pre-cleaned with the same cleaning solution at hotplates set to 80°C overnight (15-18 hours). Two series of 60 ml Teflon pots (A+B) were cleaned for 1 hour in Aqua Regia at ambient temperature, rinsed with ultrapure water, put in cleaning solution at 80°C overnight and finally carefully rinsed once again with ultrapure water and dried.

The 50 ml centrifuge tubes used in the re-dissolution step were labeled and weighed.

Digestion

For each sample 3 g of sample rock powder were weighed into the 60 ml Teflon pots of the A-series. The samples were then digested in 5 stages: **1)** 10 ml concentrated Nitric acid (HNO_3) **2)** 25 ml concentrated Hydrofluoric acid (HF) **3)** 20 ml concentrated Hydrochloric acid (HCl) **4)** 15 ml of Aqua Regia (3:1: HCl:HNO_3) and **5)** 40 ml ultrapure water. At first the nitric and hydrofluoric acids were added and then left to digest overnight (15-18 hours) at hotplates set to 150°C. After the samples had dried out completely hydrochloric acid was added and digested again overnight at 150°C. For Aqua Regia and ultrapure water digestion took place during 2 hours per stage (with the ultrapure water digestion taking place at room temperature). After Hydrofluoric and Hydrochloric digestion the caps of the Teflon pots were removed and the acids dried down at 150°C during 5 and 4 hours respectively before proceeding to the next step.

Any residue material left over from digestion was rinsed and filtered removing undissolved materials and CaF precipitates originating from the HF digestion stage. The final solution was transferred to labeled pre-weighed 60 ml plastic bottles which were then weighed.

Columns

To separate the gold from the solution of the digested samples the final solution was passed through a column. These columns contained a resin primed with di-isobutyl ketone (DIBK) a solvent with high partition coefficient for Au with a ratio of DIBK to resin of 1.6:1 (e.g. 20,8 ml DIBK and 13 g resin). The columns were placed in an elevated sample rack so that solution which had passed through them could drip down into containers below. To ensure that the DIBK bonded evenly to the resin it was added slowly and carefully mixed as the desired ratio

was approached. 6M HCl was then added until the mixture displayed a slurry texture at which point it was transferred to the columns with the use of a 5 ml pipette. 3cm of the mixture was added this way to the columns after which cotton wool was put down on top of it and pressed down with a glass mixing rod. Plastic rinse bottles were set up underneath the rack and the columns were rinsed with 5 ml 6M HCl. Then the sample solution was poured into the column trapping any gold contained in it and letting the rest of the solution pass through the column down into the bottles. A final rinse of 5 ml 6M HCl was made and once this was done the plastic bottles at the end of the column were replaced with the B-series Teflon pots.

The gold locked in the columns was extracted by an elution process of twice adding first 5 ml of 4% Ammonia solution and then 5 ml of ultrapure water. The Teflon pots were then dried down on hotplates at 150°C.

Re-dissolution

Once through the column stage the Teflon pots were filled with 1 ml of concentrated HCl and 5 ml of ultrapure water. The whole sample was put into contact with the acid after which the pots were sealed and placed on the hotplates at 80°C for 30 minutes. The content of the Teflon pots were then transferred to the labeled and pre-weighed centrifuge tubes with the help of 5 ml rinsing ultrapure water. Ultrapure water was used to fill the tubes up to 15 ml with the final solution weighing 15 g (checked on an electric balance).

ICP analysis

For the final step of the gold analysis the samples were run in an ICP-MS at ITM Stockholm University, department of applied environmental science by Karin Holm.

v. Hydride Generation – Atomic Fluorescence Spectrometry (HG-AFS)

HG-AFS

The Hydride Generation–Atomic Fluorescence Spectrometer (HG-AFS Millenium Excalibur) is an analytical instrument with super low detection limit (10ppt) designed for analyzing trace concentrations of Arsenic, Antimony, Selenium, Tellurium, Mercury and Bismuth in solution. It operates by continuously pumping sodium borohydride ($NaBH_4$) and Hydrochloric acid (HCl) into a gas/liquid separator via a mixing valve. The hydrogen gas evolved during the resultant reaction is carried through a drying tube by argon gas to fuel a flame in the atomic fluorescence spectrometer. When a sample is introduced for analysis via an auto-sampler the mixing valve switches so that the acidified sample solution mixes with the reductant and flow to the gas/liquid separator. The dissolved elements are reduced into gaseous hydrides individual for each element and are carried with the hydrogen following the argon carrier gas to the detector. The gaseous hydrides are unstable and decompose in the hydrogen flame creating an emission of atomic fluorescence which is registered in a hollow cathode lamp and recalculated to element concentrations.

The cathode lamp is element specific and must be changed in between analysis of different elements. To generate the hydrides it is required that each element is put into the right oxidation state prior to analysis which is achieved through different digest processes.

Digestion

For this project digests were prepared for As, Sb, Se and Te using the same samples as for the gold analysis and the same digest with HNO_3-HF-HCl-AR and ultrapure water. These elements were then treated the same with the exception of the final solutions of Se and Te which were heated at 120°C for 30min after digest and which reagent blank contained no KI or Ascorbic acid. These end up being 25% Aqua Regia.

Reagent blank

The reagent blank is an HCl based solution that when mixed with the reductant creates the hydrogen gas used as fuel for the fluorescence cell. The reagent blank also contains KI and Ascorbic acid ($C_6H_8O_6$, a reductant which also helps mop up the spare iodide to keep the reaction from reversing) which reduce the oxidation state of the As and Sb from +5 after digestion to +3 state desired prior to analysis. The reagent blank was mixed with the samples and standards before analysis and was also pumped through the AFS system continuously to ensure that hydrogen was always being created for the fluorescence cell. The reagent blank consisted of 3M HCl with 1% KI and 0,4% Ascorbic acid and for the one pumped through the AFS 10% 10% Aqua Regia was added.

Sample solutions

The sample solutions were made from 10 ml sample which was diluted to 50 ml with reagent blank in pre-weighed and labeled centrifuge tubes. If a lower sample volume was desired (due to high concentrations for example) 25% Aqua Regia was used to dilute the total to 5 ml. 50 ml centrifuge tubes were labeled and weighed (with caps on) for each sample.

Standard solutions

Standard solutions with known concentrations of As, Se, Te and Bi were prepared at 10 ppm, 100 ppb, 5 ppb, 2.5 ppb, 1 ppb, 0.5 ppb, 0.25ppb, 0.1ppb and 0.05ppb. These solutions were then used to test the recovery rate of the instrument to see whether it operated well within the expected sample ranges.

vi. Microthermometry of fluid inclusions

Preparation and analytical conditions

Analyses of fluid inclusion were carried out at the Department of Geological Sciences, Stockholm University. Fluid inclusions were studied in doubly polished 150 µm thick sections. One sample from each index mineral zone was made into thick sections along with 2 post-metamorphic samples from Hardhill. All these were analyzed with the exception of GE33 (staurolite zone) which proved too deformed to display fluid inclusions. A conventional microscope was used to get an overview of the samples and the distribution of fluid inclusions. All thick sections were then scanned digitally and important areas of fluid inclusions mapped out. Before analysis the sample was put in acetone for 48 hours to dissolve the glue connecting the rock chip to the glass after which any residue glue was removed with ethanol.

Microthermometric analyses on fluid inclusions in quartz and sphalerite were made with a Linkam THM 600 stage mounted on a Nikon microscope utilizing a 40x long working-distance objective. The working range of the stage is from -196° to +600°C (for details see Shepherd et al., 1985). The reproducibility of the readings was ±0.1°C for temperatures below 40°C and ±0.5°C for temperatures above 40°C. In order to fit into the sample tray of the Linkham 600 heating and cooling stage samples were cut into smaller pieces. This procedure is dangerous as cuts made in the rock chip are unpredictable and may end up destroying areas of interest. However separation of these areas is necessary as the site of measurement during analysis is restricted by the optical image of the microscope but the effects of microthermometry affect the whole sample. Cooling is normally non-destructive but heating of the sample may cause stretching leading to erroneous homogenization temperatures or decrepitation.

Theory of fluid inclusion studies

During the growth of a crystal, defects in the crystal lattice is a common occurrence and even under the most controlled laboratory experiment perfect crystals are virtually impossible to create (Shepherd et al. 1985). In nature this provides a powerful tool as these imperfections may trap so called fluid inclusions when the host mineral is precipitated. Fluid inclusions are important as the composition of the trapped fluid can yield information on the conditions which formed the host mineral such as the temperature, pressure and chemistry involved during precipitation. Fluid inclusion research has proved to be particularly useful for the

understanding of ore genesis and has provided invaluable information concerning the transportation and deposition of ore.

The main strength of the fluid inclusions also represents their limitation: The fact that the inclusions capture only the specific conditions that formed the host mineral (Shepherd et al. 1985). Ideally these conditions are directly relevant to the study such as inclusions found in ore minerals or those related to peak metamorphism. These observations are not always possible however as most ore minerals are opaque and several generations of inclusions may complicate or overprint peak metamorphic conditions (if any at all are preserved). For this reason great care must be taken when identifying different populations of fluid inclusions and their relationship to one another in order to assess what they truly represent.

One principal assumption made in order to connect fluid inclusion data with the P-T-x conditions of ancient geological systems is that trapping is representative of the mineral forming fluid. In nature this is most often the case but some process can affect the homogeneity of the fluid or alter the inclusion after trapping. These processes are important to recognize and account for in any fluid inclusion study. Fluid inclusions can re-equilibrate with their surroundings after formation and this is common for inclusions that are large or irregularly shaped. These effects are often small enough to be considered an isochemical change in relatively insoluble minerals such as quartz but in some instances it can create problems (Shepherd et al. 1985). An example of this is the process of necking-down which occur when larger elongated inclusion breaks down into a series of smaller more regular ones. If the breakdown of the larger inclusion is carried out slowly enough the fluid may differentiate as a consequence of change in pressure and temperature. This creates inhomogeneous fluid inclusions not representative of the environment of formation.

Heterogeneous trapping may still be representative and provide useful data when it occurs in a system that during formation displays a separation of phases (Shepherd et al. 1985). This process is called unmixing and is a result of immiscibility between for example CO_2 and water. This can be compared with the opening of a bottle of soda which causes a separation into a gas and a liquid state due to change in pressure but remains representative over an area incorporating both types.

Primary and secondary fluid inclusions

A mineral may contain two types of fluid inclusions: primary and secondary. Primary inclusions are formed at the same time as the host mineral and are found in alignment with faces of crystal growth. During later stage deformation or precipitation events secondary inclusions may be created. These can often be visibly distinguished from the primary as they occur in continuous lineations or planes crosscutting the crystal growth where they seal cracks in the original mineral (Shepherd et al. 1985). Primary inclusions are often the more valuable type as they are directly related to the formation of the original mineral. Secondary inclusions however also provide useful data and can be used to describe fluid migration pathways.

The analysis of fluid inclusions is principally based around phase transitions during successive heating and cooling of the sample. The timing of phase transitions during cooling have little value as water becomes metastable and requires various amounts of supercooling to freeze. Standard procedure is therefore to rapidly freeze the sample and then heat it at a controlled rate.

The implementation of fluid inclusion measurement is strongly dependent on the composition of the inclusion itself as this is coupled to the phase transitions observed. H_2O, CO_2 and salts are among most common components of fluids in nature. This is also true for the samples of this study which in addition commonly contain CH_4 and N_2. One principal requirement for microthermometric analysis is that both a gas and a liquid phase are present for the correct phase transition to be observed.

Water inclusions

At room temperature water inclusions show two phases, liquid and vapour H_2O. Upon freezing the water phase becomes solid and compresses the vapour phase resulting in an inclusion filled entirely with ice and salt. The sample is then heated until it reaches the binary eutectic point at which stage melting of the solid phase is initiated. This phase transition is difficult to recognize but can be used to identify the type of salt dissolved in the fluid and the chemistry of the salt system present in the inclusion (Shepherd et al. 1985). For example

solutions with Mg drive the point of first melting towards higher temperatures while Ca in solution act opposite causing melting at lower temperatures.

With increased heating the vapour phase is released and at the disappearance of the last ice becomes mobile. This temperature is called the freezing point depression and can be used to calculate the salinity of the fluid. Further heating above room temperature leads to homogenization between the liquid and the vapour phase as they merge into a single phase (either liquid or vapour). The homogenization temperature represents either the minimum temperature of formation of a mineralizing fluid (which has to be corrected for pressure) or the minimum temperature conditions of a boiling system.

CO_2 inclusions

Aqueous fluid inclusions which contain sufficient concentrations of gaseous phases such as CO_2, CH_4 and N_2 are more complex than inclusions containing only water and a salt system. As temperatures are lowered these gases form gas hydrates called clathrates which are crystalline solids resembling ice (Shepherd et al 1985). These clathrates consist of gas molecules binding water to their structure and occur in nature as permafrost and on the deep ocean floor where water binds strong greenhouse gases such as CH_4. Inside of fluid inclusions however clathrates interfere with the measurement of salinity as they enrich the liquid phase with salts by the binding of water. For this reason clathrate melting is used instead of ice melting in order to calculate salinity.

Experimental studies have shown that the increased addition of salt systematically lowers the quadruple invariant point (melting) of a CO_2-H_2O system much in the same manner as salts lower the triple point of melting (ice + liquid + vapour) in a H_2O-Salt system (Fall et al. 2010). Although the salinity of a CO_2 bearing fluid inclusion can be calculated the type of salt in solution cannot since first melting is obscured by presence of the gases.

As the fluid inclusion is cooled clathrates are first formed, then ice and lastly freezing of all CO_2 takes place. Upon heating melting of pure CO_2 takes place at -56,6 °C but this temperature can be lowered if there is any CH_4 and N_2 in the inclusion. From the deviation of the melting temperature the composition of the mixture can be estimated (Shepherd et al. 1985). Further heating leads to the melting of clathrates and the homogenization of CO_2. This homogenization temperature provides information about the conditions of formation and can also in combination with the melting temperature be used to estimate the composition of the CO_2 phase.

Fluid Inclusion types

Samples of Glen Esk were investigated and results showed that two major types of fluid inclusions were present: Type I inclusions which were mainly aqueous in composition and Type II which contained a gas-rich mixture of some or all of the gases CO_2-N_2-CH_4. The chart in Figure 6 was used to further classify the inclusions present by the size of their vapour phase (e.g. a Type I-b inclusion would be an aqueous inclusion with a vapour phase occupying 1.0 volume %). Type II inclusions had a tendency towards a larger vapour phase above 20 volume % while Type I mainly had a vapour phase at or below this size. A special version of the Type I inclusions was also found were solid phases of varying chemistry were identified. In the classification scheme of the analysis the letter “s” is added for such inclusions.

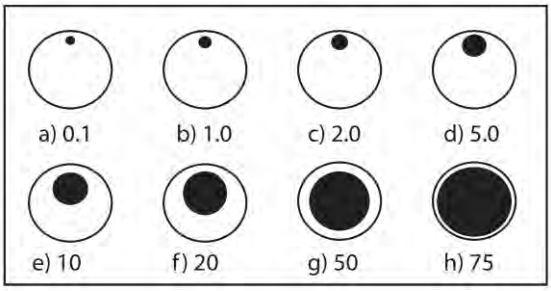

Figure 6. *Classification chart of volume percent occupied by the vapour phase (modified from Roedder 1984).*

Calibrations

The method of microthermometry is reliant on experimental data of known solutions which during recent years have become more readily available (Shepherd et al. 1985). The thermocouple readings were calibrated by means of SynFlinc® synthetic fluid inclusions and well-defined natural inclusions in Alpine quartz. These inclusions have known phase transitions and the correction curve in Figure 7 was calculated using data from them.

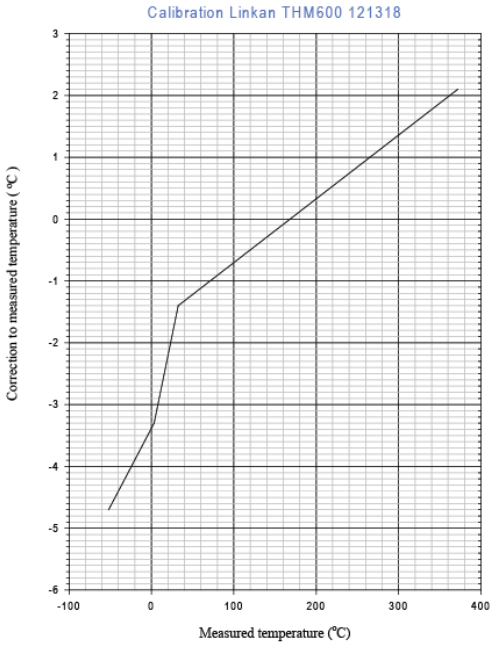

***Figure 7**. Calibration curve for fluid inclusions*

vii. Raman laser spectroscopy

Raman laser spectroscopy is an analytical method based around the measurement of scattered Raman radiation. By focusing an intense laser light source directed through an incorporated standard optical microscope into a sample, target molecules are excited. This excitement takes the form of vibration between bonded atoms in a molecule and creates scattered Raman radiation of varying frequencies dependant on which atoms are involved. By analyzing and quantifying this radiation the types of molecules present and, in the case of a gas, proportional molecular abundances can be determined. Only polyatomic species can be analyzed this way since this type of radiation is created by the vibration of atomic bonds (Shephed et al. 1985).

Raman spectra were recorded at the Department of Geological Sciences, Stockholm University, using a laser Raman confocal spectrometer (Horiba instrument LabRAM HR 800) and equipped with a multichannel air cooled CCD detector. An Ar-ion laser (λ = 514 nm) was used as the excitation source with an output power at the sample of 8 mW. The instrument was integrated with an Olympus microscope and the laser beam was focused to a spot of 1 μm with a 100x objective. The spectral resolution is about 0.3 cm^{-1}. The instrument was calibrated using a neon lamp and the Raman line (520.7 cm^{-1}) of a silicon wafer. Instrument control and data acquisition was made with LabSpec 5 software.

III. Results

i. Thin section descriptions

The vast majority of the rocks of the AE-GE and new GE collection are semi-pelitic in composition. The mineral assemblage of these samples commonly includes varying proportions of quartz, biotite, muscovite, chlorite and plagioclase. Along with similar mineral assemblages the thin sections also share common mineral reaction textures. Of these the two most prominent are the replacement of biotite by chlorite and sericitization of staurolite and other minerals (Figure 8a-b). These are common retrograde reactions in the Scottish Dalradian associated with late deformation and fluid infiltration (Yardley and Baltazis 1985, Dempster 1985). There are two notable exceptions that deviate from these characteristics: sample GE76 which contain an epidote vein with epidote-rich selvage and GE68 which hosts the entire range of the Barrovian index minerals.

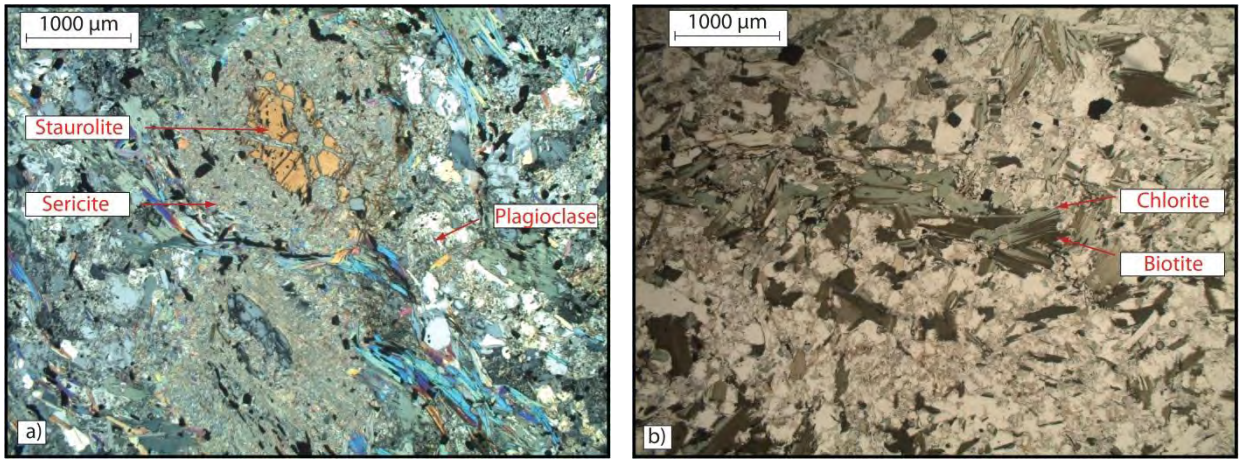

Figure 8. *Example of common mineral reaction textures* ***a)*** *Sericitization of staurolite and plagioclase from sample AE-GE13 (cross-polarized view)* ***b)*** *Replacement of Biotite by Chlorite in GE41 (polarized view).*

Qtz = Quartz, Bi = Biotite, Mu = Muscovite, Chl = Chlorite, Plg = Plagioclase, Gt = Garnet, St = Staurolite, Sill = Sillimanite, Ky = Kyanite, Ep = Epidote, Cal = Calcite

AE-GE1 - *Qtz, Bi, Chl, St, Gt, Plg, Mu*
Sample with quartz vein. Breakdown of St to sericite. Bi is replaced by Chl. Foliation.

AE-GE4 - *Qtz, Bi, Chl, Gt, Mu*
Abundant replacement of Bi by Chl. Foliation. Sericitization. Small amount of sulfides.

AE-GE5 - *Qtz, Bi, Chl, St, Mu*
Breakdown of St to sericite. Bi is replaced by Chl. Foliation.

AE-GE6 - *Qtz, Bi, Chl, St, Gt, Plg, Mu*
Sericitization is abundant both with St and other minerals. Bi is replaced by Chl.

AE-GE7- *Qtz, Bi, Chl, Gt, Mu*
Breakdown of St to sericite. The sample is dominated by quartz. Bi is replaced by Chl. Foliation.

AE-GE8 - *Qtz, Bi, Chl, Mu*
Sericitization. Bi is replaced by Chl. Foliation.

AE-GE9 - *Qtz, Bi, Chl, Gt, Plg, Mu*
Dominated by Qtz and Bi. Minor replacement of Bi by Chl. Sericitization. Foliation.

AE-GE10 - *Qtz, Bi, Chl, Gt, Mu*
Bi is replaced by Chl. Weak foliation.

AE-GE11- *Qtz, Chl, St, Mu and minor Bi*
Breakdown of St to sericite. Abundant and large mica. Bi is replaced by Chl. Foliation.

AE-GE12 - *Qtz, Chl, St, Plg, Mu*
Abundant and large mica. Sericitization is abundant in both St and other minerals.

AE-GE13- *Qtz, Chl, St, Plg, Mu and minor Bi*
Abundant and large mica. Sericitization is

abundant in both St and other minerals.

GE1 - *Qtz, Bi, Chl, Gt, Plg, Mu*
Minor replacement of Bi by Chl. Sericitization of Plag. Minor sulfides. Foliation

GE31 - *Qtz, Bi, Chl, Plg, Mu*
Sericitization of Plag. Minor replacement of Bi by Chl. Minor sulfides.

GE34 - *Qtz, Bi, Chl, Gt, Mu*
Replacement of Bi by Chl. Weak foliation.

GE39 - *Qtz, Bi, Chl, Plg, Mu*
Replacement of Bi by Chl. Abundant sericitization of Plag. Minor sulfides. Foliation.

GE41 - *Qtz, Bi, Chl, Plg, Mu*
Replacement of Bi by Chl. Sericitization of Plag. Foliation.

GE54 - *Qtz, Bi, Chl, Gt, Plg, Mu*
Replacement of Bi by Chl. Sericitization of Plag. Minor sulfides. Weak foliation.

GE58 - *Qtz, Bi, Chl, Plg, Mu*
Abundant Mu and Oxides. Sericitization of Plag. Minor Bi. Replacement of Bi by Chl.

GE60 - *Qtz, Bi, Chl, Plg, Mu*
Abundant sericitization of Plag. Minor Bi. Replacement of Bi by Chl. Weak foliation.

GE61- *Qtz, Bi, Chl, Plg, Mu*
Replacement of Bi by Chl. Sericitization of Plag. Weak foliation.

GE66 - *Qtz, Bi, Chl, St, Gt, Plg, Mu*
Replacement of Bi by Chl. Sericitization of Plag. Weak foliation.

GE68 - *Qtz, Bi, Chl, St, Gt, Plg, Mu, Sill, Ky*
Replacement of Bi by Chl. Mineral grains are larger than in other thin sections. Abundant sulfides. Weak foliation.

GE71 - *Qtz, Bi, Chl, Gt, Plg, Mu*
Replacement of Bi by Chl. Sericitization of Plag. Minor sulfides. Weak foliation.

GE74 - *Qtz, Bi, Chl, Gt, Plg, Mu*
Replacement of Bi by Chl. Sericitization of Plag. Minor sulfides. Foliation.

GE76- *Ep, Mu, Cal and Minor Qtz*
Sample with epidote vein. Differet mineral assemblage from the other thin sections. Abundant sulfides both in vein and wallrock.

Loch Lomond

LL19B - *Qtz, Mu, Cal (Semi-pelite)*
Strong foliation. Most of the calcite is found in a single vein.

LL25 - *Qtz, Plg, Mu, Cal (Psammite)*
Aubundant sericitization of Plag. Folded.

LL1- *Qtz, Plg, Mu, Gt, Cal, Chl (Semi-pelite)*
Minor sericitization of Plag. Foliation. Small garnets (sample is labeled wrong. Actually Garnet zone sample.)

LL10 - *Qtz, Bi, Chl, Plg, Mu, Cal (Pelite)*
Abundant mica (little biotite). Replacement of Bi by Chl. Fine grained foliation and folding.

LL32 - *Qtz, Bi, Chl, Plg, Mu, Cal (Semi-pelite)*
Qtz dominated sample with little Bi, Mu, Chl and Ca.

LL34 - *Qtz, Bi, Chl, Gt, Plg, Mu (Pelite)*
Abundant mica (little Bi and Chl). Replacement of Bi by Chl. Sericitization of Plag. Folding and foliation. Much Garnet (in places deformed)

Stonehaven

ST1 - *Qtz, Plg, Cal (Pelite)*
Cal dominated with small amounts of patchy Qtz. Fine grained foliation.

ST3 - *Mu, Qtz, Plg (Psammite)*
Sericitization of Plag.

ST10 - *Qtz, Bi, Chl, Plg, Mu (Pelite)*
Replacement of Bi by Chl. Sericitization of Plag.

ST30 – *Qtz, Mu, Plg (Psammite)*
Sericitization of Plag. Weak foliation

ST32 - *Qtz, Bi, Plg, Mu (Pelite)*
Abundant mica. Biotite is not in equilibrium. Sericitization of Plag.

ST39- *Mu, Qtz, St, Bi, Chl (Pelite)*
Abundant mica. Abundant Sericitization of St. Replacement of Bi by Chl (both not very abundant).

ST42 - *Qtz, Bi, Chl, St, Mu (Semi-pelite)*
Replacement of Bi by Chl. Sericitization of St. Foliation.

ST50 - *Mu, Qtz, Bi, Plg, Chl*
Sericitization of Plag. Replacement of Bi by Chl (both not very abundant). Foliation.

ii. Stonehaven - Sulfide mineralogy and SEM analysis

Chlorite zone

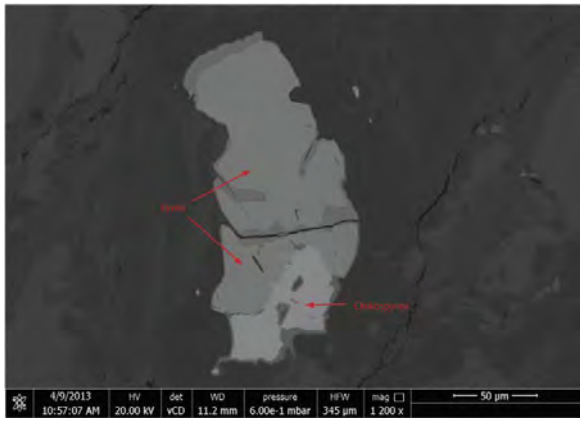

Figure 9. *Irregular composite grain of Pyrite and chalcopyrite with oxidized rims (ST1).*

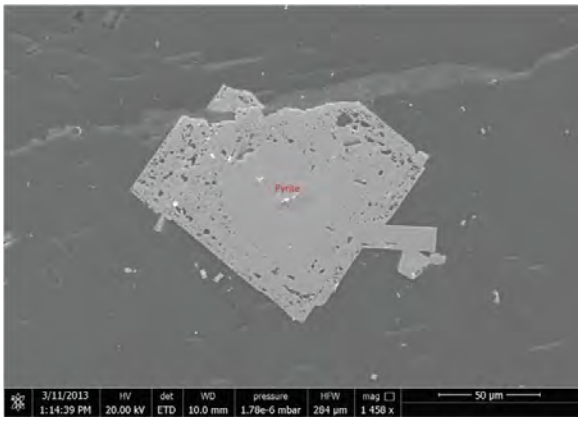

Figure 10. *Euhedral pyrite grain with porous secondary growth from sample ST3.*

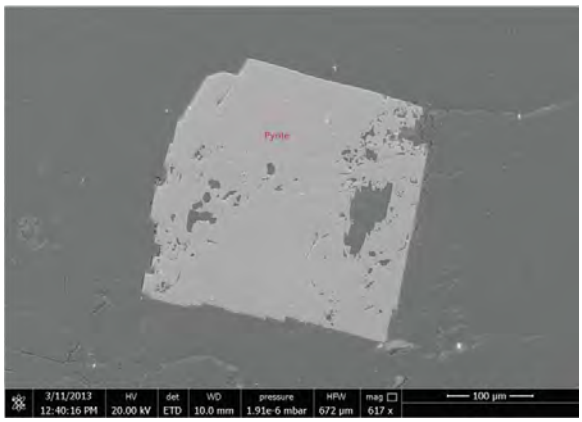

Figure 11. *Euhedral pyrite in sample ST3.*

Biotite zone

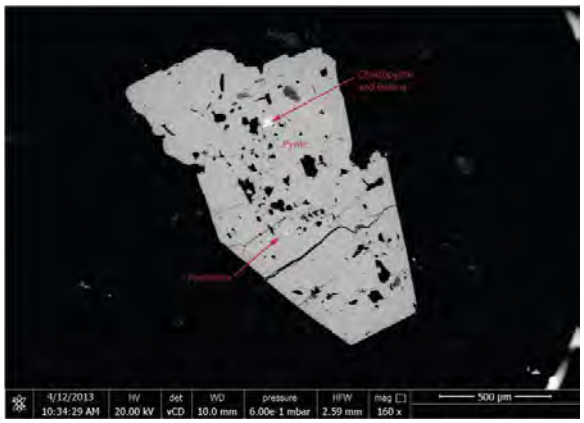

Figure 12. *Composite grain of pyrite, pyrrhotite, galena and chalcopyrite in sample ST10.*

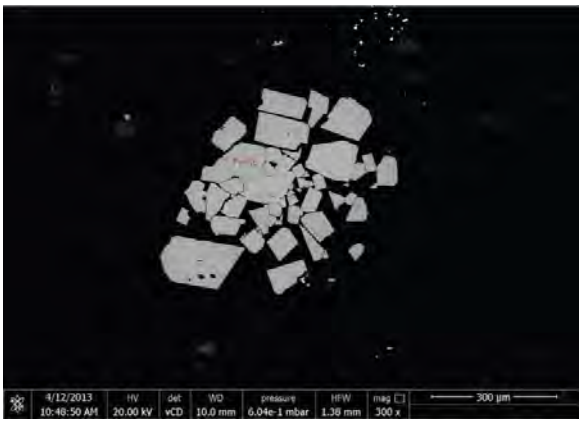

Figure 13. *Framboidal pyrite in sample ST10.*

Garnet zone

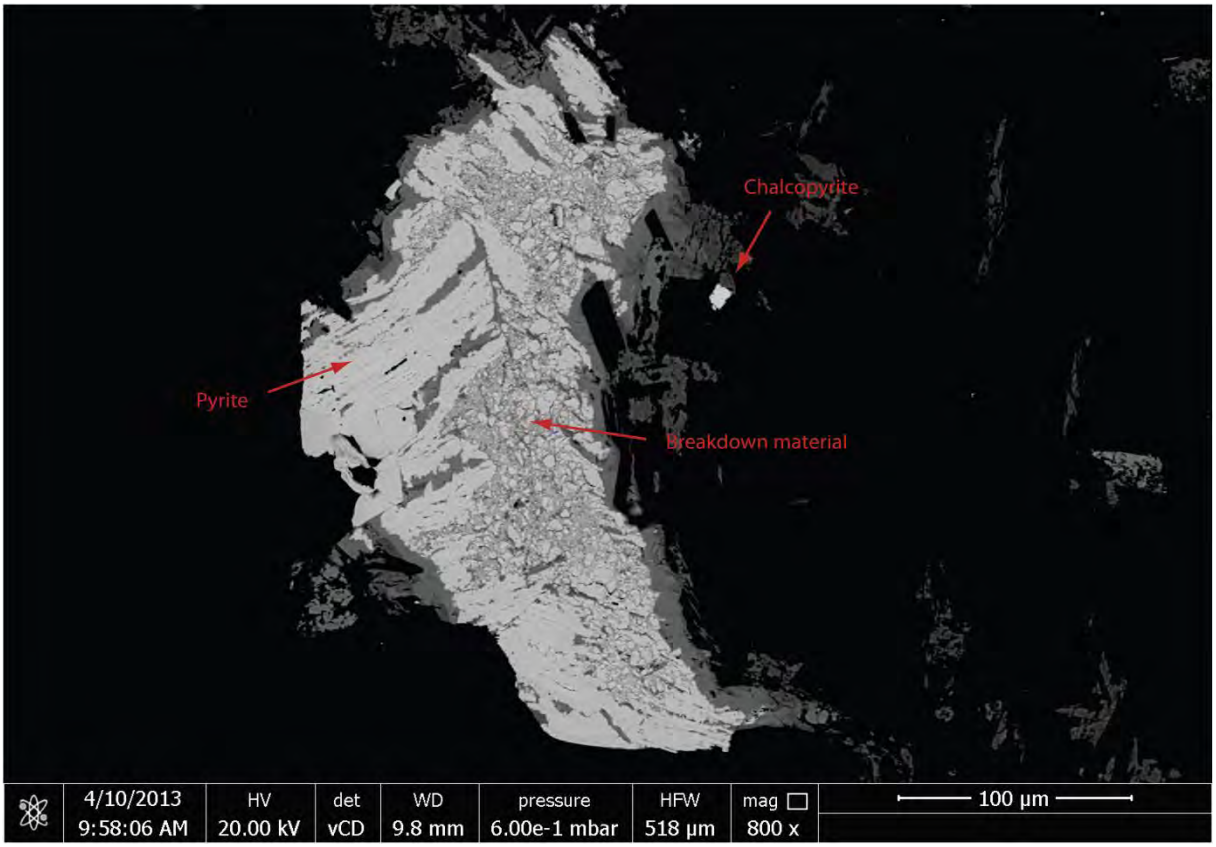

Figure 14. *Composite grain of pyrite and chalcopyrite in sample ST30. Pyrite is breaking down to form mineral grains with similar chemistry to pyrite but containing trace amounts of As and Ni.*

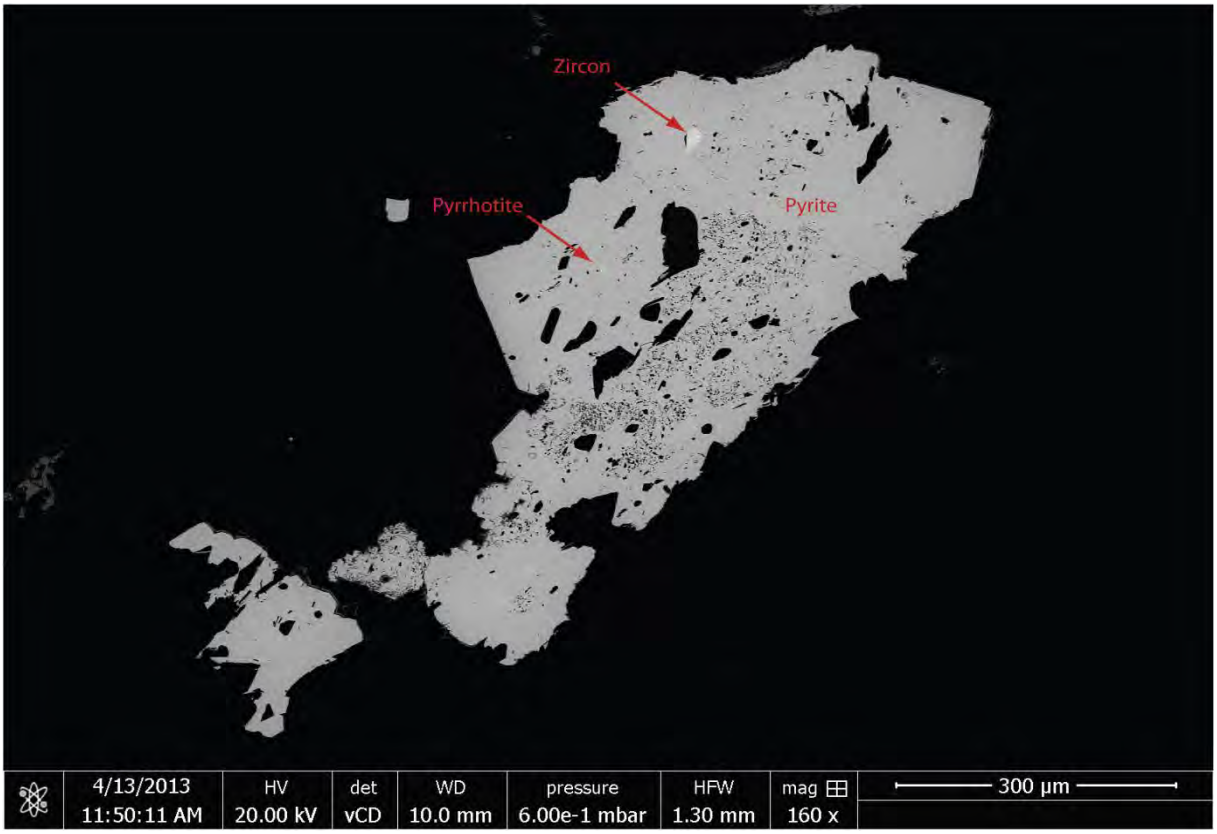

Figure 15. *Large irregular composit grain of pyrite and pyrrhotite in sample ST32.*

Staurolite zone

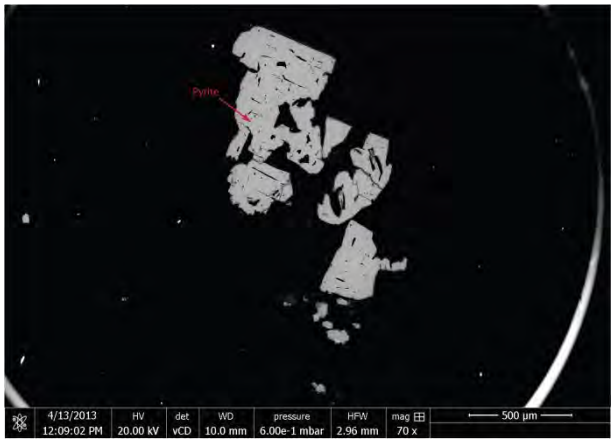

Figure 16. *Large grain of pyrite found inside a vein in sample ST39.*

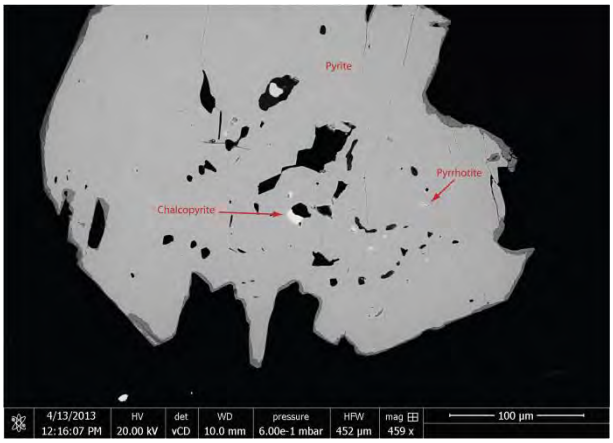

Figure 17. *Composite grain of pyrite, chalcopyrite and pyrrhotite with oxidized rim (sample ST39).*

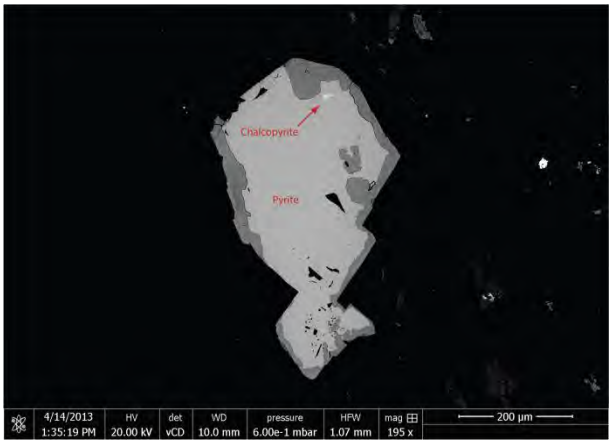

Figure 18. *Composite grain of pyrite and chalcopyrite with oxidized rim in sample ST42.*

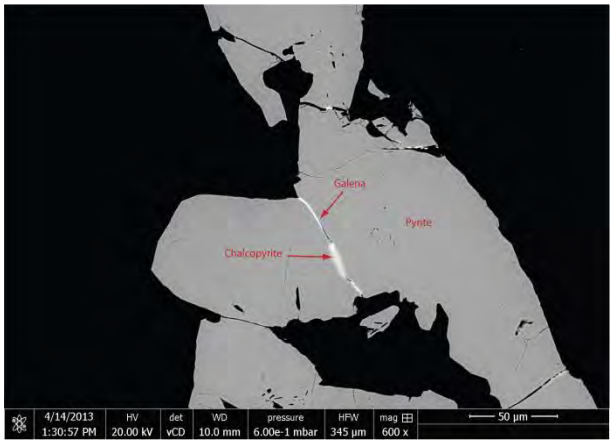

Figure 19. *Composite grain of pyrite, chalcopyrite and galena (sample ST42).*

Sillimanite zone

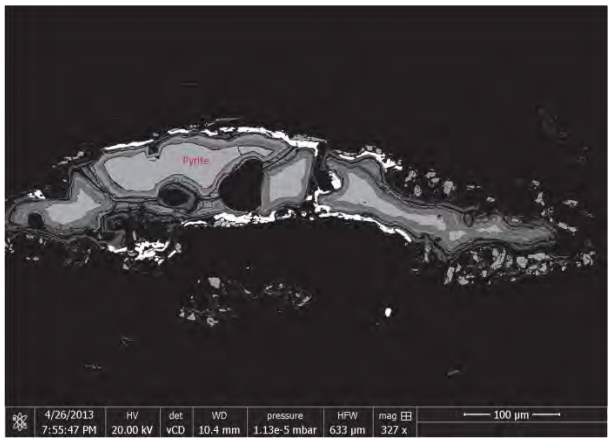

Figure 20. *Pyrite with abundant oxidation surrounded by minerals rich in REE (ST50).*

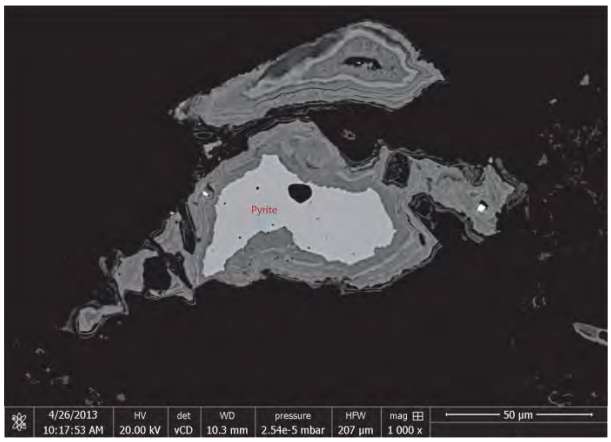

Figure 21. *Oxidized pyrite in sample ST50. The difference in brightness is due to varying proportions of Fe and O.*

Sulfide evolution with metamorphic grade - Stonehaven

The chlorite zone of Stonehaven is dominated by euhedral pyrite crystals (Figure 10-11) and pyrite-chalcopyrite composite grains (Figure 9). Pyrite grains are commonly euhedral showing signs of coalescence and two periods of growth where the second is identified by the mineral becoming more porous. Pyrrhotite, sphalerite, galena, cobaltite, gersdorffite and arsenian pyrite occur as small inclusions in pyrite and as isolated grains.

In the biotite zone coalescence of euhedral pyrite grains becomes more prominent (Figure 12, Figure 13). Pyrite is slightly more dominant as chalcopyrite drop drastically in abundance (Figure 36, Figure 39). Abundances of sphalerite, cobaltite and gersdorffite disappear completely while pyrrhotite, Galena and arsenian pyrite decrease in abundance (Figure 39).

The garnet zone samples retain similarities with the lower grade rocks but become less euhedral and more irregular in shape forming composite grains with more complex and diverse sulfide mineralogy. Pyrite is still dominant but decreases slightly while pyrrhotite and chalcopyrite increase in abundance. Sphalerite and cobaltite reemerges while cobaltpentlandite and pentlandite are introduced (Figure 39). A breakdown of pyrite is observed which in places yield a signal similar to pyrrhotite but mostly are chemically composed as pyrite with minor addition of As and Ni (Figure 14). Coalescence is observed as well as porous secondary pyrite growth (Figure 15).

Staurolite samples are dominated by pyrite but show a slight increase in pyrrhotite content (to represent 7-11%) and all sulfides adopt a more rounded crystal habit (Figures 16-19). Pyrite, pyrrhotite and chalcopyrite exist together as rounded composite grains where the first two sulfides increases in abundance and the last decrease relative to the garnet zone (Figure 16-19). Galena and cobaltpentlandite increase slightly in abundance while cobaltite and pentlandite decrease. Sphalerite remains unchanged and a small amount of coboltoan pyrite is introduced. Galena is observed precipitated in cracks of pyrite (Figure 19)

In the Sillimanite zone only two sulfides are present: pyrite and chalcopyrite. Irregularly shaped pyrite is dominant, and heavily oxidized (Figure 20, Figure 21) while chalcopyrite occur in small abundances in association with thorium aggregates.

iii. Loch Lomond - Sulfide mineralogy and SEM analysis

Chlorite zone

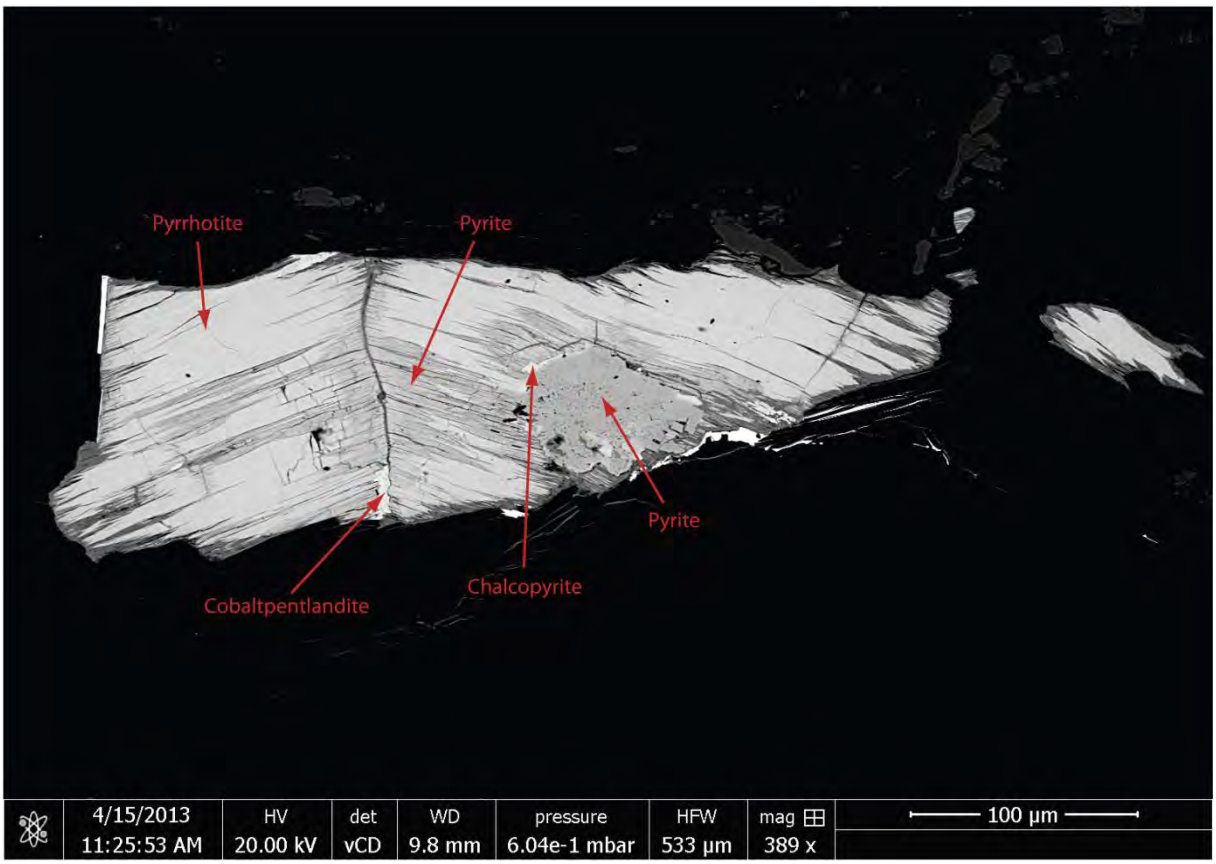

Figure 22. *Composite grain of pyrite, pyrrhotite, cobaltpentlandite and chalcopyrite in sample LL19B.*

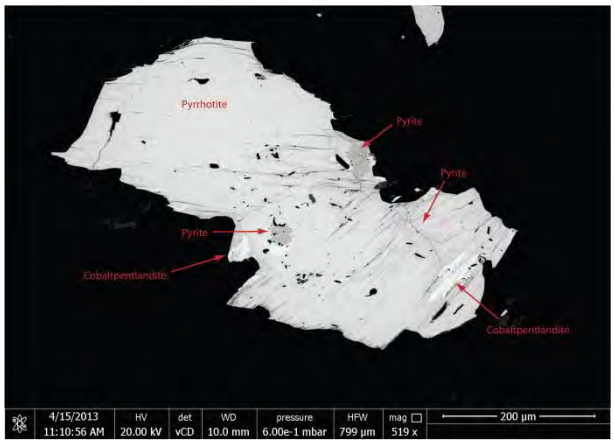

Figure 23. *Same type of composite grain as in Figure 22 but with less alteration of pyrite to pyrrhotite (LL19B).*

Figure 24. *Pyrite grain with porous secondary growth in sample LL25.*

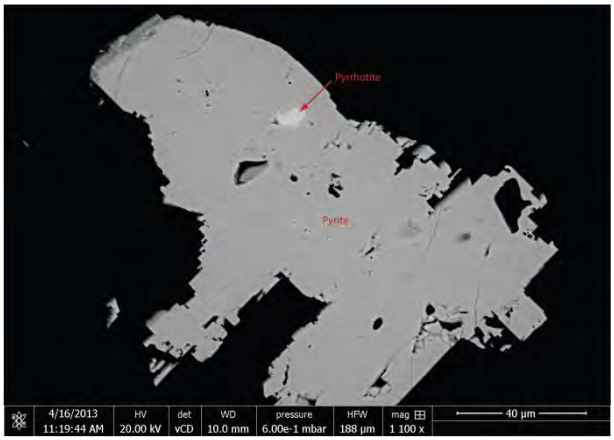

Figure 25. *Composite grain of euhedral pyrite with an inclusion of pyrrhotite (sample LL25).*

Biotite zone

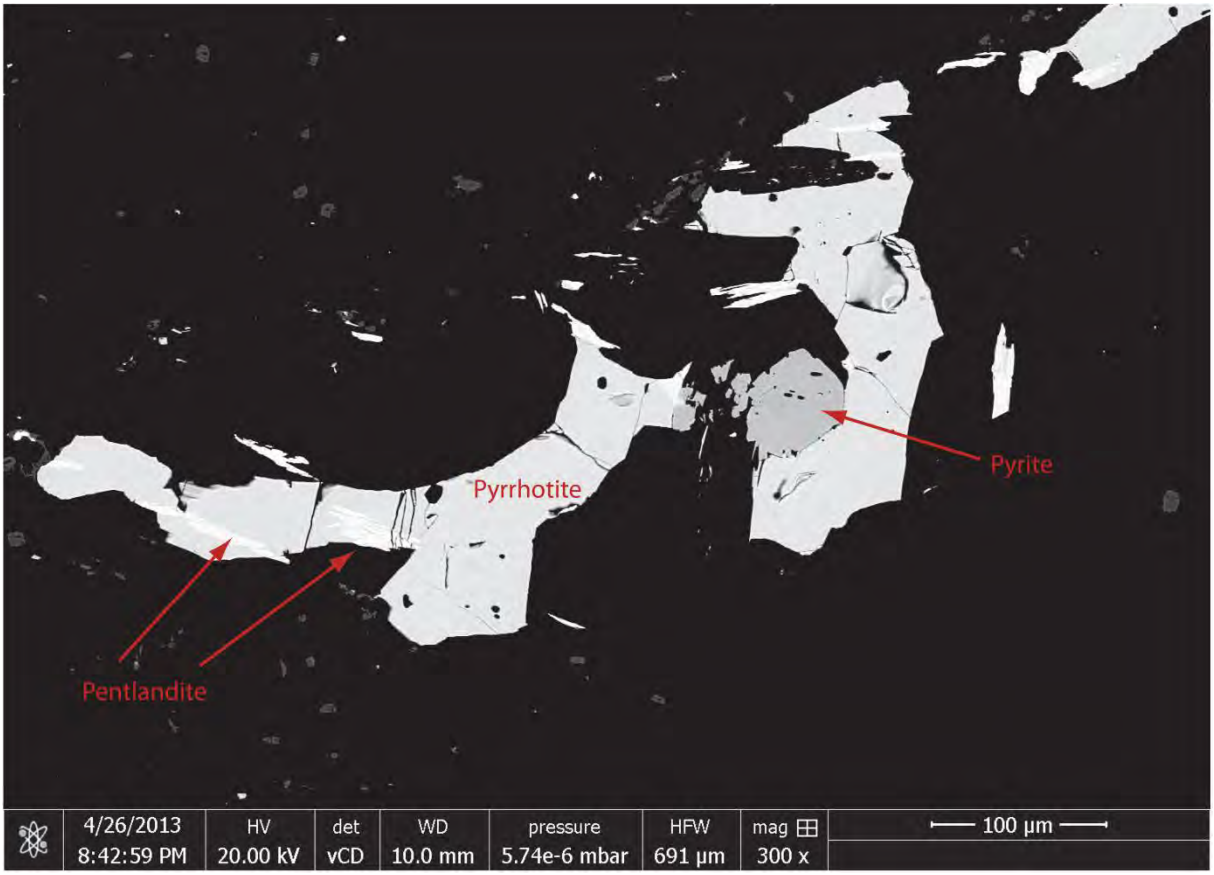

Figure 26. *Composite grain of pyrrhotite and pyrite with pentlandite lamellae (sample LL10).*

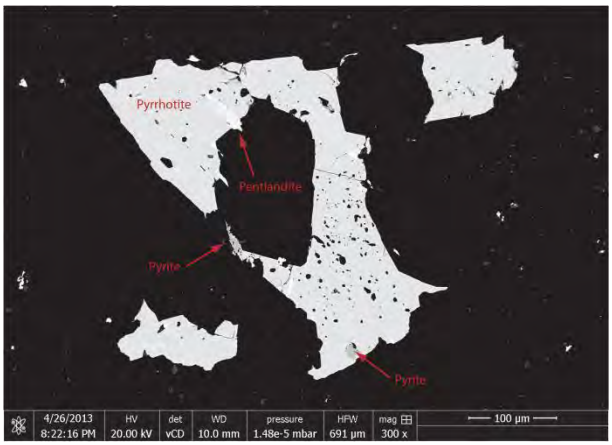

Figure 27. *Same type of composite grain as in Figure 26 but with porous pyrrhotite (LL10).*

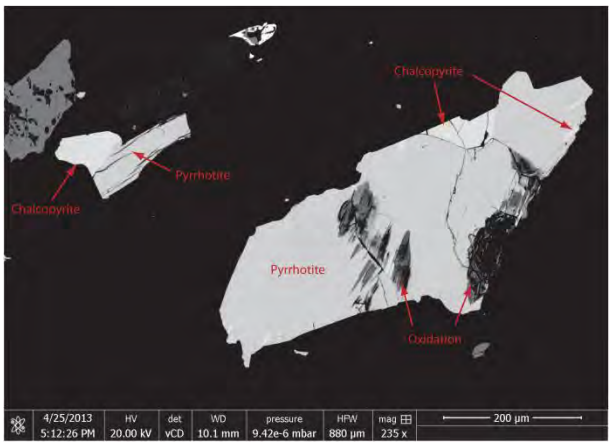

Figure 28. *Composite grain of pyrrhotite and chalcopyrite with oxidation on the sample surface (LL1).*

Figure 29. *Pyrrhotite with an inclusion of chalcopyrite from sample LL1.*

Garnet zone

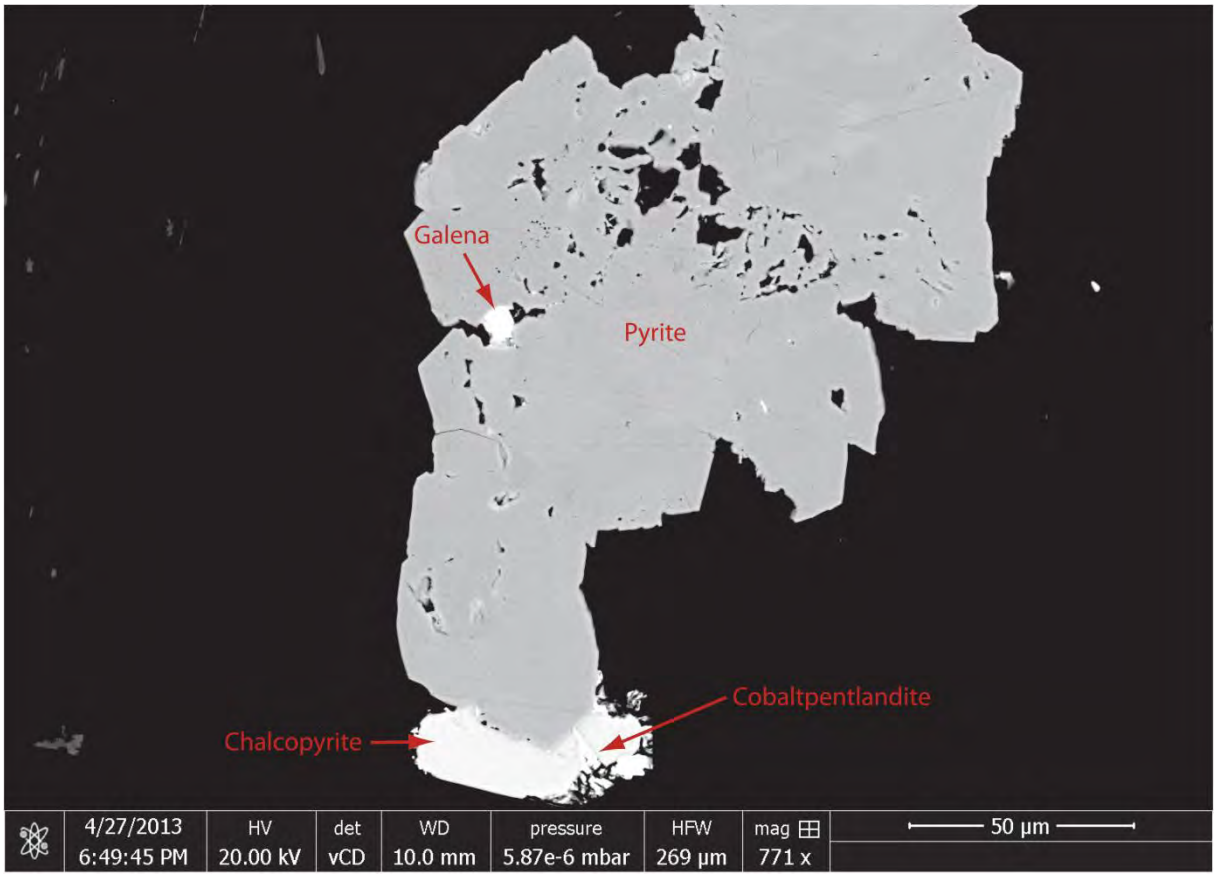

Figure 30. *Composite grain of pyrite, chalcopyrite, cobaltpentlandite and galena (sample LL34).*

Figure 31. *Pyrite with porous growth (LL34).*

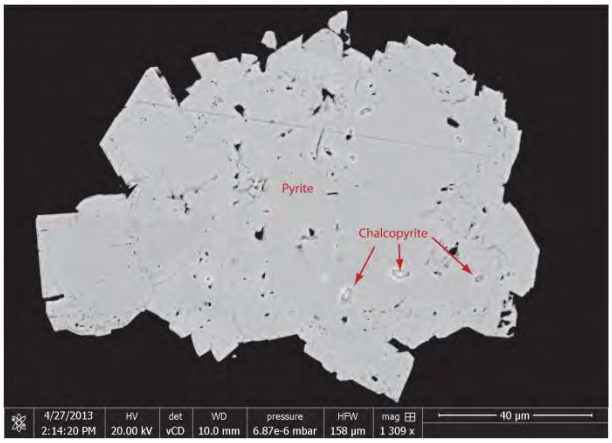

Figure 32. *Composite grain of pyrite with chalcopyrite in sample LL32.*

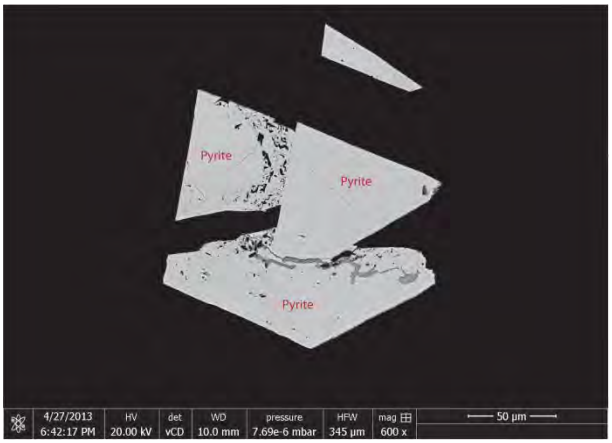

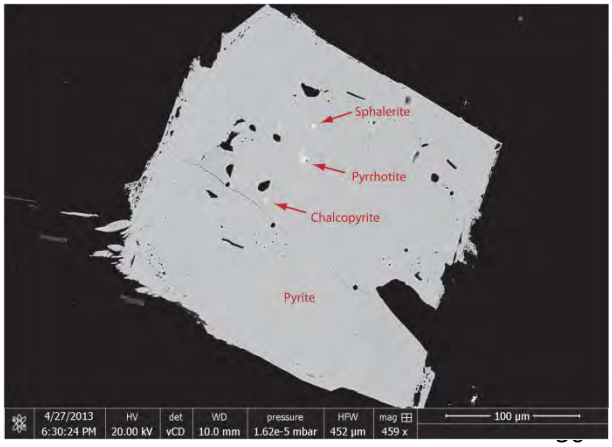

Figure 33. *Collision of euhedral pyrite grains resulting in porous secondary pyrite growth (LL34).*

Figure 34. *Composite grain with pyrite, sphalerite pyrrhotite and chalcopyrite in sample LL34.*

Sulfide evolution with metamorphic grade - Loch Lomond

The chlorite zone of Loch Lomond includes two samples with very different sulfide assemblages, one semi-pelite (LL19B) and one psammite (LL25). In LL19B pyrrhotite is the most abundant sulfide (Figure 37) and represents around 80% of the total sulfide abundance. The majority of the other sulfide minerals are pyrite and pentlandite with minor amounts of chalcopyrite, galena, arsenian pyrite, cobaltpentlandite, and coboltoan pyrite. Pyrrhotite occurs in composite grains with pyrite, pentlandite and chalcopyrite. Pyrite occurs in two modes, the first as medium-size rounded inclusions inside pyrrhotite and the second as mineralization along pyrrhotite cleavage (Figure 22, Figure 23). Pentlandite and cobaltpentlandite are abundant sulfides occurring as lamellae in pyrrhotite cleavage. Galena, coboltoan pyrite and arsenian pyrite are found as isolated grains. In LL25 pyrite is the most abundant sulfide at 85%. Coalescence is seen in pyrite (Figure 24) as well as a special type of intergrowth of euhedral pyrite (Figure 25). Other sulfides occurring in the form of small inclusions and as isolated grains are pyrrhotite, chalcopyrite, sphalerite, galena, cobaltite, gersdorffite, arsenian pyrite, cobaltpentlandite, pentlandite and cobaltoan pyrite.

The biotite zone samples are similar to the chlorite zone sample LL19B. Pyrrhotite is the dominant sulfide (Figure 37) and it occurs in composite grains together with pentlandite, chalcopyrite and pyrite. As in the chlorite zone, pyrrhotite commonly has medium sized inclusions of pyrite and also incorporates other minerals as lamellae textures (Figure 26-27). In the biotite zone however, pentlandite and chalcopyrite are more abundant as lamellae textures than cobaltpentlandite. Cobaltpentlandite and chalcopyrite increase in abundance while sphalerite, galena, cobaltite and pentlandite decrease and gersdorffite disappears completely (Figure 38).

In garnet zone samples pyrite abruptly becomes the most abundant sulfide and grains adopt a more euhedral crystal habit. Coalescence of subhedral to euhedral pyrite grains is present (Figure 32, Figure 30, Figure 33), as well as secondary porous pyrite growth (Figures 31, Figure 34 Figure 33). Chalcopyrite and cobaltpentlandite continue to increase in abundance while most other sulfides become slightly less abundant or remains unchanged (Figure 38).

Sulfide abundances

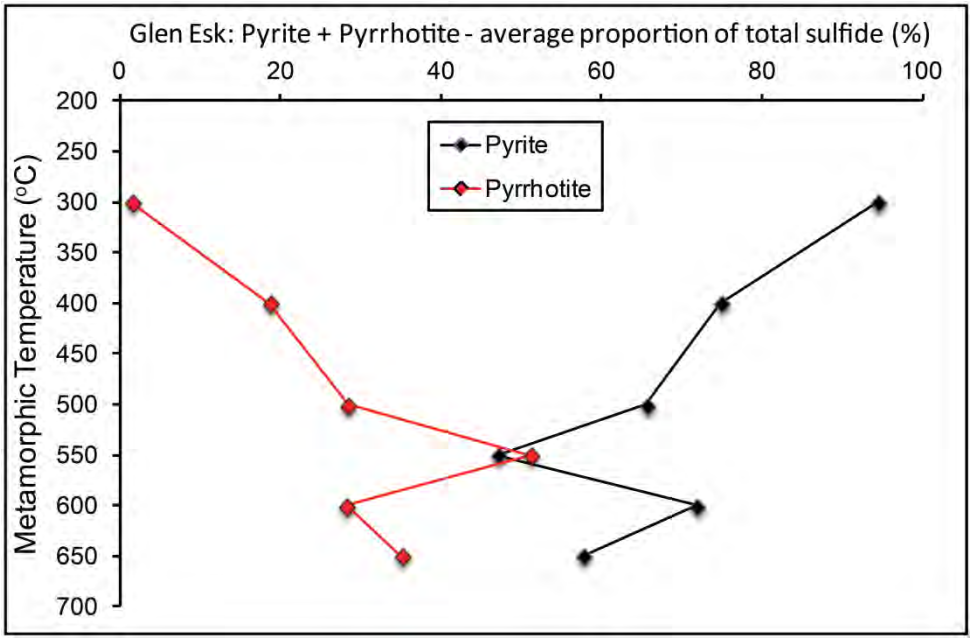

Figure 35. *Average values of each mineral isograd for proportion of total sulfide abundance between pyrite and pyrrhotite. Data taken from SEM scanning made by Dr. Iain Pitcairn on Glen Esk samples. Average values were taken from 3 samples in the chlorite zone (GE5, GE49, GE50), 5 in the biotite zone (GE8, GE9, GE12, GE14, GE18), 4 in the garnet zone (GE25, GE26, GE27, GE28), 2 in the staurolite zone (GE35, GE57), 2 in the kyanite zone (GE40, GE42) and 4 in the sillimanite zone (GE30, GE32, GE69, GE75)*

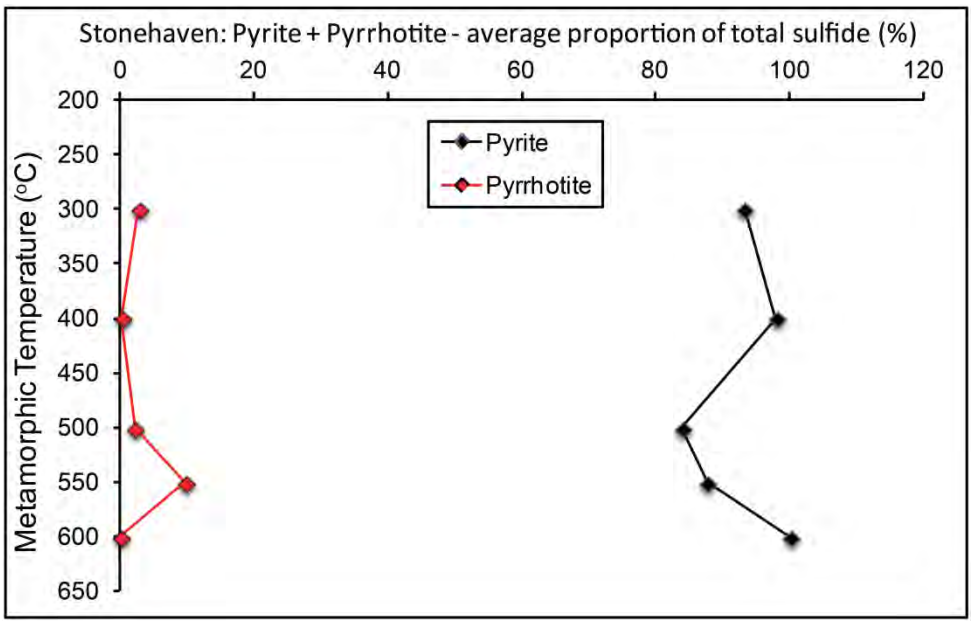

Figure 36. *Average values of each mineral isograd for proportion of total sulfide abundance between pyrite and pyrrhotite. Data taken from SEM scanning made in this study from Stonehaven samples.*

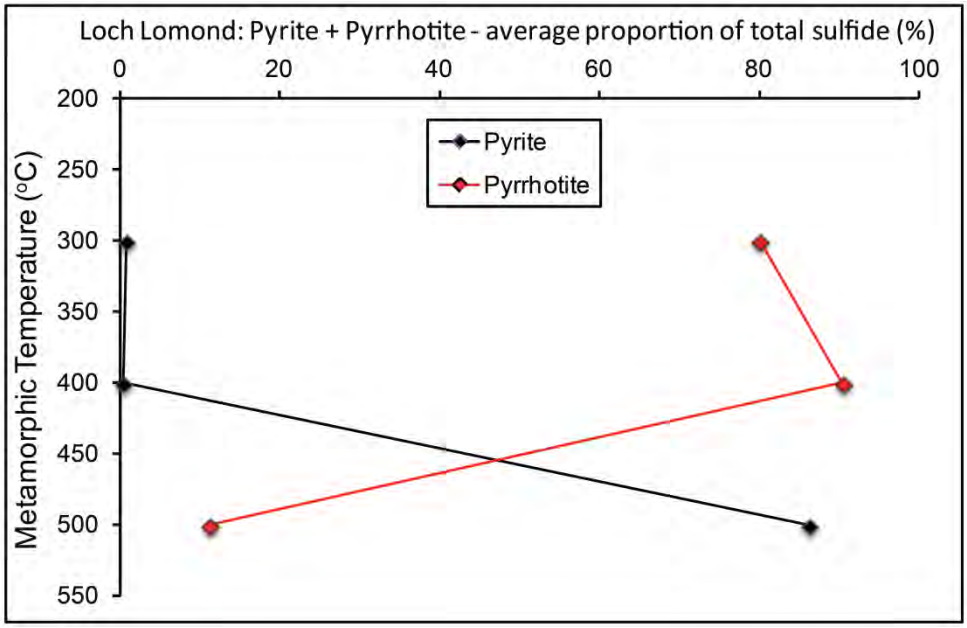

Figure 37. *Average values of each mineral isograd for proportion of total sulfide abundance between pyrite and pyrrhotite. Data taken from SEM scanning made in this study on Loch Lomond samples.*

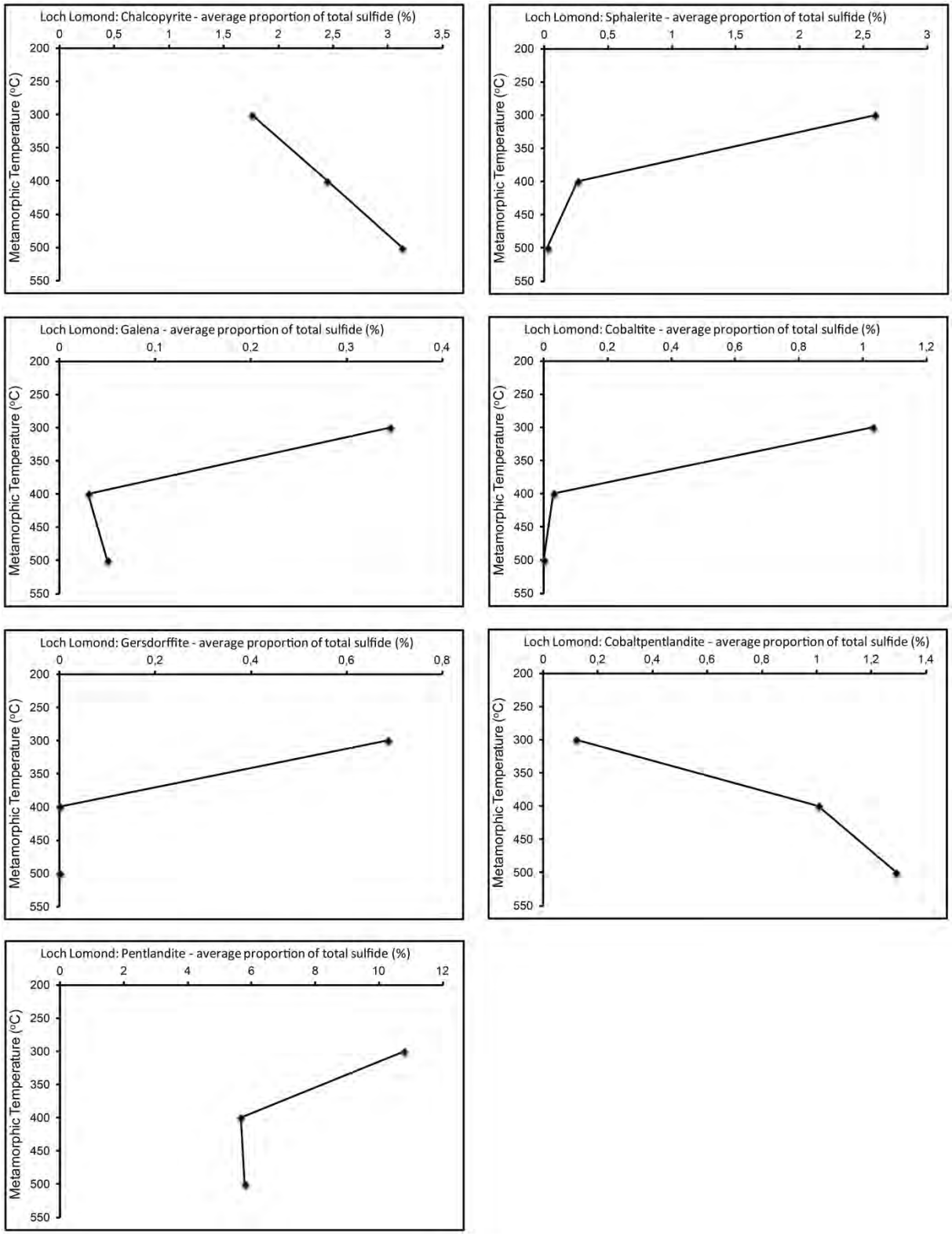

Figure 38. *Loch Lomond. Average values of each mineral isograd for proportion of total sulfide abundance for chalcopyrite, sphalerite, galena, cobaltite, gersdorffite, cobaltpentlandite and pentlandite.*

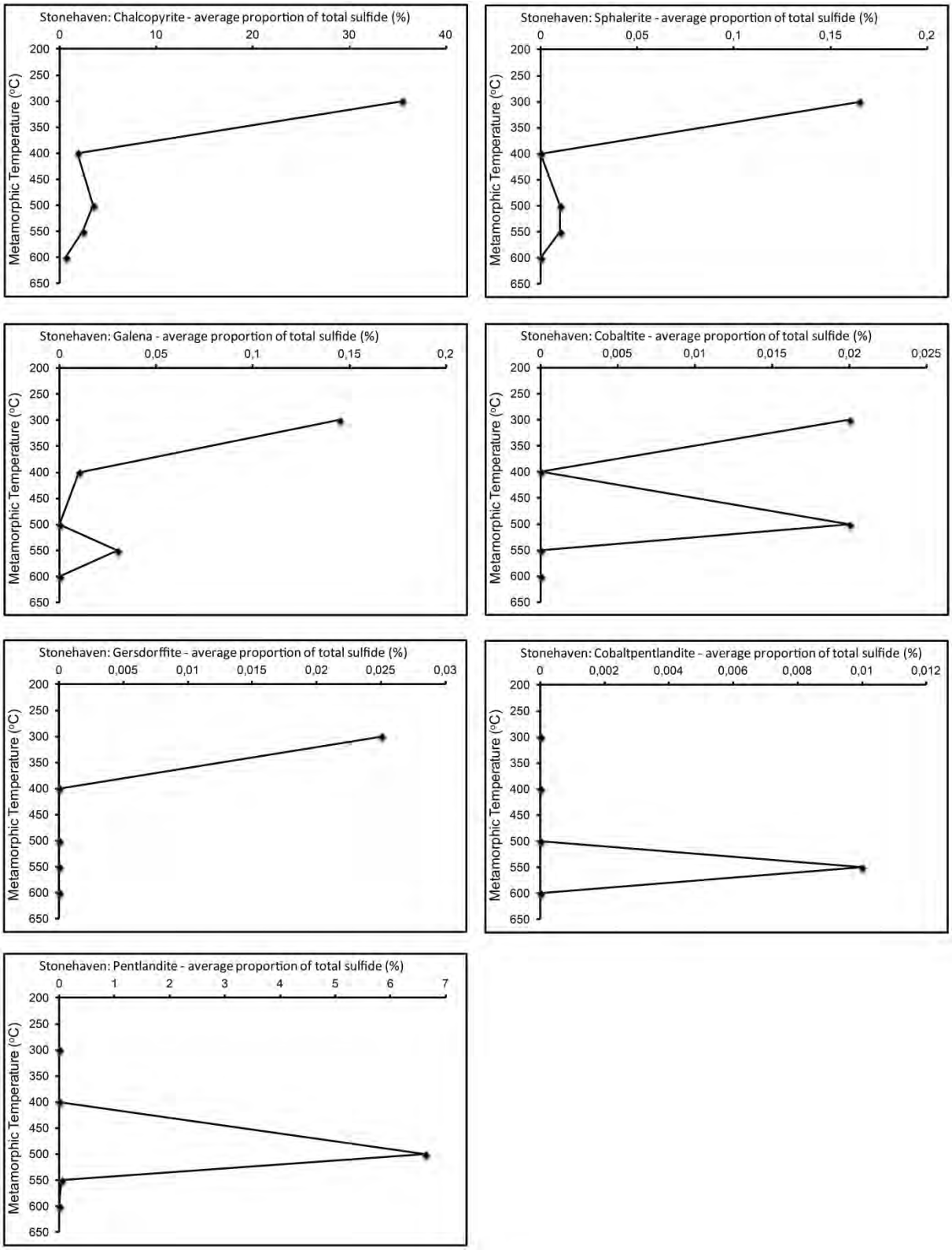

Figure 39. *Stonehaven. Average values of each mineral isograd for proportion of total sulfide abundance for chalcopyrite, sphalerite, galena, cobaltite, gersdorffite, cobaltpentlandite and pentlandite.*

iv. Whole rock analysis data

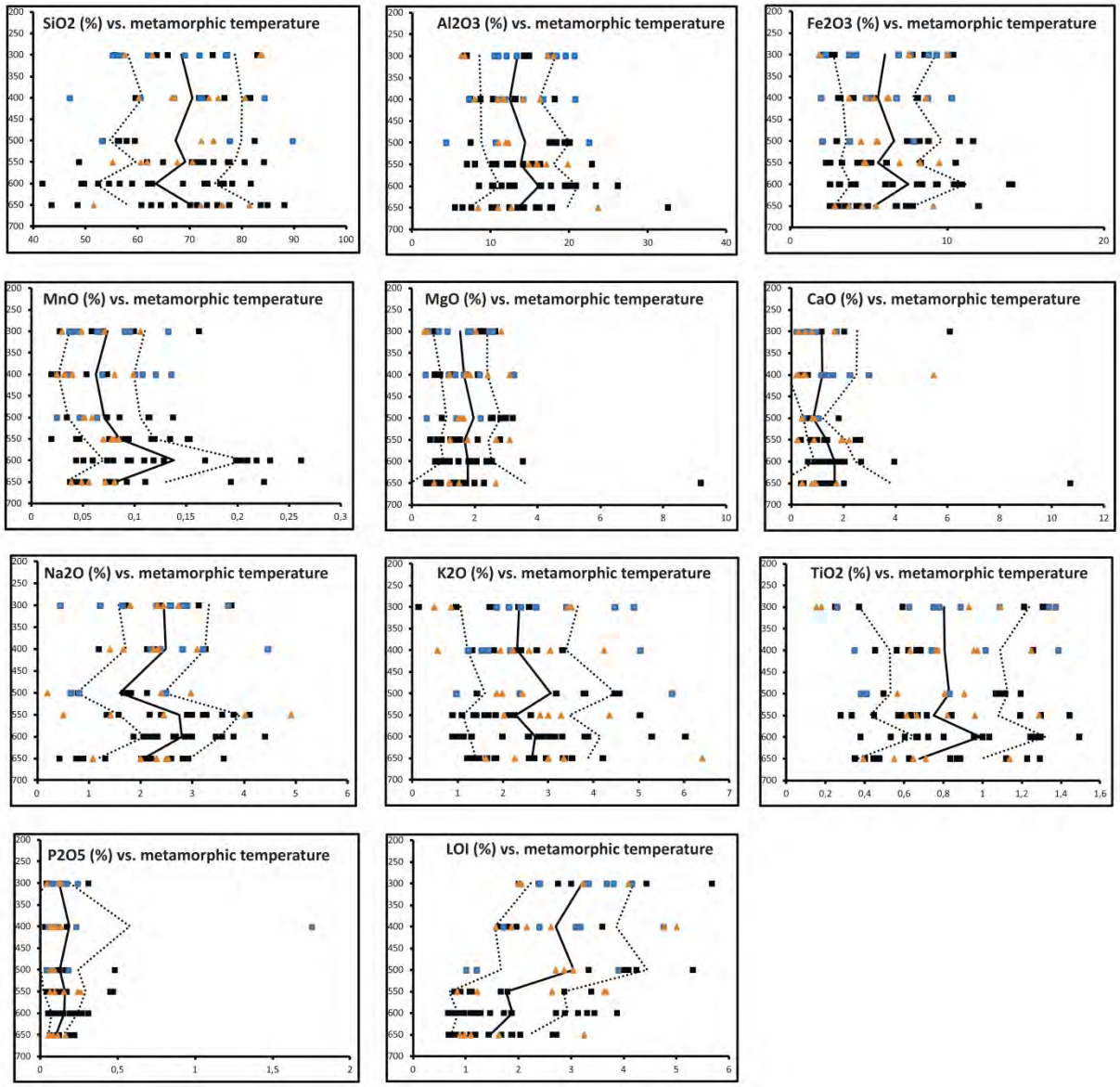

Figure 40. *Major and trace elemental trends for all localities. Black squares represent the samples from Glen Esk (all collections), the blue squares are data plotted from Loch Lomond and the orange triangles are samples from Stonehaven. The black line represents average concentrations for each mineral isograd and the dotted lines +-1 standard deviation. Extreme values in Glen Esk sillimanite zone MgO and CaO are represented by sample GE76. In the Loch Lomond biotite zone P2O5 values sample LL10 represent the extreme value.*

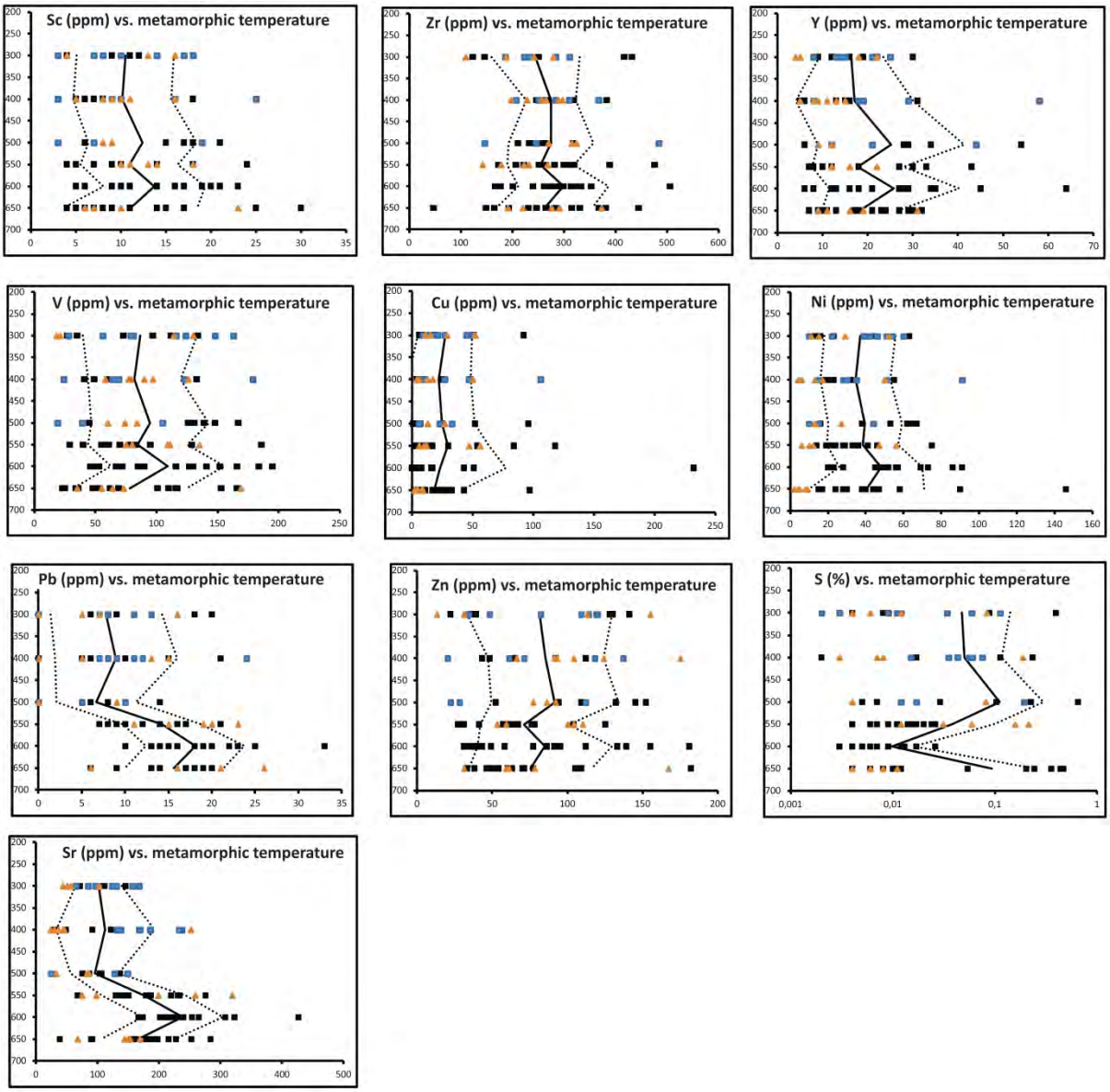

Figure 40 (continuation). *Major and trace elemental trends for all localities. Black squares represent the samples from Glen Esk (all collections), the blue squares are data plotted from Loch Lomond and the orange triangles are samples from Stonehaven. The black line represents average concentrations for each mineral isograd and the dotted lines +-1 standard deviation.*

Analyte symbol		SiO2	Al2O3	Fe2O3	MnO	MgO	CaO	Na2O	K2O	TiO2	P2O5	LOI	Total
Unit symbol		%	%	%	%	%	%	%	%	%	%	%	%
Detection limit		0.01	0.01	0.01	0.001	0.01	0.01	0.01	0.01	0.001	0.01	0.01	2
Analysis method		FUS-ICP	FUS-ICP	FUS-ICP	FUS-ICP	FUS-ICP	FUS-ICP	FUS-ICP	FUS-ICP	FUS-ICP	FUS-ICP	FUS-ICP	FUS-ICP
GE1	Staurolite	74.53	12.09	4.69	0.084	1.22	0.92	4.10	1.38	0.570	0.11	0.78	100.5
GE34	Staurolite	71.76	12.21	4.72	0.090	1.52	0.80	2.39	2.26	0.841	0.06	1.66	98.31
GE54*	Staurolite	71.30	14.16	5.15	0.075	1.39	1.30	3.20	1.84	0.669	0.08	1.79	100.9
GE39*	Kyanite	64.82	15.27	6.13	0.151	1.51	2.65	3.79	2.11	1.297	0.12	1.07	98.92
GE41	Kyanite	62.55	16.23	6.52	0.096	2.02	2.05	4.40	2.56	0.999	0.12	1.46	99.01
GE58*	Kyanite	41.68	26.19	13.97	0.231	2.03	0.64	2.05	6.03	1.492	0.27	3.87	98.45
GE60	Kyanite	52.37	20.22	10.57	0.198	3.52	1.49	2.85	3.31	1.257	0.15	3.44	99.38
GE61	Kyanite	76.52	10.20	3.15	0.073	0.73	1.90	2.99	0.99	0.531	0.05	0.77	97.90
GE31*	Sillimanite	71.30	13.79	3.50	0.044	1.62	1.65	3.60	2.69	0.455	0.06	0.88	99.60
GE66	Sillimanite	77.54	10.13	4.93	0.072	1.43	1.44	2.20	1.48	0.474	0.08	0.94	100.7
GE68	Sillimanite	43.45	32.58	12.00	0.193	1.68	0.97	0.78	4.21	1.227	0.12	2.03	99.24
GE71	Sillimanite	75.26	10.82	3.68	0.073	1.28	1.29	2.59	1.85	0.474	0.07	0.76	98.15
GE74*	Sillimanite	60.69	17.82	6.78	0.092	1.44	1.50	2.91	3.53	1.291	0.22	1.67	97.94
GE76*	Sillimanite	48.44	16.24	7.80	0.110	9.18	10.70	1.31	2.58	0.867	0.10	2.65	99.98
		SiO2	Al2O3	Fe2O3(T)	MnO	MgO	CaO	Na2O	K2O	TiO2	P2O5	LOI	Total
AE-GE1*	Staurolite	48,7	22,9	10,55	0,153	2,79	1,27	2,17	5,03	1,443	0,17	3,38	98,56
AE-GE7*	Staurolite	77,61	10,74	2,53	0,043	0,78	1	3,57	0,89	0,276	0,04	0,9	98,39
AE-GE8*	Staurolite	80,47	8,01	3,29	0,046	0,94	0,74	1,57	1,68	0,715	0,06	1,07	98,6
AE-GE5*	Kyanite	68,63	13,05	6,08	0,093	1,79	1,37	2,9	2,57	0,801	0,09	1,28	98,66
AE-GE6	Kyanite	61,96	16,25	8,09	0,218	1,93	1,57	2,63	2,79	0,955	0,26	1,87	98,53
AE-GE9	Kyanite	78,1	10,36	2,53	0,043	0,85	1,22	3,57	0,89	0,377	0,11	0,66	98,72
AE-GE10	Kyanite	73,36	12,61	3,89	0,059	1,19	1,8	3,45	1,31	0,603	0,07	0,85	99,19
AE-GE11*	Kyanite	54,49	19,45	10,45	0,203	2,54	0,89	2,27	3,81	1,271	0,25	3,3	98,93
AE-GE12*	Kyanite	49,68	23,41	10,95	0,168	1,47	0,93	1,86	5,29	1,295	0,25	3,13	98,44
AE-GE13*	Kyanite	58,89	17,7	9,32	0,261	2,05	1,08	2,68	2,87	1,275	0,22	2,88	99,23
AE-GE4*	Sillimanite	67,07	14,26	7,39	0,225	1,72	1,37	2,01	2,66	0,834	0,12	2,72	100,4

Analyte symbol		Ba	Sr	Y	Sc	Zr	V	Cu	Ni	Pb	Zn	S
Unit symbol		ppm	ppm	ppm	ppm	ppm	ppm	ppm	ppm	ppm	ppm	%
Detection limit		2	1	1	2	1	0.5	1	5		1	0.001
Analysis method		FUS-ICP	FUS-ICP	FUS-ICP	FUS-ICP	FUS-ICP	FUS-ICP	TD-ICP	TD-ICP	TD-ICP	TD-ICP	TD-ICP
GE1	Staurolite	328	151	12	9	307	78	30	35	7	61	0.011
GE34	Staurolite	582	144	10	9	282	83	2	36	10	76	0.007
GE54*	Staurolite	440	234	18	9	389	70	54	33	17	64	0.024
GE39*	Kyanite	714	276	33	14	476	95	9	41	21	78	0.020
GE41	Kyanite	625	308	16	11	293	85	17	49	16	94	0.013
GE58*	Kyanite	912	167	34	23	353	166	1	73	23	139	0.004
GE60	Kyanite	654	219	27	20	314	129	<1	91	20	181	0.009
GE61	Kyanite	346	254	13	6	299	48	1	21	13	39	0.012
GE31*	Sillimanite	647	216	21	7	231	51	24	24	17	50	0.355
GE66	Sillimanite	350	182	17	8	149	62	8	38	18	71	0.010
GE68	Sillimanite	1042	90	29	25	193	153	97	90	18	182	0.438
GE71	Sillimanite	280	155	9	5	266	52	10	28	20	107	0.012
GE74*	Sillimanite	783	192	32	14	445	117	17	44	19	77	0.011
GE76*	Sillimanite	160	284	11	30	47		27	146	6	54	0.202
		Ba	Sr	Y	Sc	Zr	V	Cu	Ni	Pb	Zn	S
AE-GE1*	Staurolite	1399	220	43	24	252	186	118	75	8	125	0,015
AE-GE7*	Staurolite	369	179	7	5	173	40	7	19	14	31	0,007
AE-GE8*	Staurolite	526	136	8	5	265	61	2	21	9	41	0,004
AE-GE5*	Kyanite	599	231	12	10	167	90	7	45	13	86	0,006
AE-GE6	Kyanite	563	235	28	14	319	116	1	47	25	95	0,009
AE-GE9	Kyanite	254	174	8	5	177	46	5	23	15	31	0,007
AE-GE10	Kyanite	322	323	13	9	333	67	8	28	10	37	0,009
AE-GE11*	Kyanite	657	202	35	17	280	141	16	86	22	155	0,007
AE-GE12*	Kyanite	1059	205	28	19	262	195	17	56	18	49	0,017
AE-GE13*	Kyanite	425	224	35	16	272	130	3	57	20	133	0,005
AE-GE4*	Sillimanite	574	165	27	15	283	101	3	58	14	70	0,008

Table 2. *Whole rock major and trace element analysis for samples from the AE-GE and new GE collections. TD-ICP = Total Digestion - ICP FUS-ICP = Lithium Metaborate/Tetraborate Fusion – ICP. Highlighted samples with an asterisk were used for Gold and HG-AFS analysis.*

Analyte Symbol		SiO2	Al2O3	Fe2O3(T)	MnO	MgO	CaO	Na2O	K2O	TiO2	P2O5	LOI	Total
Unit Symbol		%	%	%	%	%	%	%	%	%	%	%	%
Detection Limit		0.01	0.01	0.01	0.001	0.01	0.01	0.01	0.01	0.001	0.01		0.01
Analysis Method		FUS-ICP	FUS-ICP	FUS-ICP	FUS-ICP	FUS-ICP	FUS-ICP	FUS-ICP	FUS-ICP	FUS-ICP	FUS-ICP	FUS-ICP	FUS-ICP
LL-19	Chlorite	68,98	13,3	7,63	0,063	1,86	0,54	1,21	2,13	0,778	0,12	3,28	99,89
LL-25	Chlorite	77,02	10,45	3,74	0,039	0,84	0,95	1,64	2,39	0,624	0,07	2,39	100,2
LL-1	Biotite	72,26	10,9	4,97	0,068	1,15	2,24	2,2	1,54	0,737	0,11	3,17	99,34
LL-10	Biotite	46,89	20,75	10,27	0,1	3,23	2,97	2,19	5,03	1,384	1,75	4,75	99,32
LL-32	Garnet	89,64	4,32	2,03	0,024	0,45	0,45	0,64	0,97	0,378	0,04	1,2	100,1
LL-34	Garnet	53,08	22,51	7,86	0,063	2,17	1,03	0,8	5,73	0,829	0,18	3,89	98,15
ST-3	Chlorite	83,4	6,68	1,81	0,029	0,48	0,8	2,31	0,85	0,151	0,04	1,99	98,54
ST-10	Biotite	60,14	16,27	8,61	0,08	3,09	0,54	1,66	4,23	1,246	0,13	5	101
ST-30*	Garnet	72,92	10,64	5,34	**0,103**	1,16	0,9	0,16	1,78	0,594	0,07	6,8	100,5
ST-32	Garnet	52,82	24,24	7,58	0,064	1,65	0,23	0,76	5,17	1,046	0,13	5,72	99,41
ST-39*	Staurolite	44,65	30,06	7,04	**0,104**	1,65	0,65	2,16	5,28	1,36	0,13	5,86	98,93
ST-42	Staurolite	55,13	19,8	9,48	0,08	3,09	0,87	1,41	4,35	1,285	0,26	3,66	99,41
ST-50	Sillimanite	73,93	11,35	4,5	0,057	1,12	1,64	2,24	1,99	0,534	0,28	1,26	98,9

Analyte Symbol		Ba	Sr	Y	Sc	Zr	V	Cu	Ni	Pb	Zn	S
Unit Symbol		ppm	ppm	ppm	ppm	ppm	ppm	ppm	ppm	ppm	ppm	%
Detection Limit		2	2	1	1	2	5	1	1	5	1	0.001
Analysis Method		FUS-ICP	FUS-ICP	FUS-ICP	FUS-ICP	FUS-ICP	FUS-ICP	TD-ICP	TD-ICP	TD-ICP	TD-ICP	TD-ICP
LL-19	Chlorite	456	97	21	10	311	81	21	42	< 5	109	0,059
LL-25	Chlorite	777	65	13	7	283	56	14	22	7	48	0,034
LL-1	Biotite	373	138	19	9	367	64	27	35	24	61	0,056
LL-10	Biotite	1199	233	58	25	251	179	106	91	8	137	0,06
LL-32	Garnet	250	25	12	3	484	19	6	10	5	22	0,017
LL-34	Garnet	1361	149	44	19	146	105	33	44	10	112	0,193
ST-3	Chlorite	214	57	4	4	109	18	15	13	16	31	0,083
ST-10	Biotite	863	37	15	16	257	126	50	54	13	175	0,187
ST-30*	Garnet	447	46	15	8	368	56	46	44	7	15	0,051
ST-32	Garnet	968	109	22	20	170	122	27	52	20	84	1,07
ST-39*	Staurolite	1532	137	34	26	218	152	50	68	21	57	0,178
ST-42	Staurolite	1287	98	22	18	232	135	47	64	23	104	0,157
ST-50	Sillimanite	405	125	18	8	177	58	36	25	15	58	0,05

Table 3. *Whole rock major and trace element analysis for samples from Loch Lomond and Stonehaven. Sample ST-30 and ST-39 high MnO values which may be a consequence of weathering. TD-ICP = Total Digestion - ICP FUS-ICP = Lithium Metaborate/Tetraborate Fusion – ICP. Highlighted samples with an asterisk were used for Gold and HG-AFS analysis.*

The elemental concentrations for the samples from the higher index mineral zones analyzed in this study are listed in Table 2. In the major elements SiO_2 content of the sample ranges from 80% to 43% with lower concentrations often associated with an increase of Al_2O_3 (32% - 8%), TiO_2 (1.4 - 0.2%) and Fe_2O_3. (13 - 2%). MgO and CaO values commonly range between 3.5 - 0.7% and 2.6 – 0.6% respectively but show high values in sample GE76 (9% and 10%). MnO ranges in between 0.26 – 0.04%, Na_2O between 4.4 - 0.7%, K_2O between 6.0 - 0.8% and P_2O_5 between 0.25 - 0.04%.

In the trace element data Pb and Sr range from 25-6 ppm and 323-90 ppm respectively while S ranges between 0.438 - 0.004%. Seen in the context of the full Dalradian elemental data set illustrated in figure 40 this is an increase in the staurolite and kyanite zones for Pb and Sr and a decrease of S in the kyanite zone. Other trace elements range from: Ba 1399 – 160ppm, Y 43 – 8 ppm, Sc 30 – 5 ppm, Zr 476 – 47, V 195 – 46 ppm, Ni 146 – 19, Cu 118 – 1 and Zn 182 – 31.

v. Gold analysis data

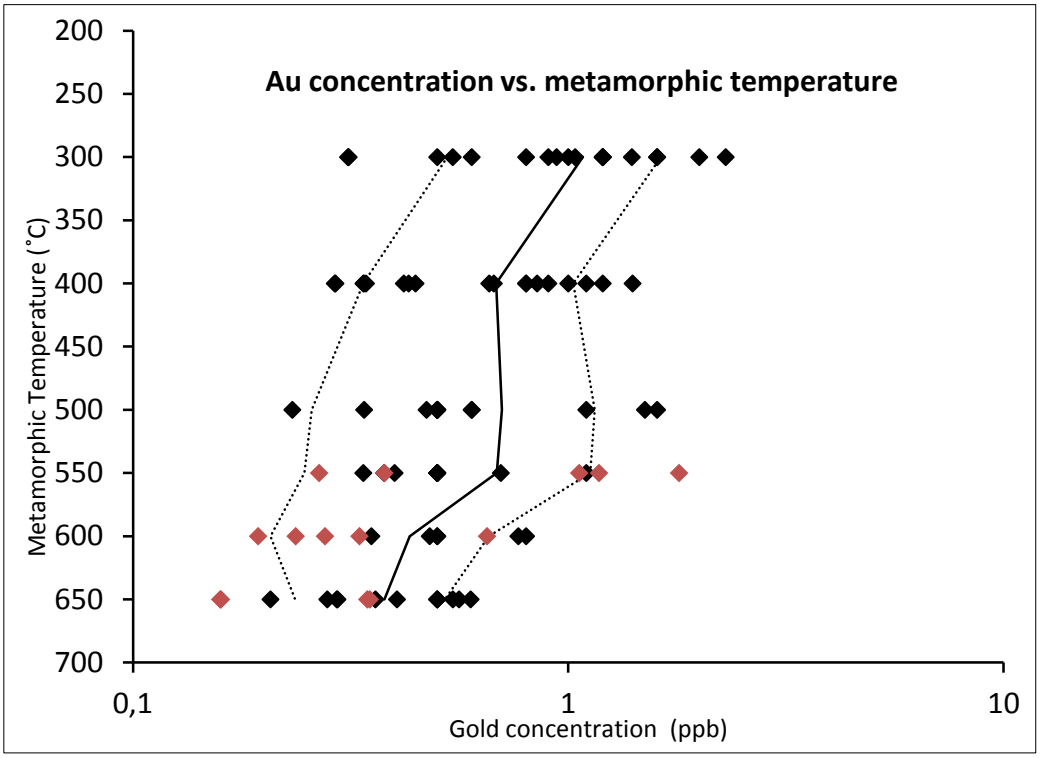

Figure 41. *Gold concentrations plotted against metamorphic temperature. Black points are from gold analysis made by Dr. Iain Pitcairn on samples from Glen Esk, Loch Lomond and Stonehaven. Red points represent samples from this study (AE-GE and the new GE collection, summarized in table 4). The black line represents average concentrations for each mineral isograd and the dotted lines +-1 standard deviation. Detection limit is 10ppt (Pitcairn et al. 2006b)*

vi. HG-AFS data

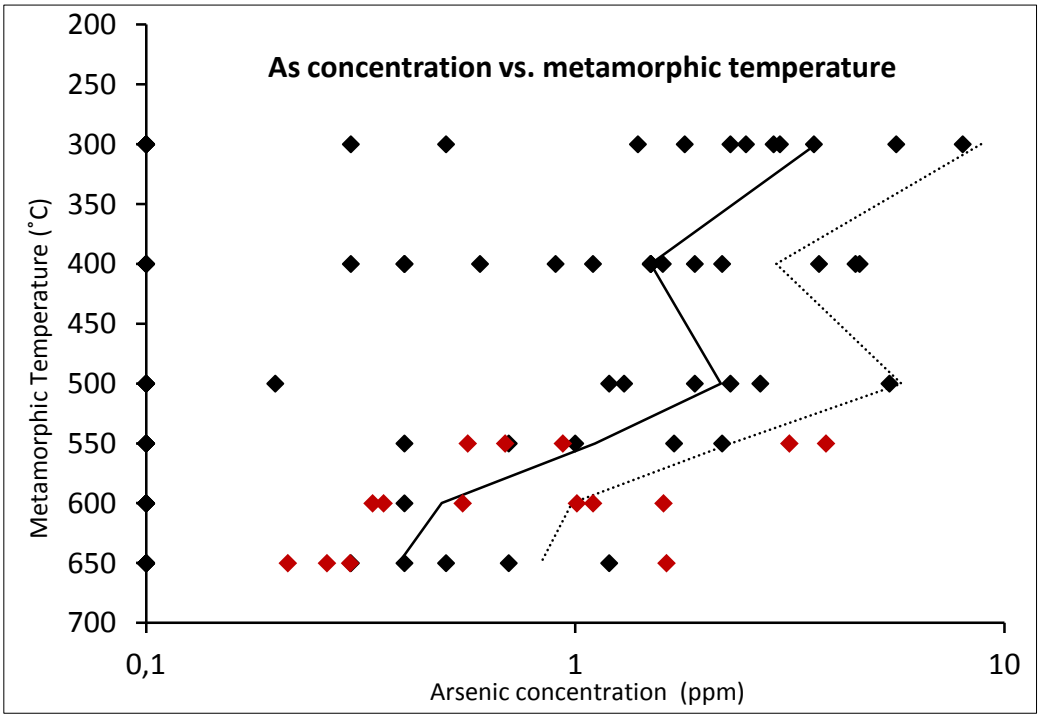

Figure 42. *Arsenic concentrations plotted against metamorphic temperature. Black points represent samples analyzed by Dr. Iain Pitcairn (Aqua Regia ICP-MS). Red points are values obtained from this study using HG-AFS analysis. The black line represents average concentrations for each mineral isograd and the dotted lines +-1 standard deviation. Detection limit is 10 ppt.*

Sample ID	Metamorphic temperature	Au (ppb)	As (ppm)
AE-GE1	Staurolite - 550	1,0594	0,9358
AE-GE7	Staurolite - 550	1,7969	3,8406
AE-GE8	Staurolite - 550	1,1764	0,5617
GE34	Staurolite - 550	0,2676	0,6866
GE54	Staurolite - 550	0,3781	3,1555
AE-GE5	Kyanite - 600	0,6506	0,3371
AE-GE11	Kyanite - 600	0,3313	0,3576
AE-GE12	Kyanite - 600	0,2761	1,6061
AE-GE13	Kyanite - 600	0,1938	1,1005
GE58	Kyanite - 600	0,0950	1,009
GE39	Kyanite - 600	0,2364	0,5467
AE-GE4	Sillimanite - 650	0,1586	0,2988
GE31	Sillimanite - 650	0,3453	0,2639
GE76	Sillimanite - 650	0,1592	1,632
GE74	Sillimanite - 650	0,3500	0,2139

Table 4. *Gold and Arsenic data for each sample presented in Figures 41 and 42.*

vii. Fluid inclusion study

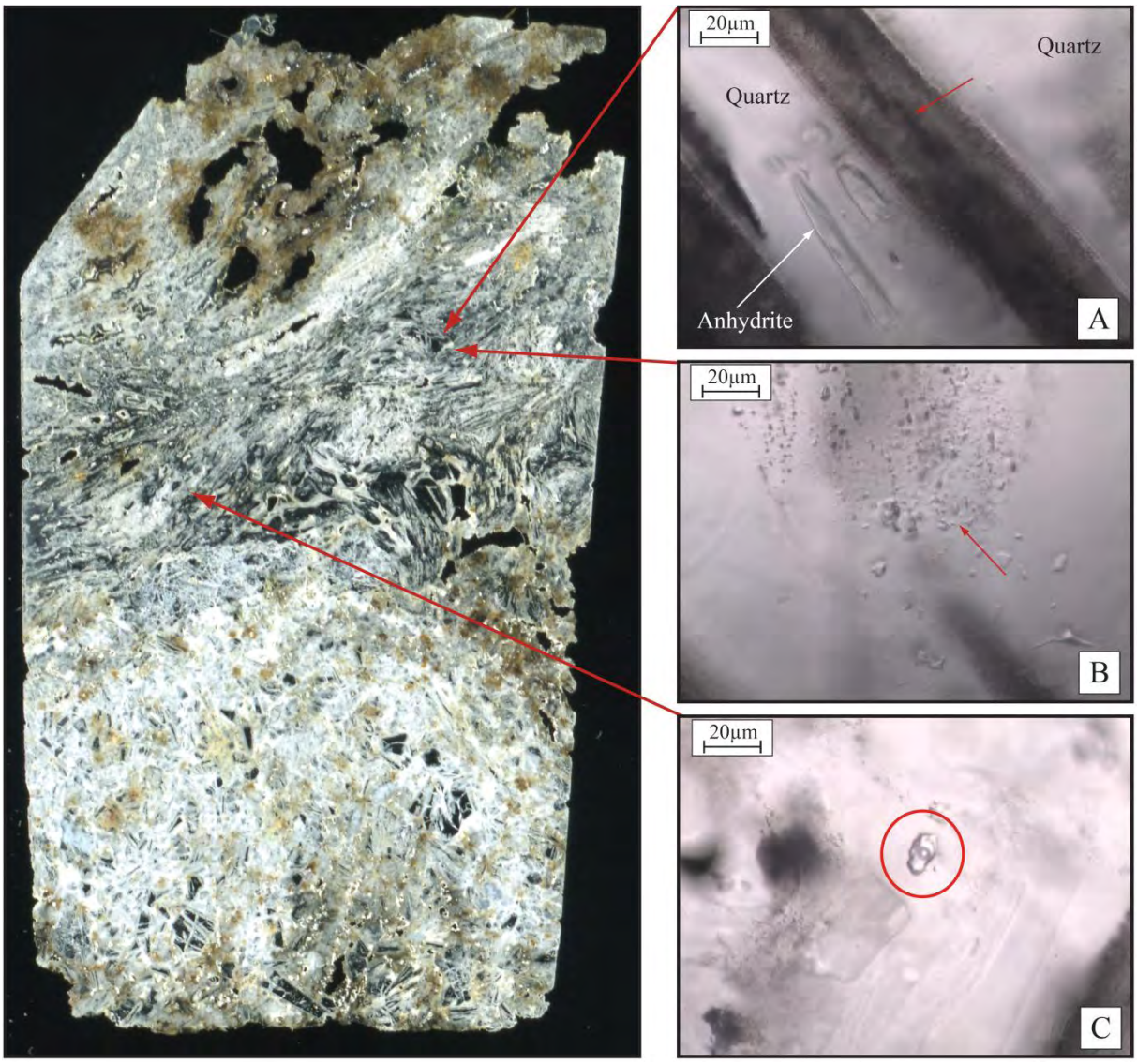

Figure 43. *Sample AE-GE2a, post-metamorphic vein of Hardhill (center)* ***A)*** *Mineral inclusions of anhydrite in quartz. Red arrow indicates border between two quartz grains. At the outer part of the quartz grain a growth zone displaying a "dirty" appearance consistent of boiling residue material can be observed.* ***B)*** *Small aqueous inclusions located at the edge of a growth zone in quartz.* ***C)*** *Large aqueous inclusion in the center of a quartz grain.*

The center of the Hardhill vein (Dip direction 010, Dip 90) consists of numerous small quartz crystals which are randomly orientated. The edges of the quartz grains are well defined and have a "dirty" appearance caused by a large amount of impurities (Figure 43-A and Figure 44). The quartz crystals often contain large inclusions of anhydrite ($CaSO_4$) which are incorporated into the crystal structure aligned along the border of the host mineral. Fluid inclusions are rare and exclusively aqueous in composition. They are found only in the quartz and occur either as large single inclusions towards the center of the grain (Figure 43-C) or smaller, more numerous at the edge (Figure 43-B). Small amounts of pyrite and sphalerite with oxidized rims are also found.

Homogenization temperatures are divided into two distinct groups with the first ranging from 78 °C to 80 °C (Figure 43-B) and the other from 140 °C to 300 °C (Figure 43-C). The low temperature group is the most abundant and has a salinity of approximately 20 weight % NaCl equivalent while the higher temperature group has a slightly lower salinity of 15 Wt % (Figure 64). Both types are calcic in composition (Melting temperature of ~ -56°C, Table 7).

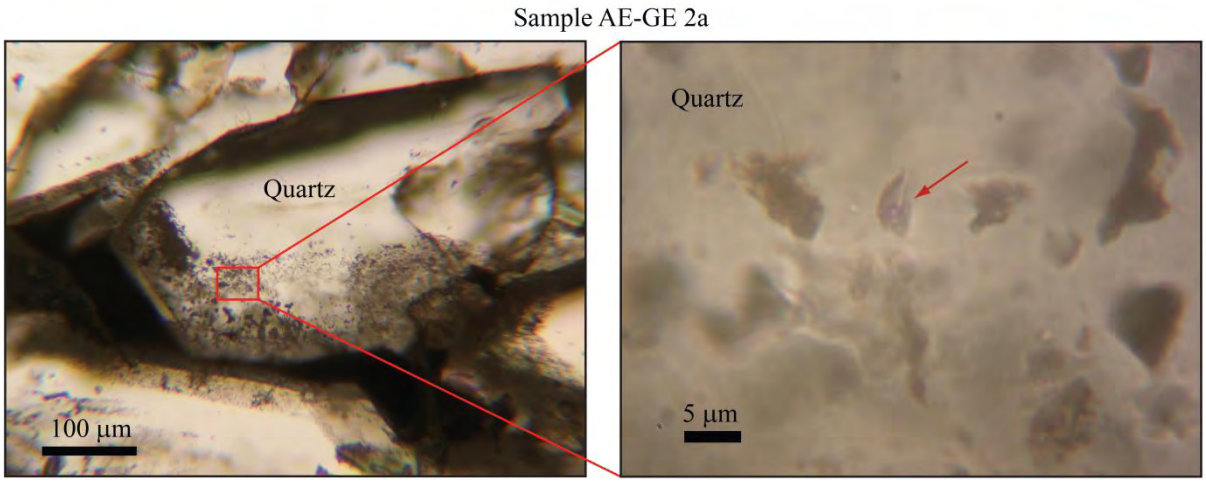

Figure 44. *An aqueous fluid inclusion in the "dirty" part of a quartz crystal in sample AE-GE2a.*

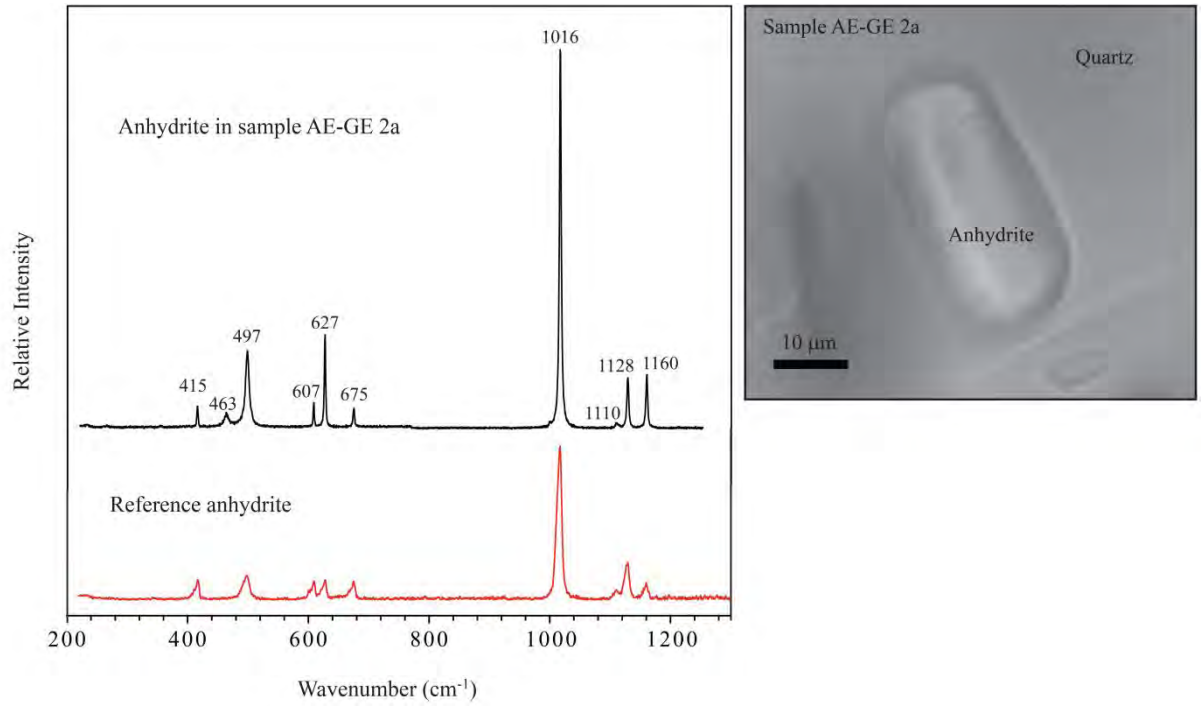

Figure 45. *Raman Spectrum of a white mineral in quartz (photo) identified as anhydrite (sample AE-GE2a). Reference spectrum from anhydrite $CaSO_4$ RRUFF ID: R061102.2 from the RRUFF™ project (Downs 2006).*

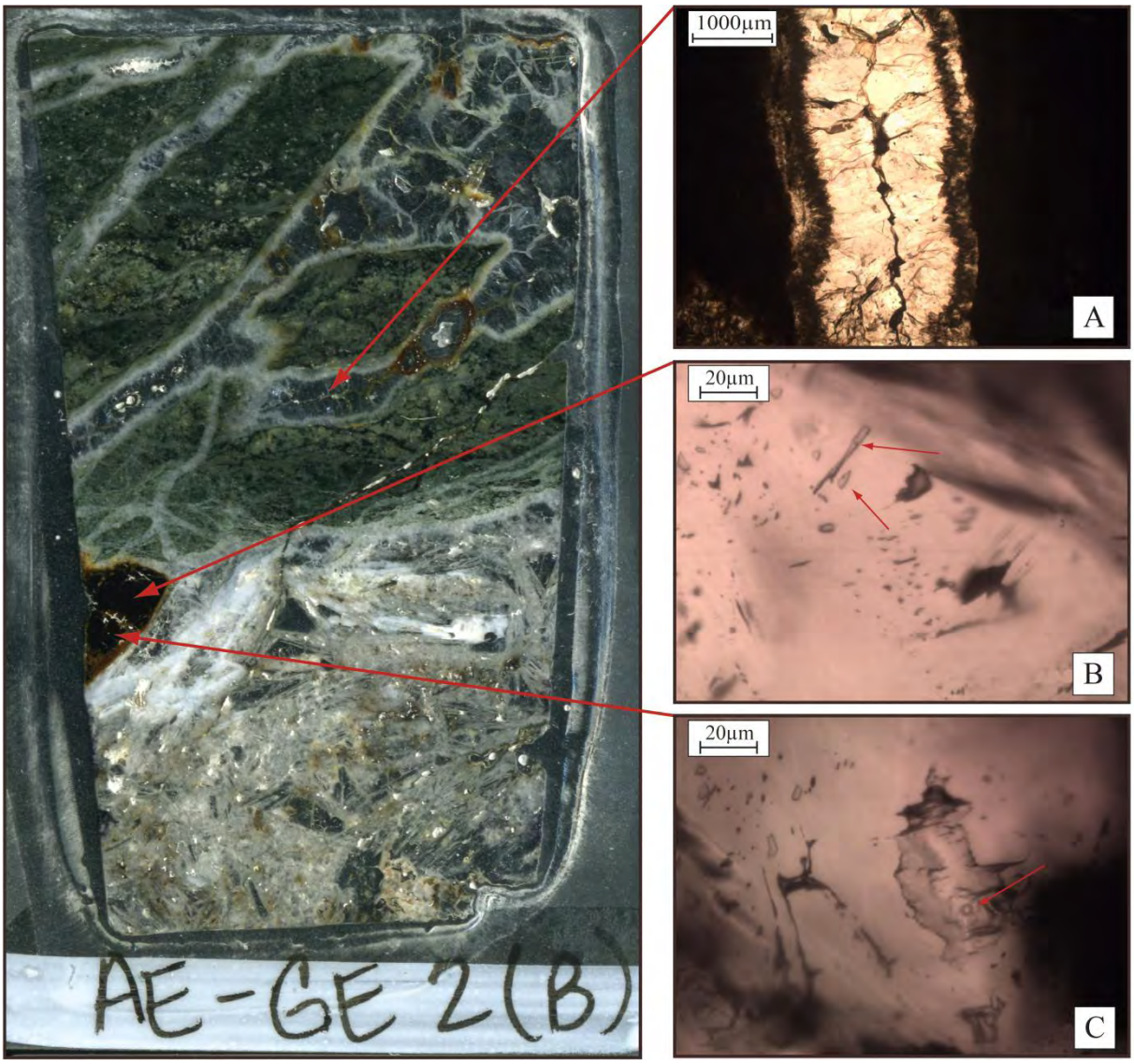

Figure 46. *Sample AE-GE2b, post-metamorphic vein of Hardhill (contact between vein and country rock)* ***A)*** *Exsolution reaction of two types of quartz healing cracks created by brecciation.* ***B)*** *Small aqueous inclusions in sphalerite.* ***C)*** *Large aqueous inclusion in sphalerite.*

The country rock (metasedimentary rock from the sillimanite zone) in contact with the vein has been brecciated and healed by two generations of quartz nucleating from the wall rock into the cracks (Figure 46-A). This reaction is also occurring in the center of the vein (sample AE-GE2a) but to a much lesser extent. At the contact between vein and country rock large crystals of sphalerite have precipitated. These contain two types of aqueous fluid inclusions, one large (30-75µm) type (Figure 46-C) and one smaller type (10-15µm, Figure 46-B) which are similar in composition. Minor amount of pyrite is also found close to the vein margin and inside of the wall rock.

Homogenization temperatures are exclusively from inside of sphalerite and range from 70 to 80 °C with a salinity of approximately 20 weight percent NaCl equivalent (Figure 65). Melting temperatures suggests a calcic composition (-56 to -60 °C).

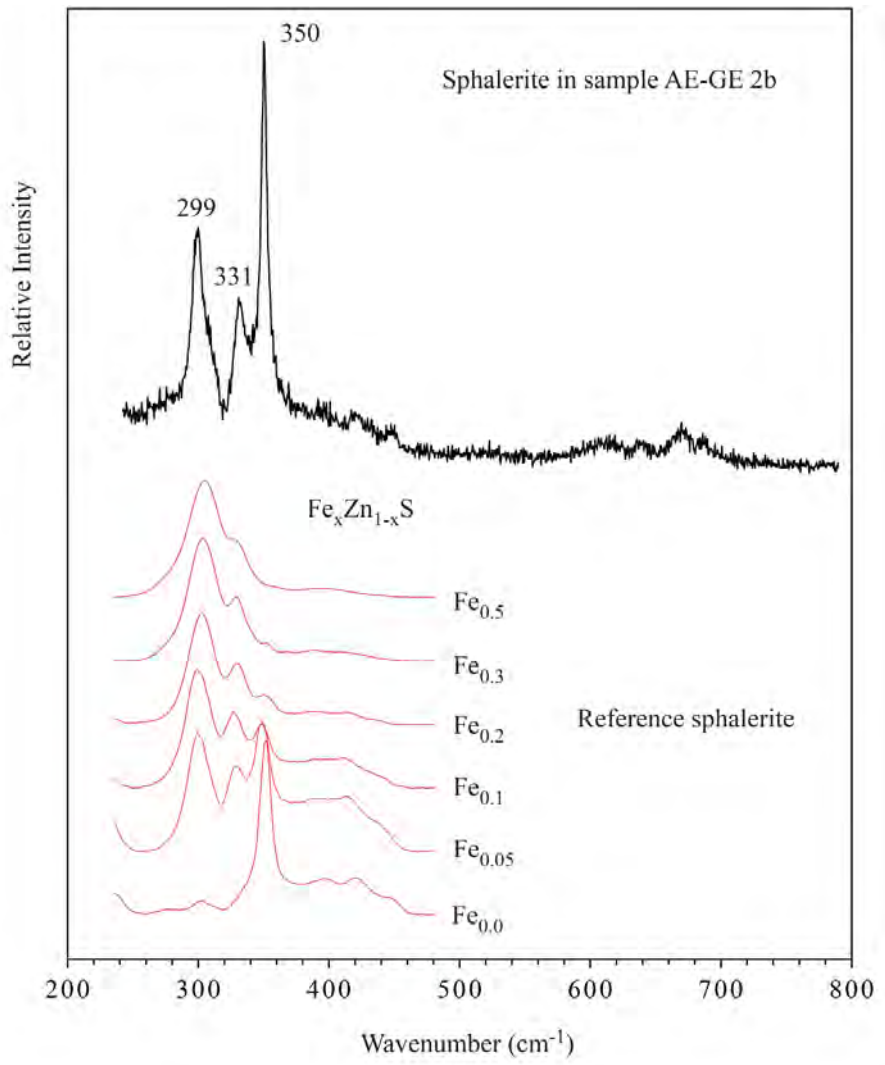

Figure 47. *Raman spectrum of sphalerite in sample AE-GE2b. Reference sphalerite shows the spectra of sphalerite with different Fe content (Osadchii and Gorbaty 2010). The spectrum of the analyzed sphalerite indicates a mole fraction of Fe = 0.05.*

Similar elemental proportions between Fe and S were also identified with SEM.

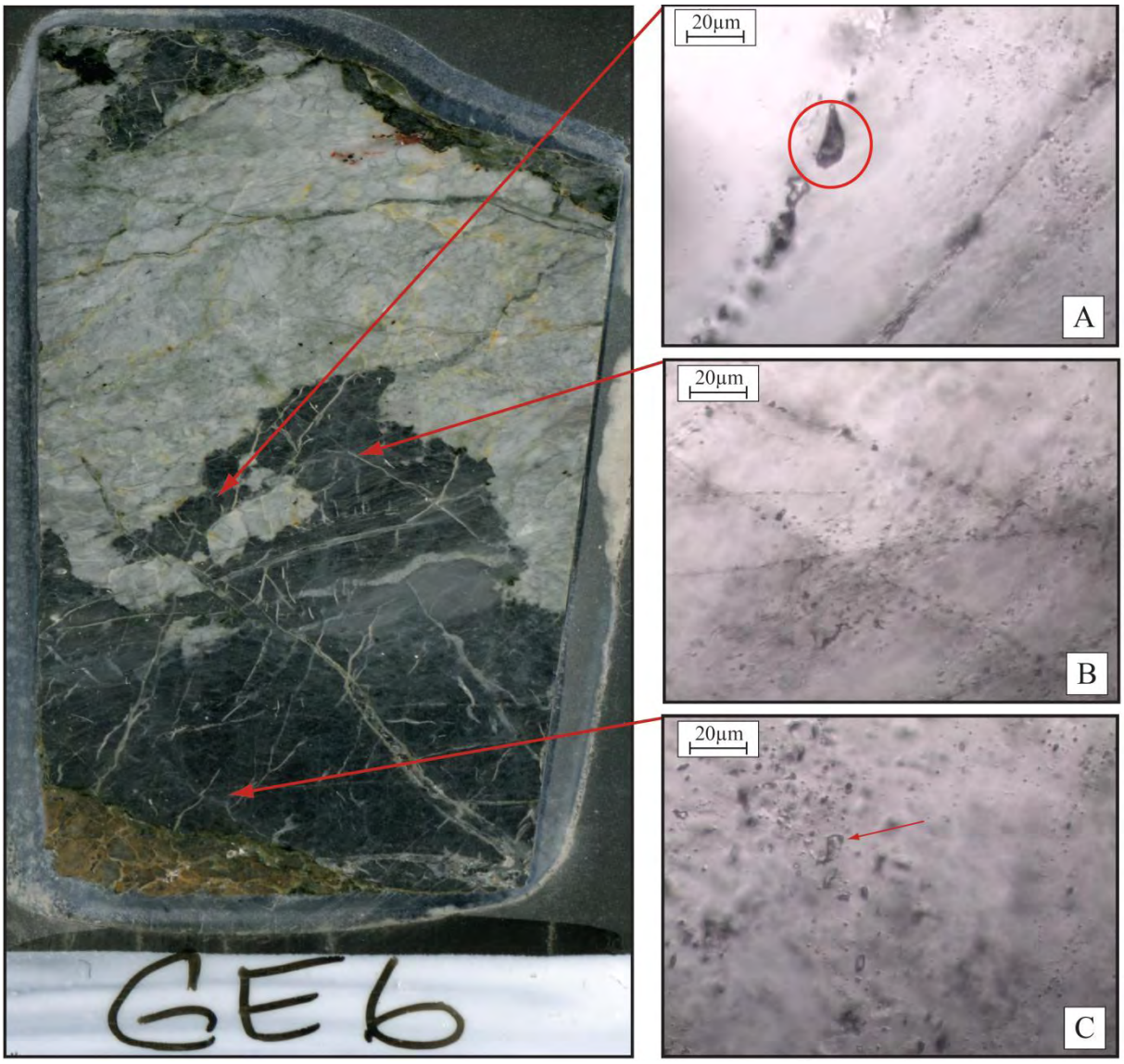

Figure 48. *Sample GE6, chlorite zone of Glen Esk* ***A)*** *Gas-rich fluid inclusion with N_2 and CH_4.* ***B)*** *Healed fractures are a common sight in the sample. Most fluid inclusions found in the fractures have either leaked or been destroyed.* ***C)*** *Small aqueous inclusions hosted by quartz.*

Quartz and calcite vein from the location of Dalbog. The vein is oriented along a foliation of 60°/340° and also contain chlorite and an unusual margin of albite (the latter found in the lower left corner of Figure 48 and confirmed by Raman spectroscopy). Fluid inclusions are rare in the quartz and almost non-existent in the calcite (Table 5-6). The thick section contains both Type I and Type II inclusions. Aqueos inclusions of the sample range between Type Ia-d while the gas-rich are only found as Type II-h. The Type II inclusions of GE6 are composed of N_2 and CH_4 and contain the only gas-rich inclusions analyzed in this study which have no trace of CO_2. The sample contain many healed fractures (Figure 48-B) and the vast majority of the fluid inclusions are found in these. Both the calcite and the albite contain abundant pyrite while the quartz contain no sulfides.

Homogenization temperatures seems to belong to a single group which range from 140 to 180 °C containing 10-13 weight percent NaCl equivalent (Figure 65). Melting temperatures give a $CaCl_2$ dominated composition for the salt system (-37 to -40 °C).

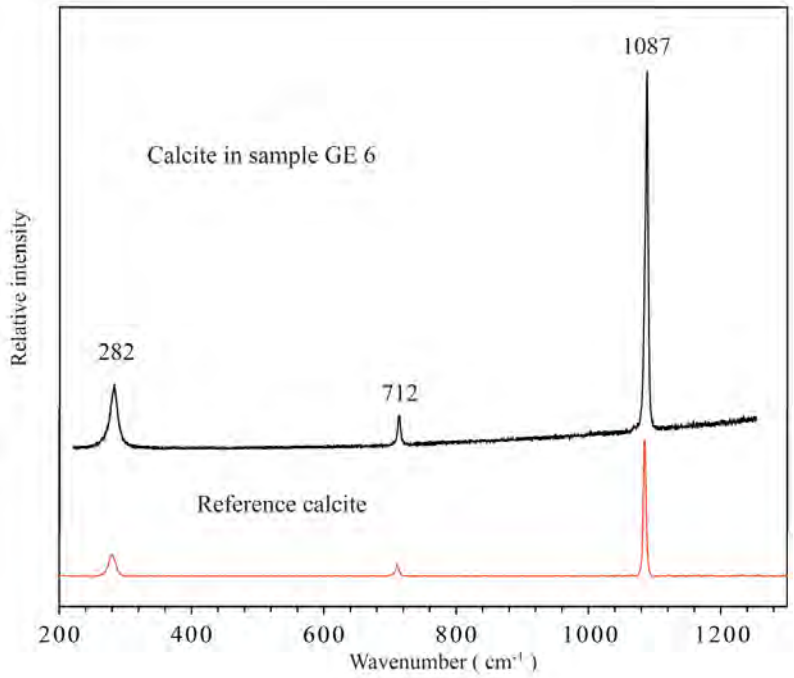

Figure 49. *Raman spectrum of a carbonate mineral (photo Figure 48) in the vein identified as calcite (sample GE6). Reference spectrum from calcite $CaCO_3$ RRUFF ID: R050128 from the RRUFF™ project (Downs 2006).*

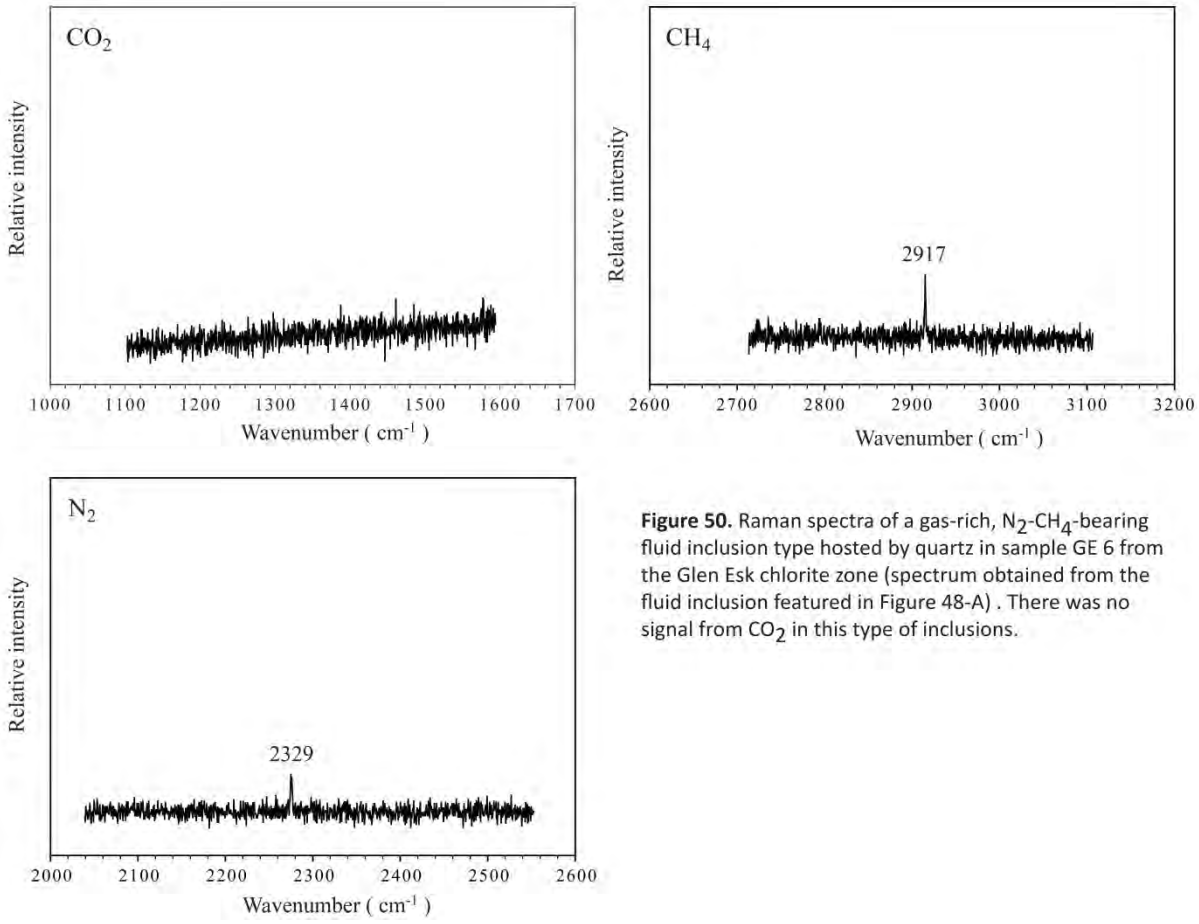

Figure 50. Raman spectra of a gas-rich, N_2-CH_4-bearing fluid inclusion type hosted by quartz in sample GE 6 from the Glen Esk chlorite zone (spectrum obtained from the fluid inclusion featured in Figure 48-A) . There was no signal from CO_2 in this type of inclusions.

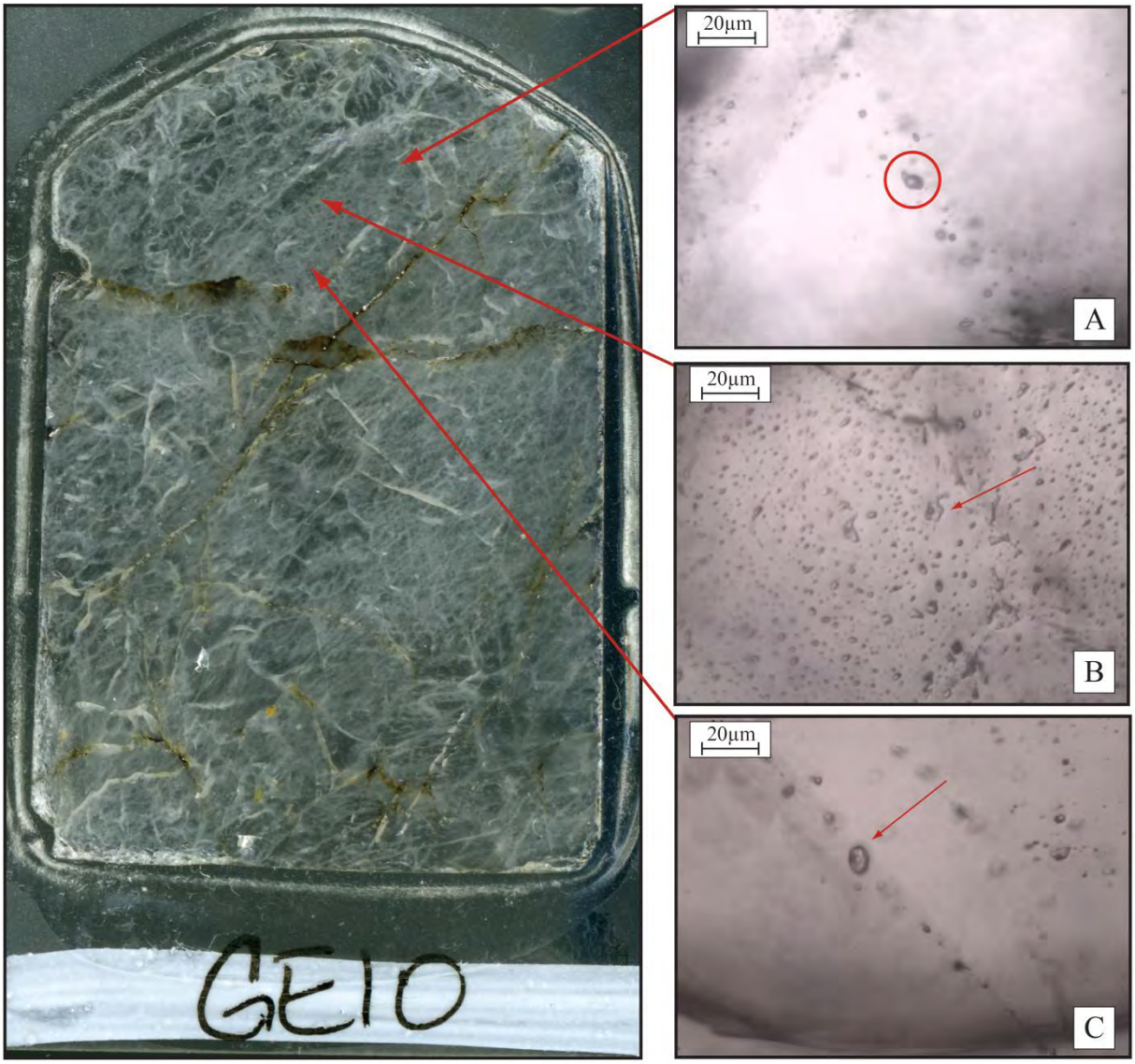

Figure 51. *Sample GE10, biotite zone of Glen Esk* ***A)*** *Gas-rich fluid inclusion with CO_2, N_2 and CH_4.* ***B)*** *Cluster of small aqueous fluid inclusions.* ***C)*** *Aqueous inclusions occuring in lineations.*

Quartz vein in the biotite isograd locality Burn of Mooran Gorge. The vein is oriented layer parallel to foliation of 80°/310° with an ellipsoid appearance and a maximum width of 60cm. Surrounding rocks are rich in biotite. Fluid inclusions are abundant including both Type Ic-h (more commonly around 20 volume % and below) and Type IIh with CO_2, N_2 and a small amount of CH_4. GE10 also contain fluid inclusions of Type I-s with three types of solid phases (Figures 52-54). These have been identified by Raman spectroscopy as the minerals witherite ($BaCO_3$), Mg-rich Siderite ($FeCO_3$ with substitution of Fe to Mg) and Chalcopyrite ($CuFeS_2$). All solid phases vary in size between inclusions and only occur in some places.

Fluid inclusions of both types occur both together and separately. Most commonly they are found in lineations but at places they also form clusters. Homogenization temperatures and salinities identify two separate groups of inclusions which indicate the presence of unmixing (Figure 65). The first group has homogenization temperatures of 260 to 330 °C with a salinity of approximately 10 weight percent NaCl equivalent. The second group has a lower homogenization range of 120 to 260 °C and lower salinities around 5 weight percent NaCl equivalent. Both the first (~-60°C Tm) and the second (-47 to -50°C) groups are calcic in composition.

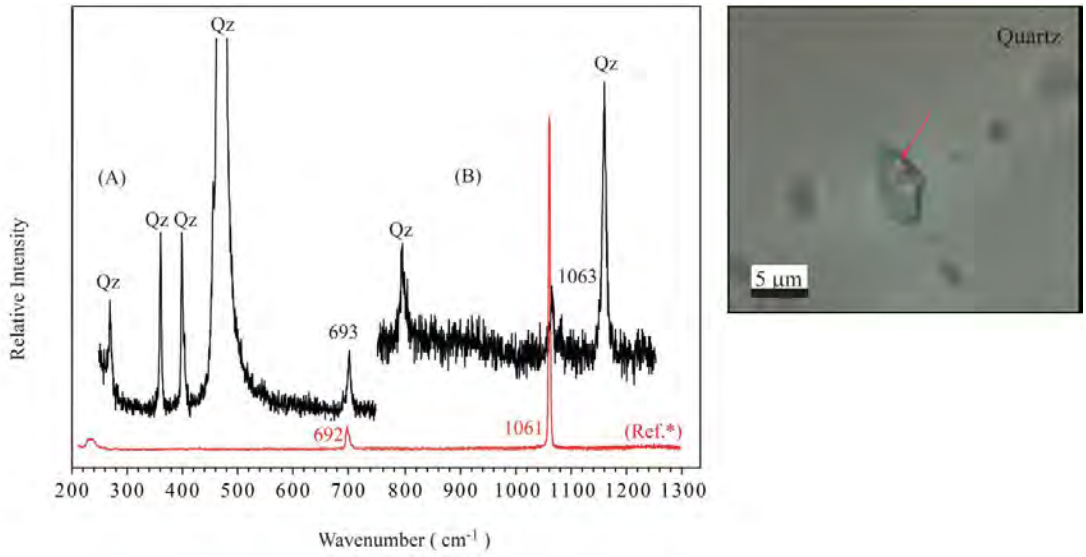

Figure 52. *Raman spectra (A and B) of a white solid phase (see arrow) identified as witherite ($BaCO_3$) in a fluid inclusion in sample GE10. Please note that different scales of the Y-axis are used in A and B because of less intense bands in B. Bands from the host quartz is marked "Qz".*

Ref. = Reference spectrum from witherite $BaCO_3$ RRUFF ID: R040040 from the RRUFF™ project (Downs 2006).*

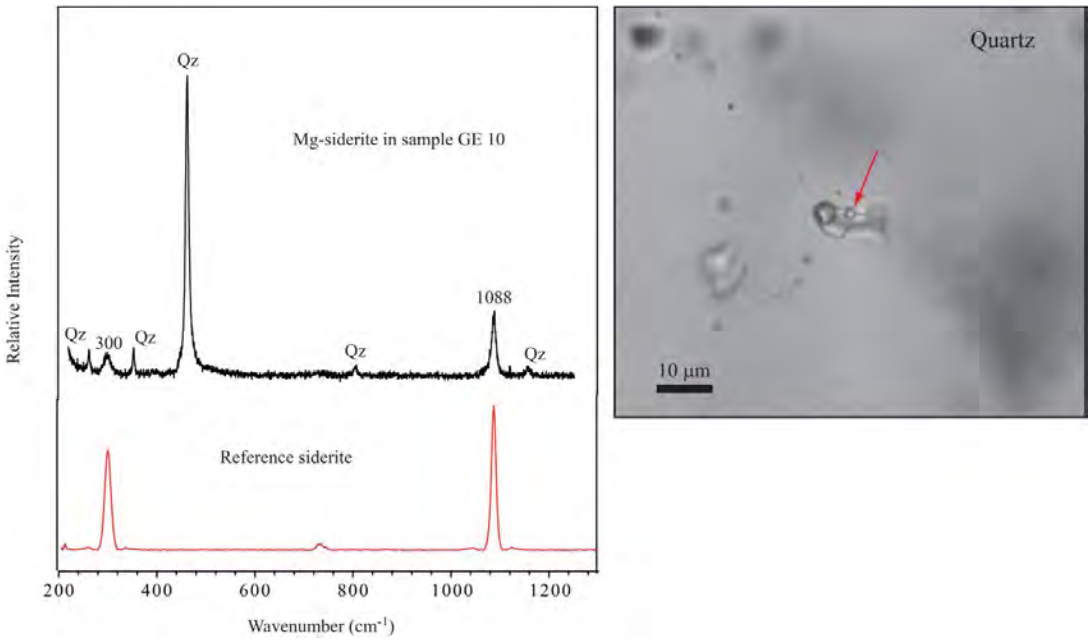

Figure 53. *Raman spectrum of a white solid phase (see arrow) identified as Mg-siderite in a fluid inclusion in sample GE10. Bands from the host quartz is marked "Qz". Reference spectrum from siderite RRUFF ID: X050144 from the RRUFF™ project (Downs 2006). A Fe-pure end member of siderite $FeCO_3$ has a Raman peak at 290 cm-1, the position of this peak is shifted towards higher wavenumber with increasing Mg content (Boulard et al. 2012). The analyzed sample (peak position at 300 cm^{-1}) has a composition of about Mg 0.3 Fe 0.7 CO_3 similar as the reference siderite.*

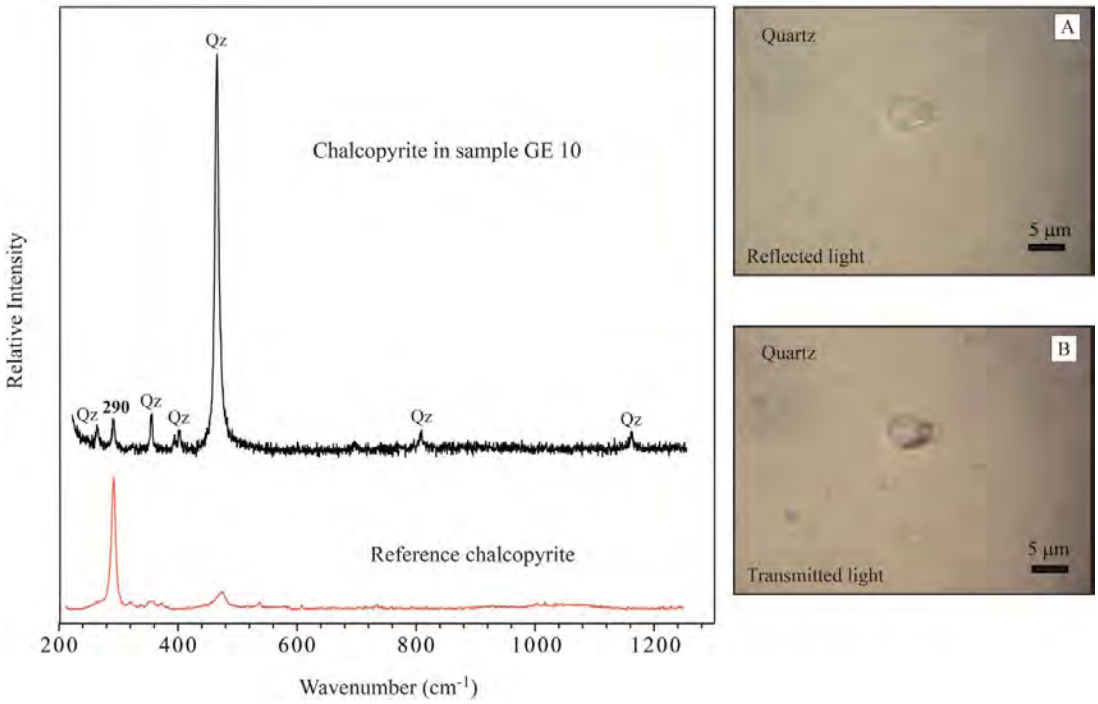

Figure 54. *Raman spectrum of a yellow (black in transmitted light, see photos) mineral in an aqueous fluid inclusion hosted by quartz (photos) and identified as chalcopyrite (sample GE 10). Bands from the host quartz is marked "Qz". Reference spectrum from chalcopyrite $CuFeS_2$ RRUFF ID: R050018.2 from the RRUFF™ project (Downs 2006).*

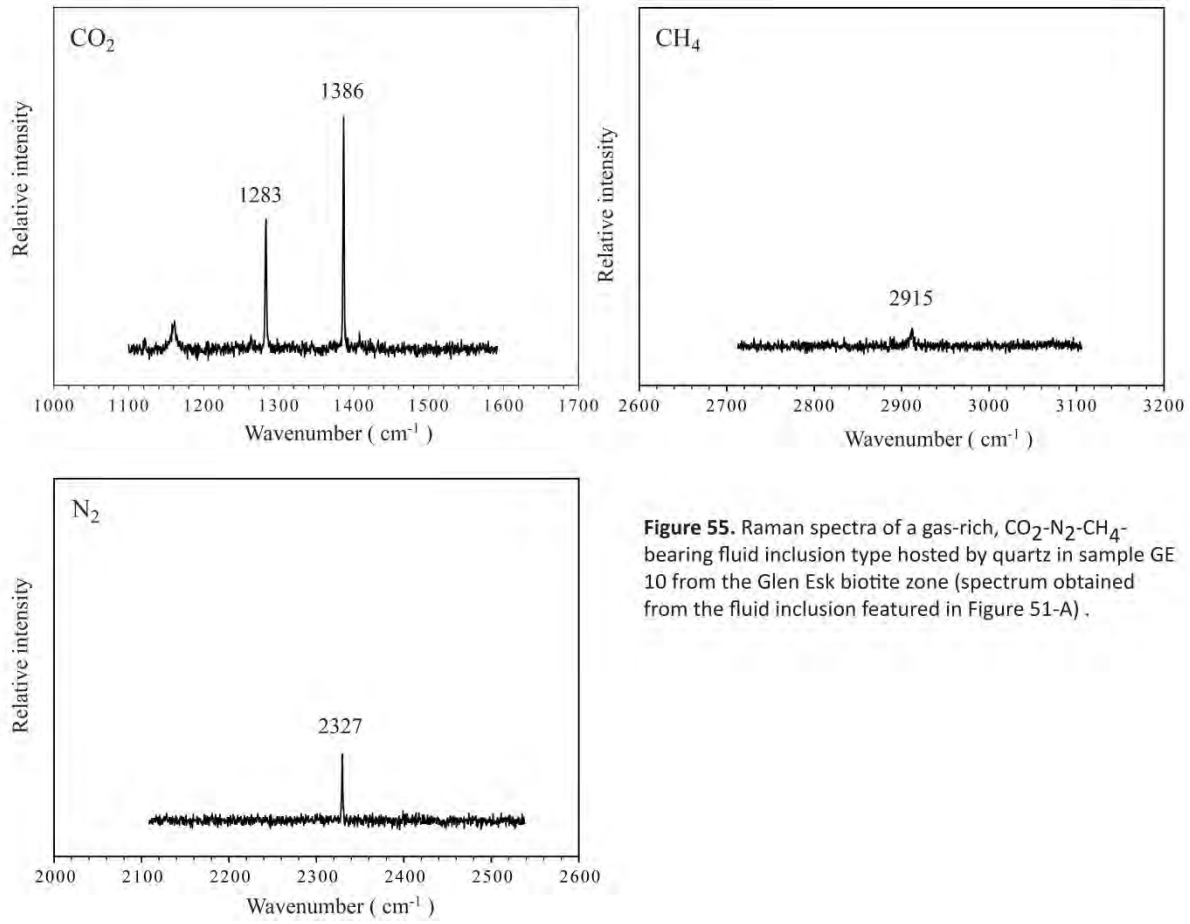

Figure 55. Raman spectra of a gas-rich, CO_2-N_2-CH_4-bearing fluid inclusion type hosted by quartz in sample GE 10 from the Glen Esk biotite zone (spectrum obtained from the fluid inclusion featured in Figure 51-A) .

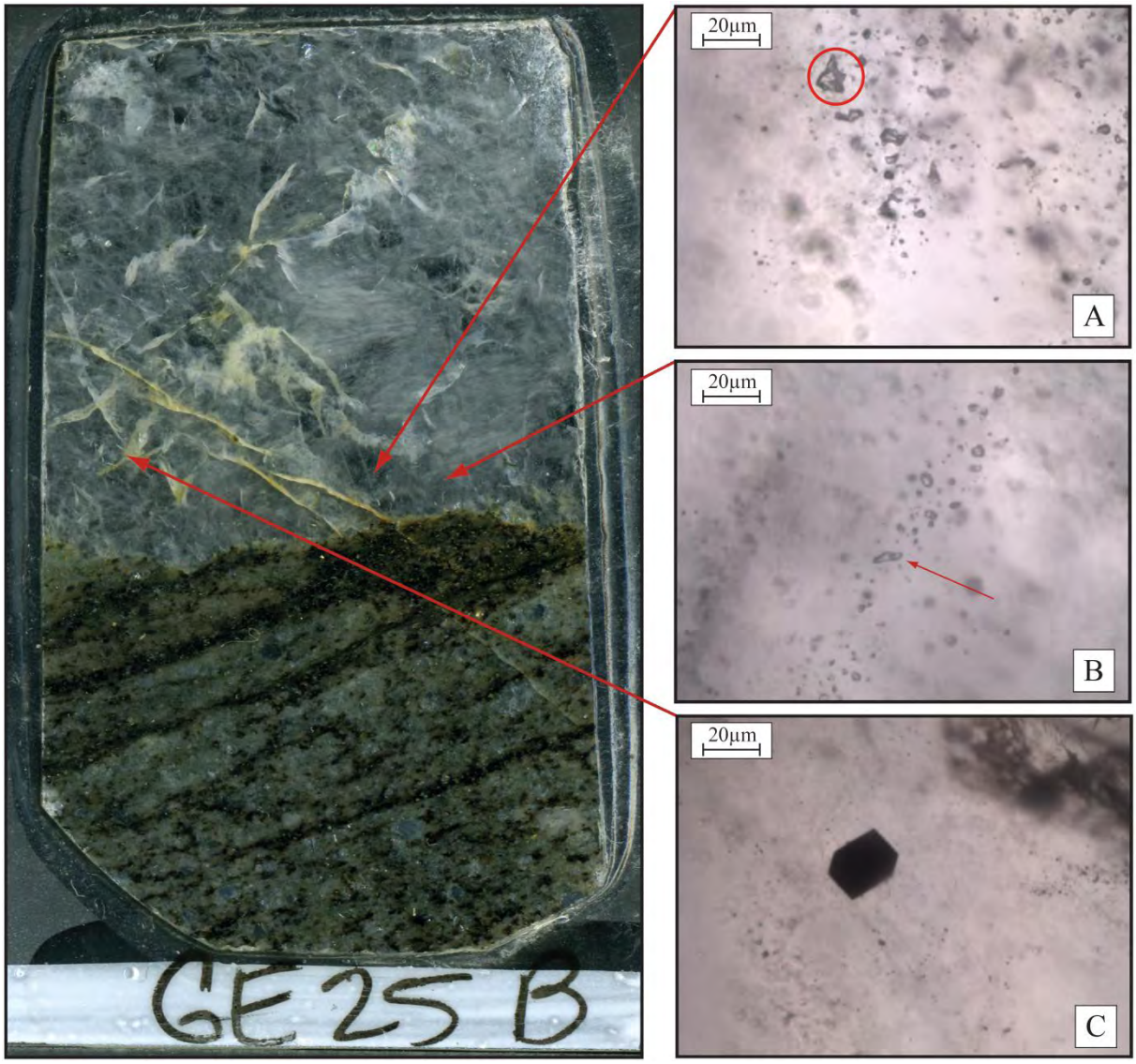

Figure 56. *Sample GE25b, garnet zone of Glen Esk* ***A)*** *Gas-rich fluid inclusion with CO_2, N_2 and CH_4 occurring in a cluster .* ***B)*** *small aqueous fluid inclusions.* ***C)*** *Pyrite mineral inclusion in quartz.*

GE25b is a layer parallel quartz vein (75°/305°) sampled from The Long Pool containing both Type Ic-e and Type IIh fluid inclusions. The two types are often found isolated from one another, with the Type I occurring in lineations and the Type II as large clusters on the border of the grains (Figure 56-A and B). The gas-rich inclusions contain a mixture of CO_2, N_2 and CH_4. In contact with the country rock the vein has created a selvage where abundant pyrite, a smaller amount of chalcopyrite and pyrrhotite has precipitated. To a smaller extent this mineral precipitation is found in the vein itself (Figure 56-C). Inside recrystallized quartz mineral inclusions in the form of rounded grains of zircons are found.

Two groups of inclusions were identified in GE25B. Both groups have a very narrow homogenization temperature range from 215 to 220 °C but the first group has a calculated salinity of approximately 5 weight percent NaCl equivalent while the other range from 10 to 15 weight percent NaCl equivalent (Figure 63, Figure 64). Both lower salinity (-36 to - 42°C) and the higher salinity (-50°C) group indicates a salt system that is dominated by $CaCl_2$.

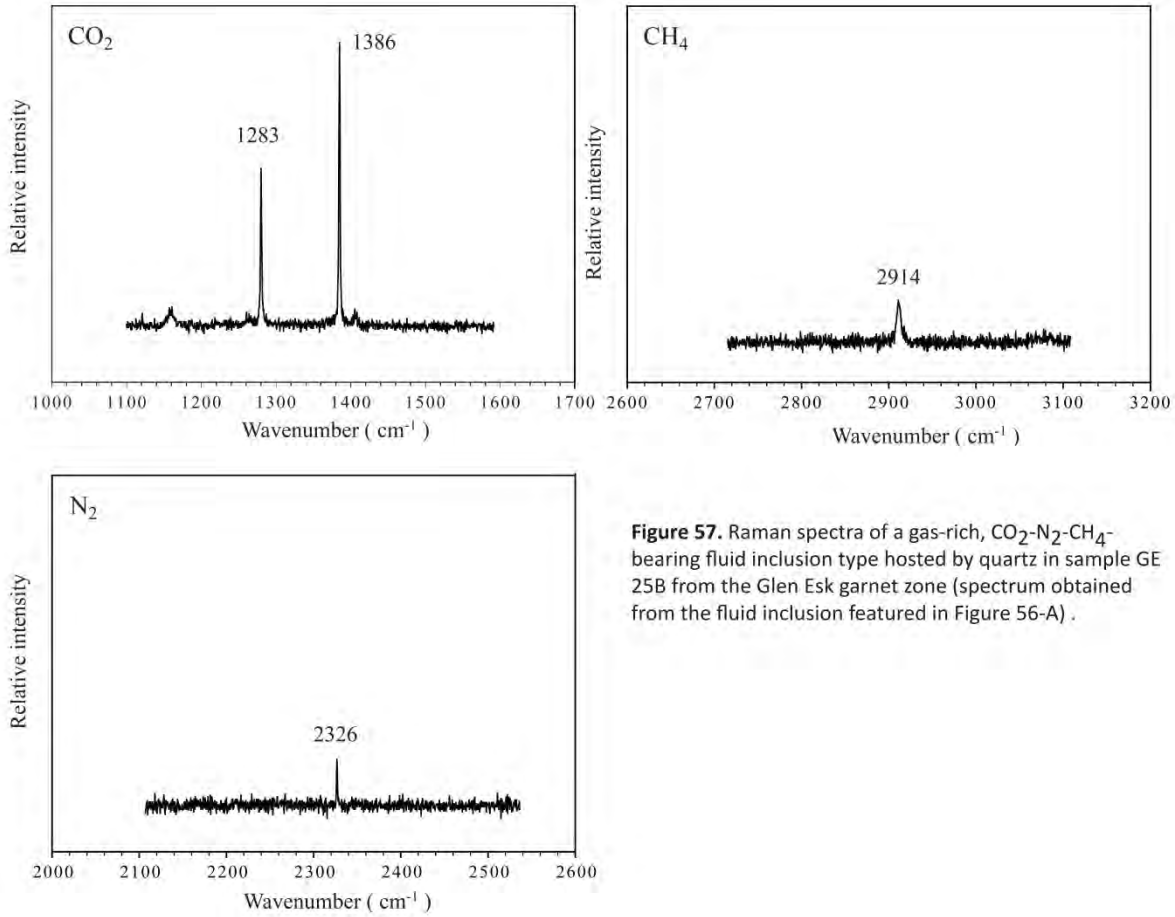

Figure 57. Raman spectra of a gas-rich, CO_2-N_2-CH_4-bearing fluid inclusion type hosted by quartz in sample GE 25B from the Glen Esk garnet zone (spectrum obtained from the fluid inclusion featured in Figure 56-A) .

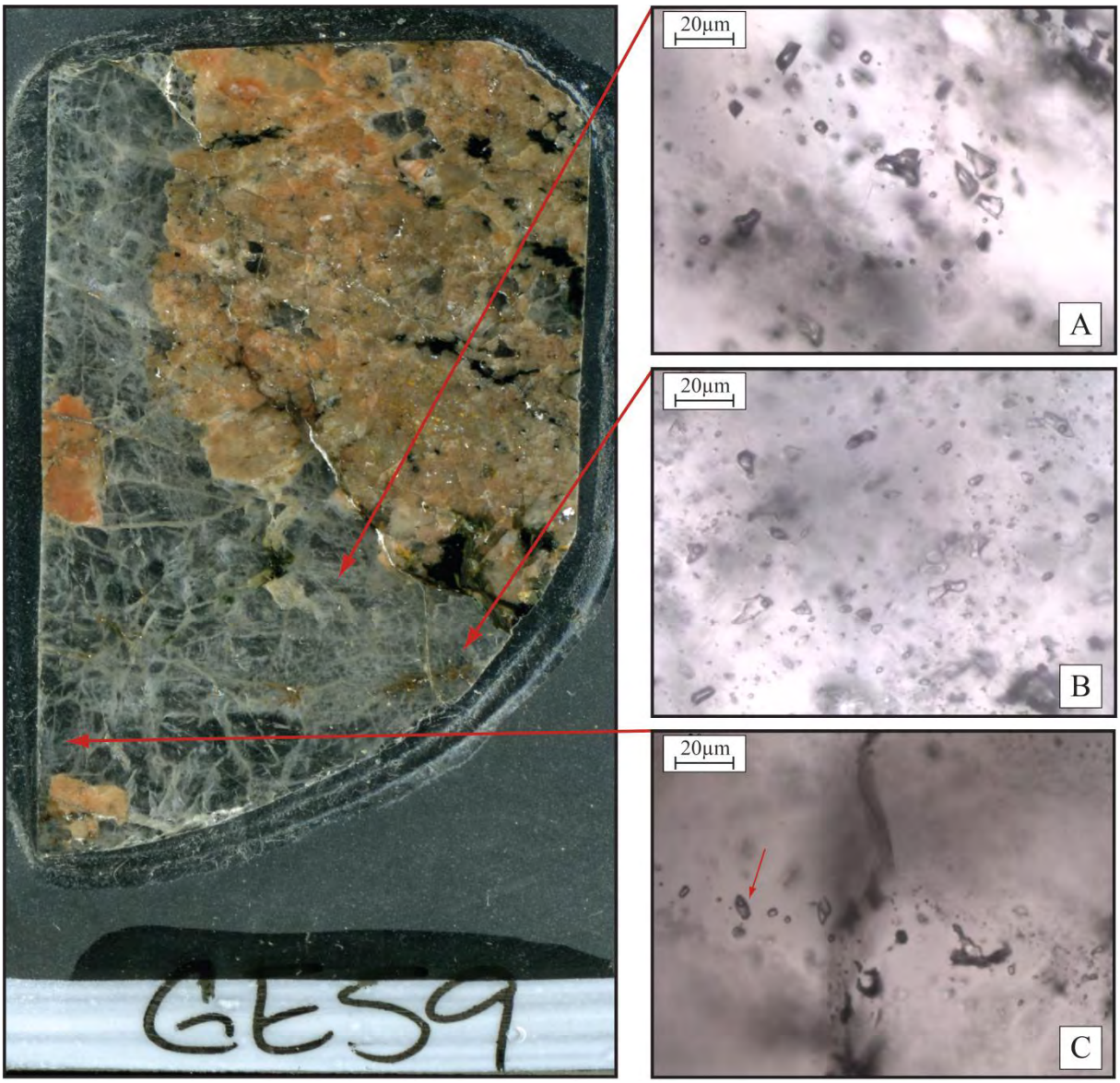

Figure 58. *Sample GE59, kyanite zone of Glen Esk* ***A)*** *Cluster of gas-rich fluid inclusion with* CO_2 *and* N_2 ***B)*** *Aqueous iclusions occurring in a cluster with a lack of preferential orientation* ***C)*** *Aqueous inclusions occurring in lineations close to a fractured zone.*

Sample from the locality of Craigoshina in the kyanite zone. The vein is parallel to surrounding layers (85°/340°) and contains large porphyroblasts of kyanite and some mica. Fluid inclusions are very abundant in GE59 and include both Type I and Type II. In contrast to the samples of the other mineral isograds the gas-rich inclusions are the most dominant type found in GE59 and are widely distributed. Both gas and aqueous fluid inclusions occur together and separate, in clusters and in lineations. No trace of CH_4 was found in any of the gas-rich inclusions.

Minerals of the host rocks included albite, muscovite, quartz, magnetite, tourmaline and rutile. These minerals were identified using Raman spectroscopy but their spectra are omitted in this thesis. Also identified was a large grain of magnetite surrounded by an alteration rim of goethite. Two different types of fluid inclusion groups were identified. The first had homogenization temperatures ranging from 170 to 215°C and low salinities of 1 to 3 NaCl weight percent equivalent and the other had temperatures ranging from 190 to 270 °C with salinities of 8 to 12 weight percent NaCl equivalent (Figure 65, Table 7). The melting temperatures of both groups indicates a salt system dominated by $CaCl_2$ (-43 to -54°C).

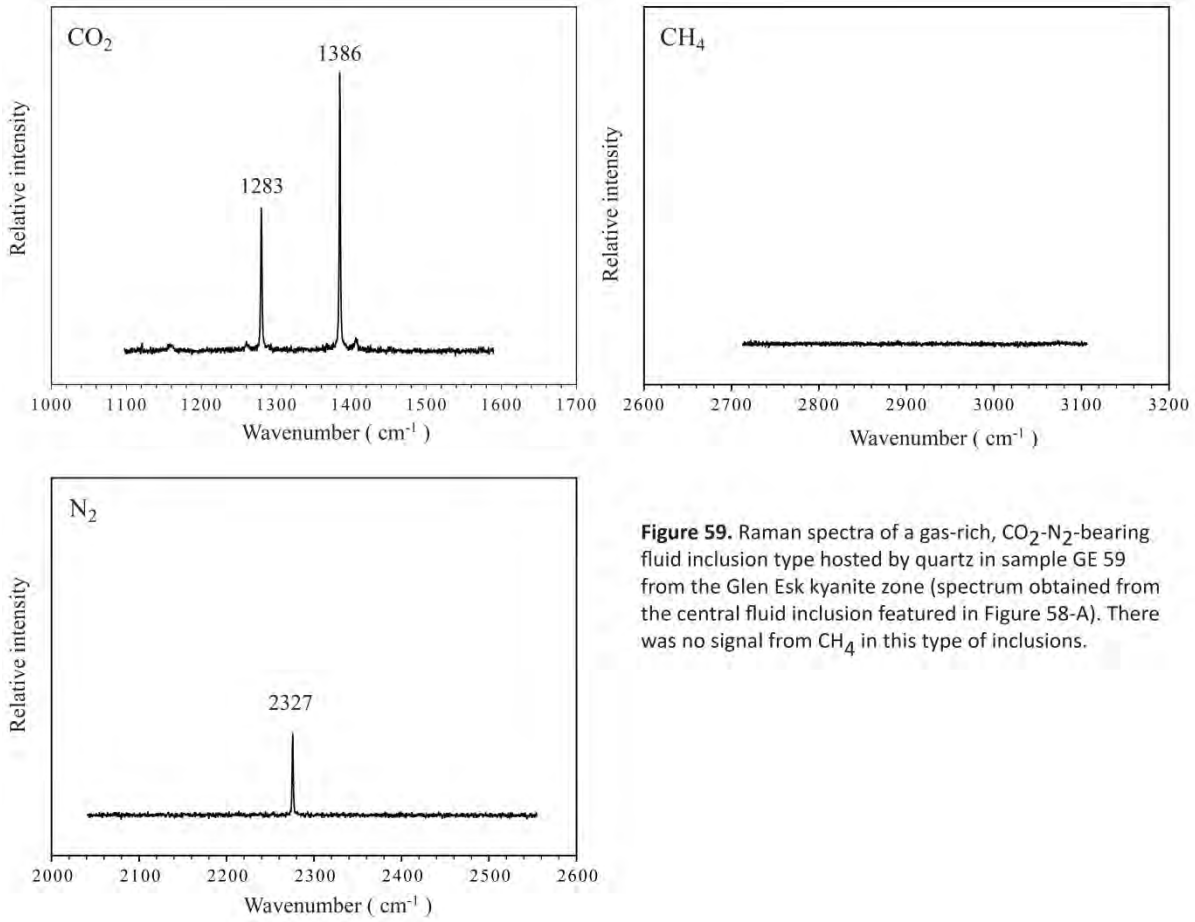

Figure 59. Raman spectra of a gas-rich, CO_2-N_2-bearing fluid inclusion type hosted by quartz in sample GE 59 from the Glen Esk kyanite zone (spectrum obtained from the central fluid inclusion featured in Figure 58-A). There was no signal from CH_4 in this type of inclusions.

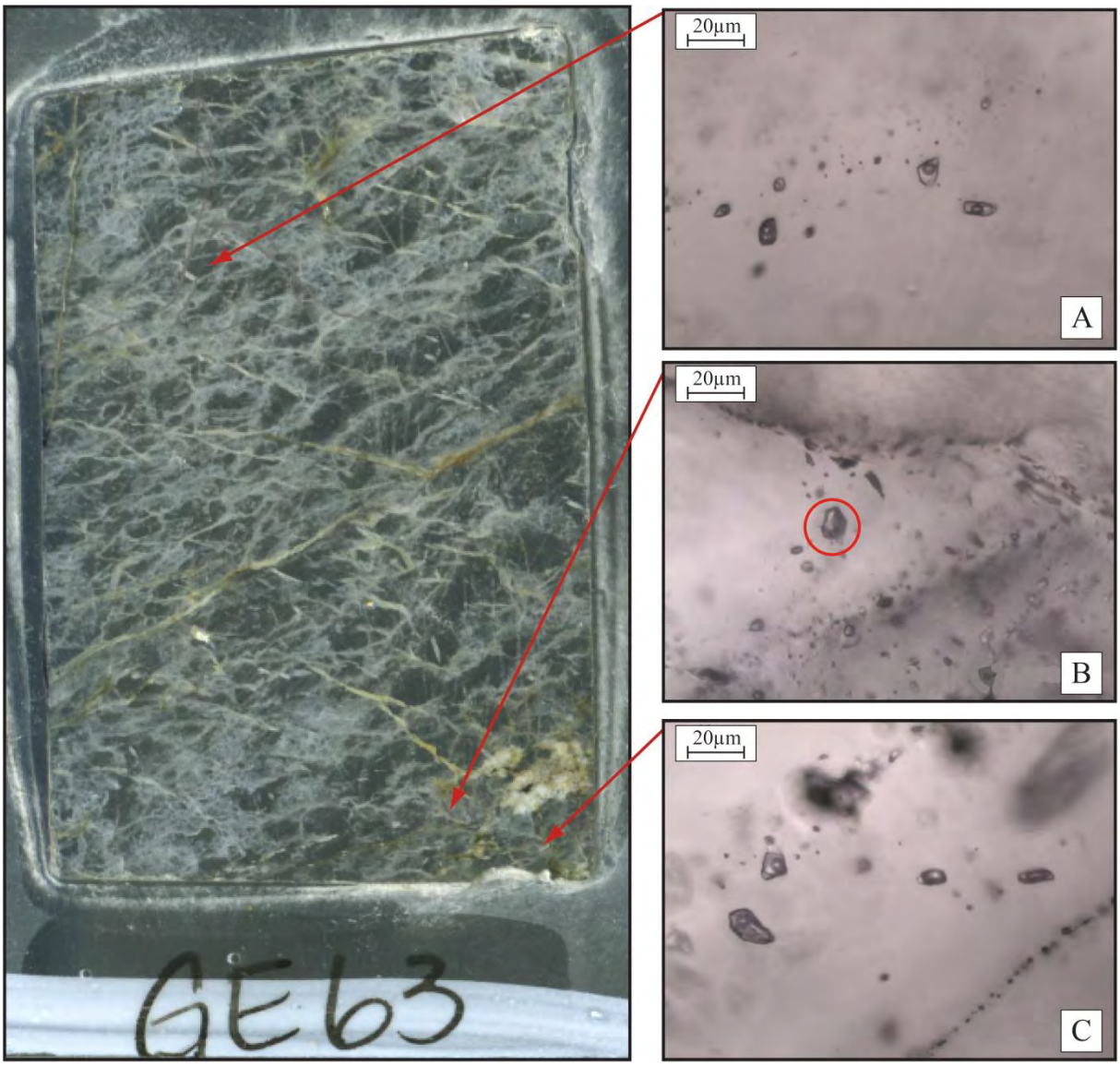

Figure 60. *Sample GE63, sillmanite zone of Glen Esk **A)** Cluster of small aqueous fluid inclusions **B)** Gas-rich fluid inclusion with CO_2 and N_2 very similar to those found in GE59. **C)** Gas-rich fluid inclusions.*

Sillimanite zone sample form the locality of Hillock. The quartz vein is parallel with surrounding layers (90/040) which contain fiberous sillimanite. Fluid inclusions are both aqueous and gas-rich in composition (type I and type II). Both types are relatively abundant occurring both together and separately, in clusters, lineations and in relative isolation. The composition of the gas-rich inclusions is very similar to GE59 from the kyanite zone with both CO_2 and N_2 present. No CH_4 was found in any of the inclusions.

In some aqueous inclusions a white solid phase identified as calcite ($CaCO_3$) was found (Figure 61). The calcite crystals vary in size and occur only in some inclusions. Fluid inclusions are divided into two distinct groups indicative of unmixing (Figure 65). The first group is at high salinity (10 to 13 weight percent NaCl equivalent), high homogenization temperatures (380 to 400 °C) while the other group displays low salinity (1-2 weight percent NaCl equivalent) and low homogenization temperatures (220-240°C). Both groups have melting temperatures of -52 to -54 °C indicating a calcic composition.

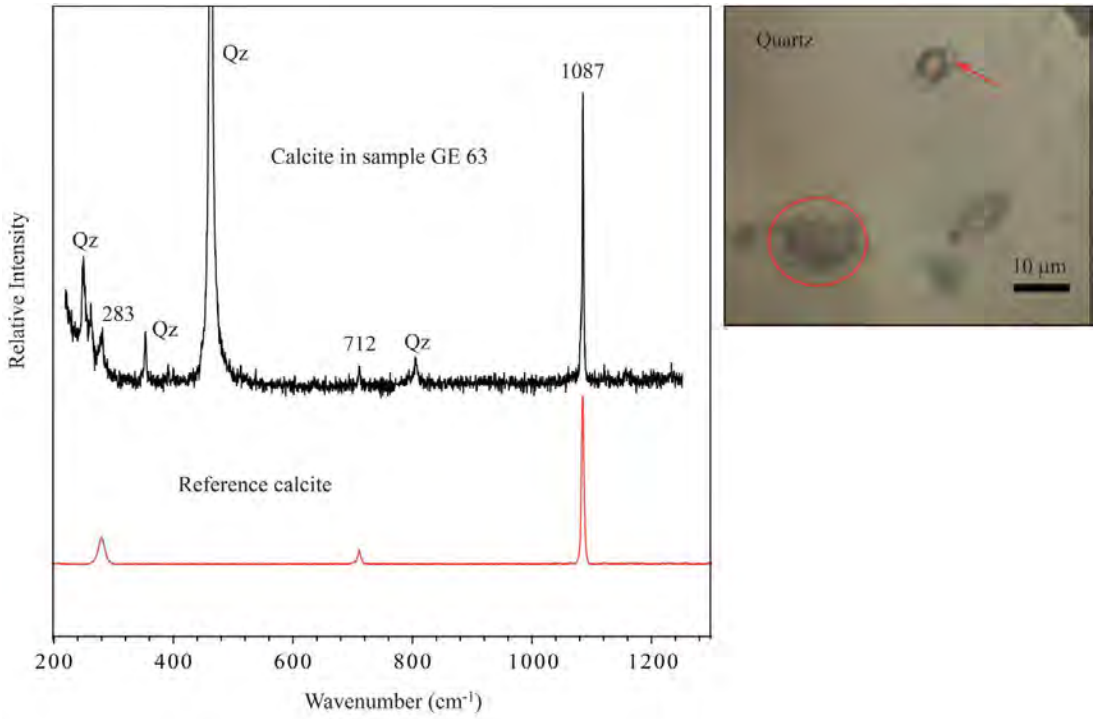

Figure 61. *Raman spectrum of a white solid phase (see arrow) identified as calcite in a fluid inclusion in sample GE63. Bands from the host quartz is marked "Qz". Reference spectrum from calcite $CaCO_3$ RRUFF ID: R050128 from the RRUFF™ project (Downs 2006).*

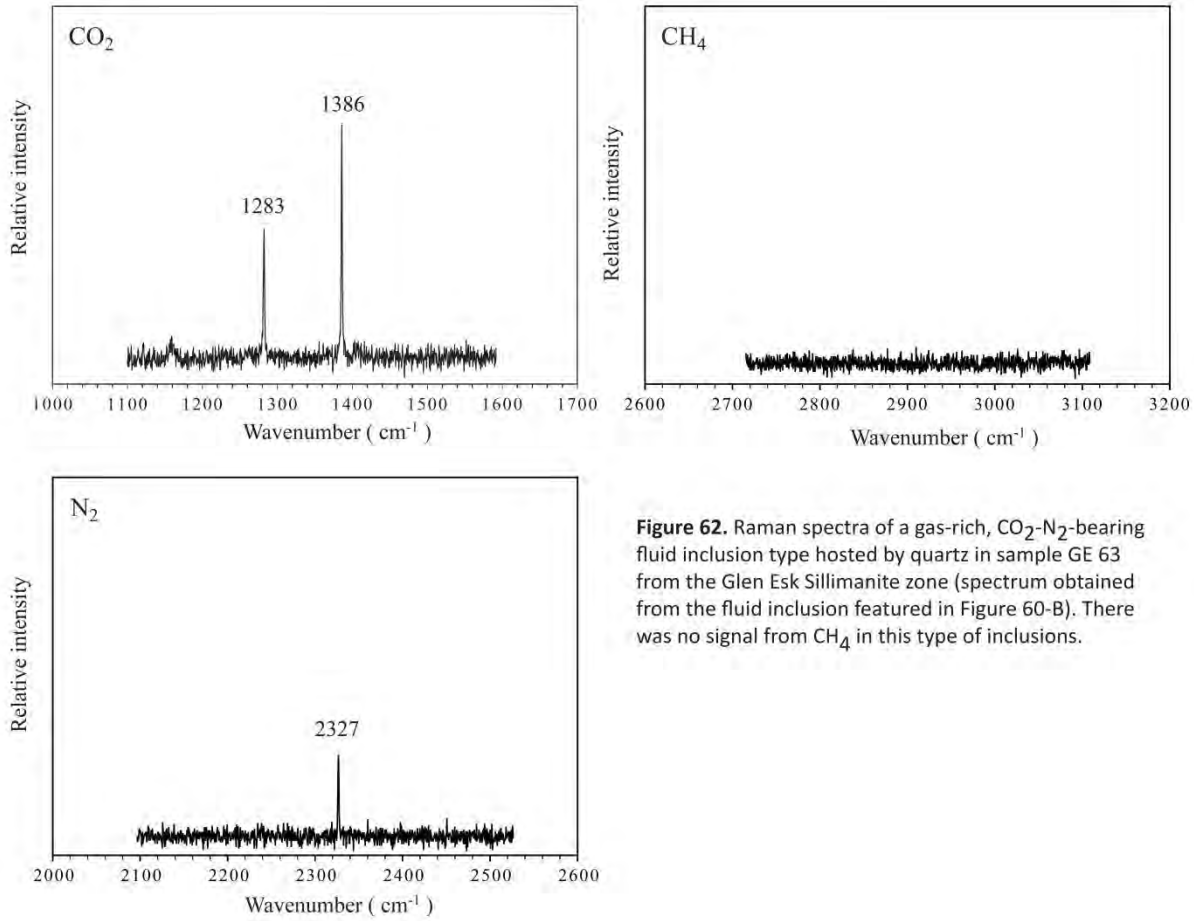

Figure 62. Raman spectra of a gas-rich, CO_2-N_2-bearing fluid inclusion type hosted by quartz in sample GE 63 from the Glen Esk Sillimanite zone (spectrum obtained from the fluid inclusion featured in Figure 60-B). There was no signal from CH_4 in this type of inclusions.

Sample	Composition	Number of inclusions	Tm	Th
GE 6 - Chlorite	20 mole % N_2; 80 mole % CH_4	1	-	**-90,5**
			-	-
GE 10 - Biotite	73 mole % CO_2; 25 mole % N_2; 2 mole % CH_4	11	**-63,25**	**-17,85***
			(-66,5 to -60,4)	*(-51,4 to 7,1)*
GE 25b - Garnet	85 mole % CO_2; 11 mole % N_2; 4 mole % CH_4	13	**-63,23**	**-2,96**
			(-64,3 to -61,8)	*(-5,9 to 4)*
GE 59 - Kyanite	75 mole % CO_2; 25 mole % N_2	15	**-59,24**	**1,31***
			(-61,7 to -56,7)	*(-30,1 to 7,4)*
GE 63 - Sillimanite	75 mole % CO_2; 25 mole % N_2	7	**-61,46**	**-5,66**
			(-62 to -61)	*(-6 to -5,5)*
AE-GE 2a - Post-meta	No gases	-	-	-

Table 5. *Semi-quantitative estimation of the gas composition (in mole %) for the carbonic inclusions calculated using the Raman peak areas and the relative Raman cross-sections (specific Raman activity) for the gaseous compounds (Van der Kerkhof and Thiery 2001 with method from Burke 2001). The gas-rich fluid inclusions of sample GE 59 and GE 10 each have two different populations containing varying proportions of gas composition affecting the average homogenization temperature. For GE 10 there are 6 inclusions ranging in between -51,4 to -16,6 and 3 ranging from 7,1 to 5,8. In GE59 the majority of the inclusions (8) range from 7,4 to 5,6 while a minority of the inclusions (2) at negative temperature range from -30,1 to -9,5.*

Metamorphic grade	Number of fluid inclusions	Size (µm)	First melting of ice (eutectic) **Tfm** or melting of CO2 **TmCO2**	Melting temperature of solid phases **Tm** Ice, clathrate **or** salts (halite)	**Salinity from melting** NaCl equavilent Wt%	**Homogenization temperature Th (°C)**
Chlorite	16	**6,1**	**-38,8**	**-8,2**	**11,9**	**155**
		(21 to 2)	*(-43 to -37)*	*(-9,5 to -6,5)*	*(13,4 to 9,9)*	*(180 to 140)*
Biotite	47	**6,9**	**-50,8**	**-3,5**	**8,5**	**196**
		(15 to 2)	*(-66,5 to -38)*	*(-11,7 to 6,2)*	*(15,7 to 5)*	*(331 to 126)*
Garnet	25	**7**	**-57,5**	**-6,4**	**11,2**	**215**
		(24 to 3)	*(-64,3 to -36)*	*(-9,9 to 0)*	*(15 to 4,5)*	*(220 to 215)*
Kyanite	44	**8,6**	**-55**	**-3,4**	**5,7**	**199**
		(19 to 3)	*(-61,7 to -43)*	*(-9,1 to -1)*	*(12,9 to 1,4)*	*(268 to 119)*
Sillimanite	35	**11,9**	**-60,6**	**1**	**6,5**	**347**
		(25 to 5)	*(-62 to -56)*	*(11,2 to -13,8)*	*(17,6 to 0)*	*(407 to 220)*
Post-meta (Hardhill)	15	**17,6**	**-56**	**-20,6**	**20,9**	**107**
		(75 to 4)	*(-60 to -53)*	*(-24,9 to -11,7)*	*(23 to 15,7)*	*(312 to 70)*

Table 6. *Summary of both carbonic and aqueous inclusion data. Melting and homogenization temperatures are measured in °C while salinity is estimated in terms of NaCL equivalent weight percent (salinities for inclusions calculated using Fall et al. 2010 with salinities of AE-GE2 from Oakes et al. 1990). Unmixing is a common occurrence in many samples leading to the averages reflecting unrepresentative mean values. Where this is the case it is stated in the individual sample description.*

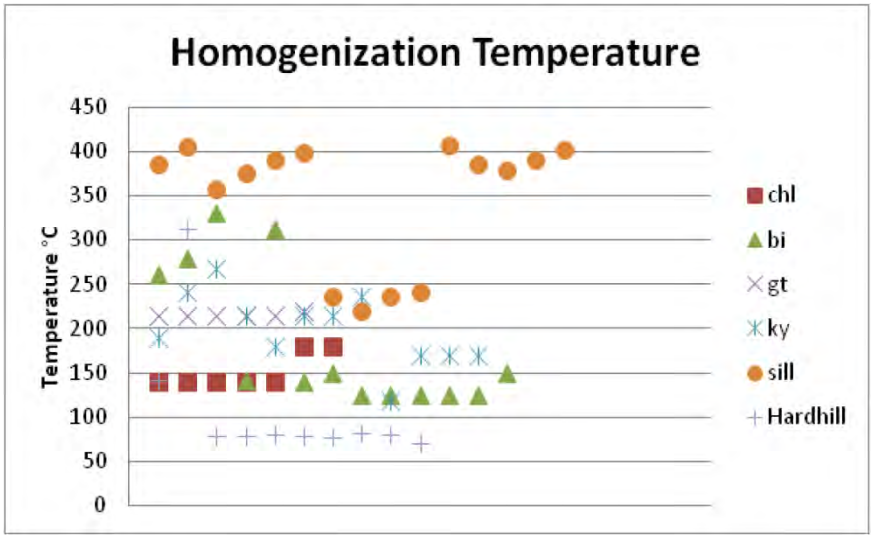

Figure 63. *Homogenization temperatures for all Glen Esk samples.*

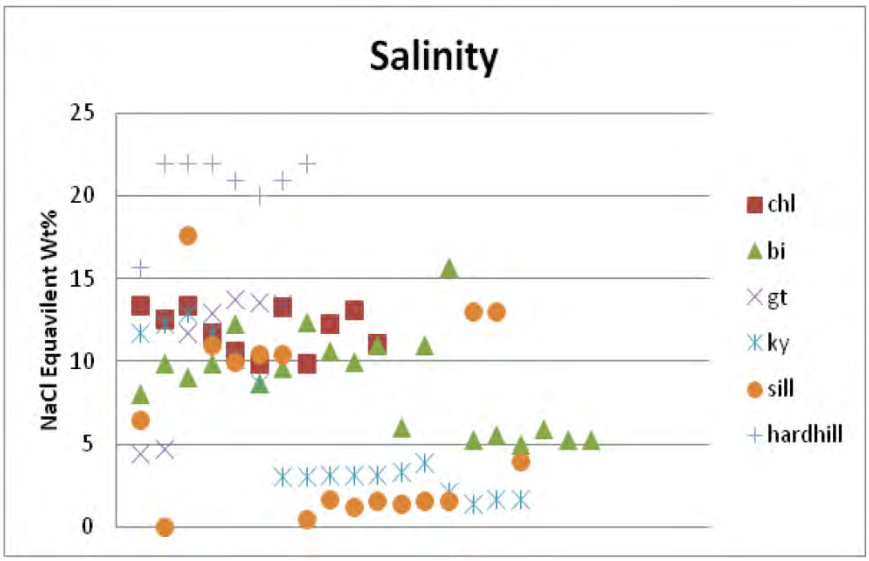

Figure 64. *Salinity of all Glen Esk samples.*

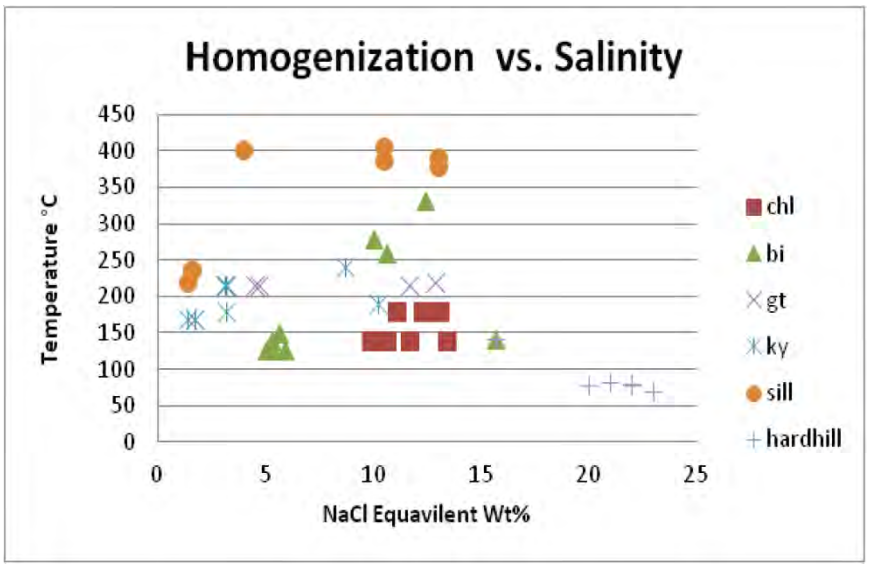

Figure 65. *Homogenization plotted against salinity.*

IV. Discussion

i. Whole rock chemistry, gold mobilization and SEM scanning

Analysis of whole rock major and trace elements show no great differences between the localities of Stonehaven, Loch Lomond and Glen Esk (Figure 40). With the exception of decreasing LOI, no major trends of systematic elemental depletion with metamorphic grade were found. However, certain differences are identified between the zones which can be attributed to change in bulk composition possibly related to the chemical reactions forming the index minerals. In particular, the kyanite zone diverges from the other zones in terms of anomalously high Mn and low S content. High MnO values may be related to weathering causing oxidation of sulfides but as not all samples are weathered, desulfidation of pyrite is believed to be partly responsible for this drop of S content starting after the garnet zone (Figure 40). The lack of S is also reflected in the abundance of sulfides for this zone which are only found in one sample (GE39). In the sillimanite zone S content is increased corresponding to sulfidation observed in these higher grade rocks (Figure 35). Si content decrease in the kyanite zone with a simultaneous increase of Al, Fe and Ti. Pb and Sr show enrichment towards the staurolite and kyanite zones. These two trends are likely to be the result of a change in mineralogy of these zones possibly implying a difference in provenance.

In figure 66 concentrations of Au, As, S and LOI are plotted against metamorphic temperature for the three different localities investigated in this study. In terms of Au, As and LOI the different localities follow similar paths of depletion with the exception of As concentrations from chlorite to garnet grade rocks in Glen Esk. S concentrations vary between localities with major depletions occurring in the higher grade rocks (garnet to staurolite grade in Glen Esk and staurolite to sillimanite in Stonehaven). For both Loch Lomond and Glen Esk the concentration of S increase towards the highest grade rock corresponding to observed sulfidation. Although occurring at slightly different temperature the different localities Glen Esk, Loch Lomond and Stonehaven are inferred to display the same kind of depletion.

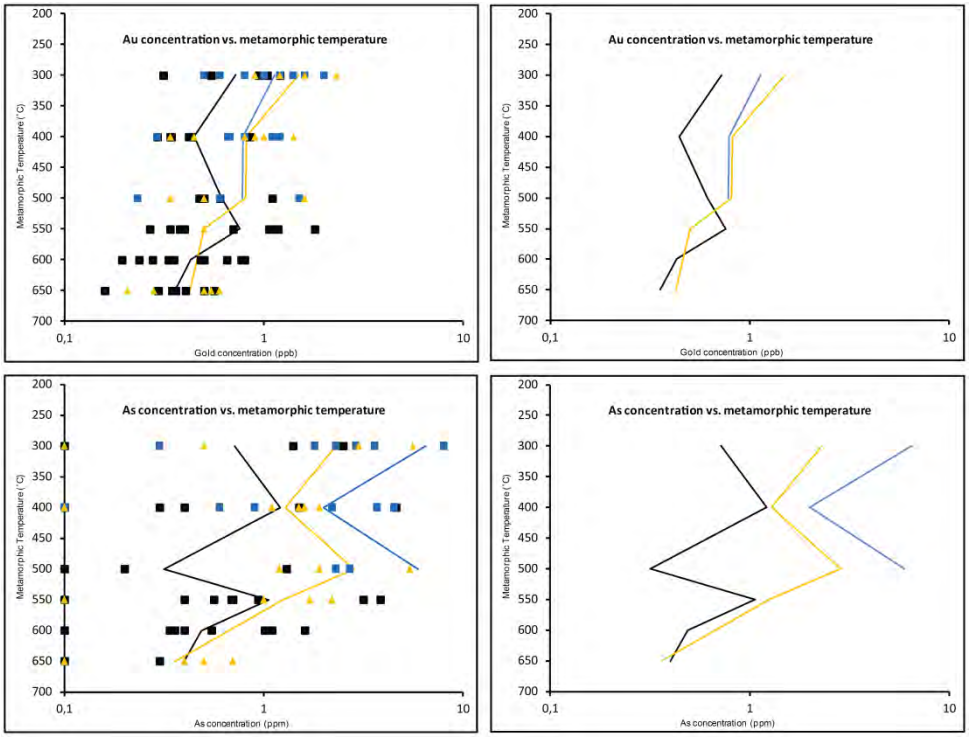

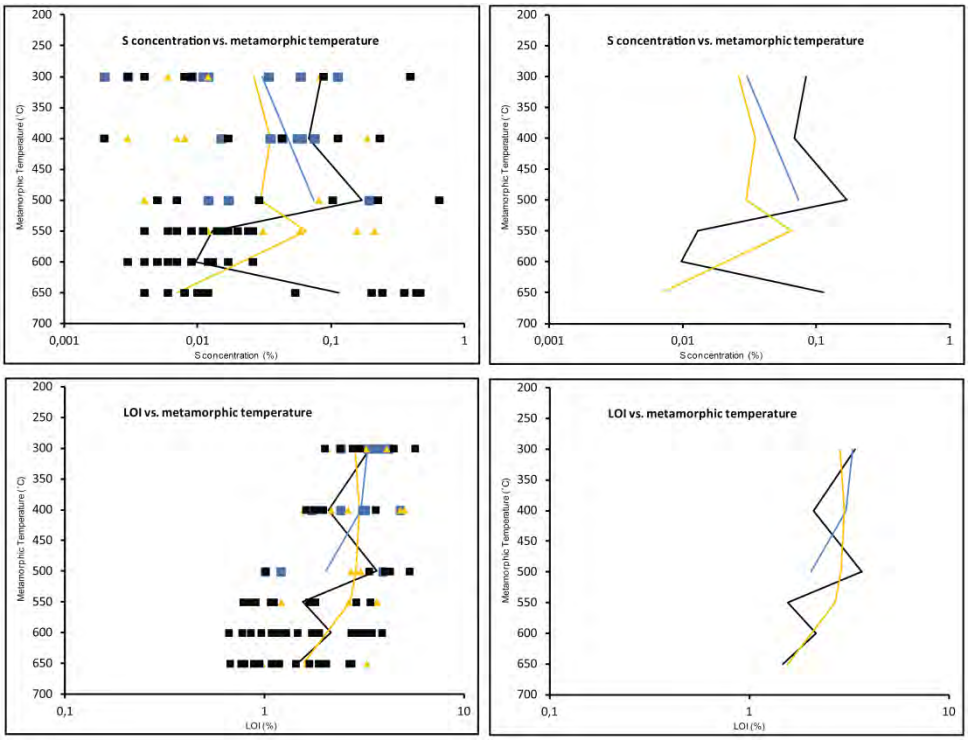

Figure 66. *Au, As, S and LOI for the different localities of the Dalradian. Boxes to the left provide the complete dataset while average concentrations are separated in the boxes to the right. Black squares and lines = Glen Esk samples and average values. Orange triangles and lines = Stonehaven samples and average values. Blue squares and lines = Loch Lomond samples and average values.*

The concentration of gold and arsenic show a systematic depletion with increasing metamorphic grade (Figure 41-42). Average values of Au change from 1.08 ppb in the chlorite zone to 0.38 ppb in the sillimanite zone which approximately corresponds to 65% depletion. Arsenic is depleted by 88% (5.01 ppm to 0.61 ppm) from chlorite to sillimanite zone (using average values from both AR ICP-MS and HG-AFS) or 67% (1.83 ppm to 0.60 ppm) from the staurolite to sillimanite zone (using only HG-AFS). This depletion is similar to observations made in Otago (Pitcairn 2006:2010), implying a relation between metal mobility and increasing metamorphic grade and in addition providing support for the theory that orogeny always release fluids which have the potential to mobilize gold.

Previous investigation of the sulfide paragenesis in Glen Esk show a progressive transition of pyrite into pyrrhotite that occurs between the chlorite and staurolite zones (Peulicke 2012, Pitcairn 2012). However, scanning of thin sections from Loch Lomond and Stonehaven made in this study provides evidence for a more complex history for the sulfide evolution of the Dalradian. At Stonehaven several textures are observed which coincide with the sulfide evolution related to increasing metamorphism seen at Otago in other places of the world (Pitcairn 2010 and Carpenter 1974). The chlorite and biotite zones are dominated by euhedral pyrite which coalescence and recrystallize into larger subhedral grains. These are prograde features indicating an arrested state of growth where the shape of the crystal is not influenced by adjacent minerals (Carpenter 1974). In the garnet to staurolite zone these composite grains become progressively more rounded in appearance as they are recrystallized and adjust their growth by surrounding grains. This recrystallization mobilizes sulphur and adds increased diversification to present sulfide assemblages. In the sillimanite zone, pyrite and chalcopyrite are the only sulfides present with pyrite being intensely irregular and oxidized and chalcopyrite occurring in low abundance. Although this textural change demonstrates increased sulphur mobility and recrystallization with increasing metamorphic grade the abundance of pyrrhotite is overall restricted to small inclusions in pyrite with the exception of the staurolite zone where it peaks to approximately 10% of the total sulfide area.

The samples of Loch Lomond provide textures which greatly contrasts the gradual alteration seen at Stonehaven. Already in the chlorite and biotite zone pyrrhotite is dominant in abundance and occurs together with several other types of sulfides. Pyrrhotite grains have a retrograde appearance adjusting its mineral growth by its surroundings as it recrystallizes and fully euhedral shapes are completely absent. Other types of sulfides such as pentlandite and cobaltpentlandite are also relatively abundant and grow in the crystallographic cleavage planes of pyrrhotite. This is indicative of interior replacement of pyrrhotite by the hosted mineral and corresponds well with the envisaged elemental mobility upon the conversion of pyrite to pyrrhotite leading to diversification of the sulfide assemblage (Carpenter 1974 and Pitcairn 2010). Pyrite occur in two modes, the first as rounded medium sized inclusions associated with chalcopyrite and other sulfides inside of pyrrhotite and the second as lamellae along well-developed cleavage planes in pyrrhotite. The rounded inclusions are interpreted to represent remains of the original pyrite grain which have largely been recrystallized as pyrrhotite. This direct replacement is a common feature in carbonaceous rocks which have the appropriate components to drive the pyrite to pyrrhotite alteration reaction in situ. In a rock lacking these components desulfidation products would be leached from pyrite which would be replaced by silicates and other minerals and precipitated elsewhere (Carpenter 1974). The pyrite lamellae are inferred to represent either incomplete desulfidation of pyrite or a product of a later stage fluid infiltration along cleavage which by means of sulfidation has altered pyrrhotite to pyrite. Sample LL25 represent an exception to the above given description and is dominated by pyrite only containing small inclusions of pyrrhotite. This may be a caused by the fact that LL25 is a psammite and possibly lacks the organic carbon necessary to facilitate the pyrite to pyrrhotite desulfidation thus highlighting the importance of difference in lithologies. In the garnet zone pyrite becomes the most abundant sulfide and pyrrhotite occur only rarely as small inclusions.

The difference in sulfide evolution between Stonehaven and Loch Lomond can be caused by many factors. At Stonehaven the absence of a clear pyrrhotite transition can be a consequence of either insufficient desulfidation or the overprint of pyrite through sulfidation. Lack of desulfidation is likely to be a result of redox conditions inhibiting sulphurs ability to go into solution during metamorphism. This could for example happen when there already is abundant sulphur present in the fluid. At Loch Lomond the desulfidation reaction appears to have almost reached completion in all zones with pyrite overprinting occurring in the garnet zone. The efficiency of the reaction can possibly be attributed to abundance of components to drive the reaction and high solubility conditions for sulphur. Although the retrograde event of pyrrhotite sulfidation present problems for assessment of sulfide paragenesis elemental mobility of Au and As does not seem to be affected. Whatever factors are ultimately responsible for the formation of sulfide paragenesis of Stonehaven, Loch Lomond and Glen Esk the localities different geological evolution in terms of PT and time frames of metamorphism are likely to have played an important role.

ii. Fluid inclusion study

The vein samples collected at Glen Esk are interpreted to represent two different mineralization events in the geological history of the Dalradian Supergroup. Samples from Hardhill are associated with brecciation of the wallrock indicative of rapid release of fluid overpressure and hydraulic fracturing in the brittle regime. The fluid that formed the vein was a high salinity (15 to 20 weight percent NaCl equivalent) low temperature (70-140°C) H_2O-salt fluid with calcic composition. Preservation of primary quartz crystals along with brittle behavior of the wallrock and spatial relationships to the other veins suggest that the Hardhill mineralization was a later event. Vein samples from the different index mineral zones of Glen Esk preceding the veins of Hardhill were formed in the ductile regime and were subject to fluid unmixing (Figure 65). This process separates fluid CO_2 and H_2O producing erroneous homogenization temperatures which are slightly higher than the actual values. In the biotite and the sillimanite zone the effect of unmixing is most evident where fluid inclusions are separated into two groups, the first with higher temperatures and higher salinities and the second with lower temperatures and lower salinities (Figure 65). The chlorite zone fluid inclusions show no separation into groups but are also limited in their abundance. Gas-rich inclusions in particular are rare in this zone which displays a more

secondary appearance with a unique composition believed to be a result of extensive interaction with surrounding calcite and wallrock. Taking the process of unmixing into consideration there is no major trend in temperature indicating that mineralization of these veins were unrelated to peak metamorphism. There is a trend of the fluid becoming more reducing towards the three lower index mineral zones where the inclusions contain variable proportions of CH_4. The spatial distribution of sulfides both in selvages and in the inclusions coincides with this pattern and is restricted to these three samples. Solid phases found in GE10 and GE63 vary in size between the inclusions and occur only sporadically. They are inferred to have been transported with the fluid rather than being precipitated from it as they would be otherwise been more widespread and occurred with a size proportional to the hosting inclusion. The fluid that formed the veins at Glen Esk was most likely a uniform low salinity (0-15 weight percent NaCl equivalent) medium temperature (150 to 250 °C) CO_2-N_2-H_20-salt fluid with local variations attributed to host rock control on fluid chemistry (variable CH_4 content). Pressure estimations from isochores indicate a low pressure environment of formation at 1-3kbars (Figure 67).

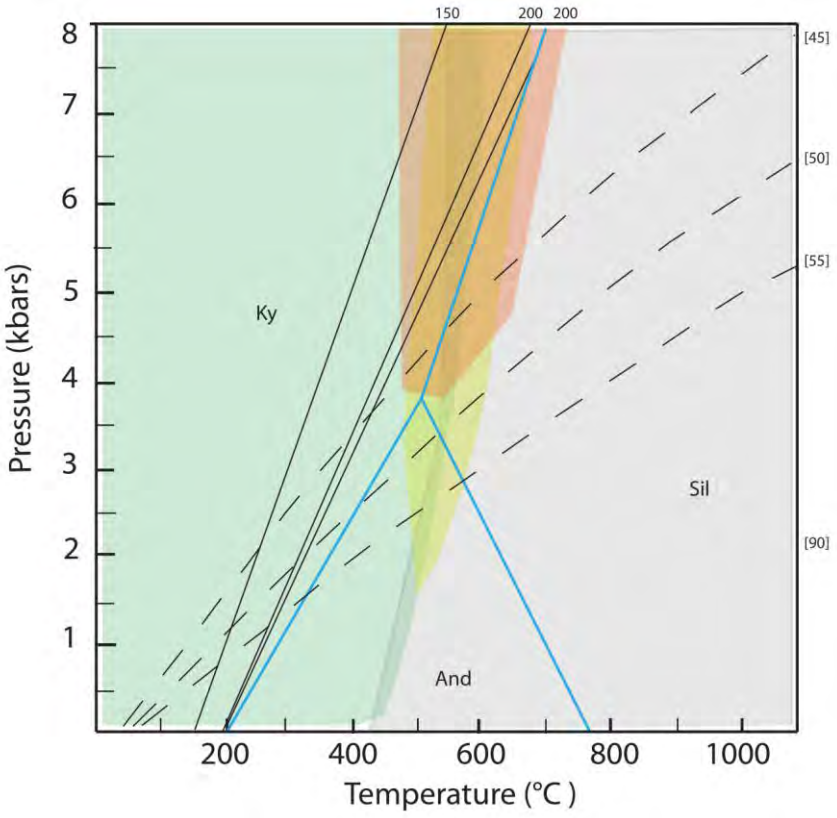

Figure 67. *Diagram showing isochores for fluid inclusion data from the index mineral zone samples. Isochores are lines of constant density which can be used to estimate the pressure of formation for fluid inclusions if parameters such as salinity, homogenization temperature and melting of gas phases are known (Shepherd et al. 1985). Solid lines are isochores for aqueous inclusions based on a salinity range of 5-10% NaCl weight percent equivalent and homogenization temperatures of 150–200 °C taken from Bodnar 2003. These salinities and homogenization temperatures are representative of the dataset in the mineral isograds. The two isochores of 200°C illustrates the small effect of salinity (left one represents 5% while the right represents 10% NaCl weight equivalent for 200°C) on isochore alignment. Dashed lines are isochores from gaseous inclusions CO2 melting (Roedder 1984) Grey line = isochore for methane in GE6. Stability fields: Blue lines = Sillimanite-Kyanite-Andalusite, Green = Chlorite, Grey = Biotite, Red = Garnet, Yellow = Staurolite (Stability fields from Bucher & Rodney 2011). As unmixing is observed in the samples gaseous and aqueous phases existed together when they formed inclusions. Estimation of the pressure of formation can therefore be identified at the section where the range of aqueous and gaseous inclusions crosses. The two types of isochores cross in the chlorite zone and infer a formation pressure of 1-3 kbars.*

The vein composition at Hardhill bears much resemblance to Carboniferous calcic brines which in the British Isles are widely distributed and recognized to host base-metal sulfide mineral deposits (Lusty et al 2007). Examples of this type of mineralization were described by Baron and Parnell (2005) in samples from multiple abandoned mines on Islay and in Northern Ireland where mineralization of base-metals had been precipitated by a low to moderate temperature (Th 70 to 240°C), low to moderate salinity (0 to 20 wt% NaCl eq.) H_2O-salt fluid. In the Dalradian of the Sperrin Mountains of Northern Ireland and at Tyndrum in southwest Scotland carboniferous basinal brines are found overprinting gold mineralization of Caledonian age (Craw 1990 and Parnell et al. 2000). Both these were H_2O-salt fluids formed during low to moderate temperature (70 to 200°C) and low to moderate salinity (0 to 25 wt% NaCl eq.) conditions. In the majority of the base-metal deposits Pb and Zn were main products coinciding well with the occurrence of large sphalerite grains of Hardhill which have also been mapped to contain Ag and Pb (these elements are likely to be absent from the samples of this survey due to having been mined).

The veins from the index mineral zones are harder to correlate with larger scale events as they are less characteristic in composition. However, if a Carboniferous age for the Hardhill vein can be assumed the other veins of Glen Esk are constrained between this age and peak metamorphism of the Dalradian in the Ordovician (475-465 Ma, Vorheis and Ague 2011, Oliver et al. 2008, Fettes et al. 2011, Breeding et al. 2004). The low pressure and low temperature estimates for this H_2O-CO_2-N_2-Salt fluid corresponds well to characteristics of a retrograde metamorphic devolatilization fluid released during uplift and erosion of the Caledonians but relation to igneous processes cannot be completely precluded. H_2O, CO_2 and N_2 are all common products of metamorphic dehydration reactions and the veins of the index mineral zones share many similarities to veins of this origin located in the south west Dalradian (Baron and Parnell 2005). The grouping caused by unmixing with high temperature, high salinity and low temperature, low salinity is the reverse of what would be expected to be found in nature and may imply mixing with meteoric fluids.

V. Conclusions

This thesis has investigated the mobility of metals during metamorphism in the Dalradian of Scotland and possible implications for the formation of orogenic gold deposits. The main conclusions are:

- Ultralow detection limit methods show systematic depletion of Au and As with increasing metamorphic grade. Average Au concentrations are depleted by 65% from the chlorite zone to the sillimanite zone while As is depleted by 88% in the same interval. This depletion suggests a connection between metal mobility and metamorphic grade providing support for the theory that orogenic processes always release fluids which have the potential to mobilize gold.
- No other elements in a suite of 10 major and 12 trace elements showed sign of systematic depletion.
- SEM scanning of thin sections identifies a complex evolution of sulfides through the Dalradian supergroup as represented by the localities of Glen Esk, Stonehaven and Loch Lomond. At Loch Lomond the pyrite to pyrrhotite transition is located in the chlorite to biotite zones while at Stonehaven transition is weak but suggested to occur in the staurolite zone.
- Investigation of fluid inclusions at Glen Esk identifies two distinct types of fluids. The first type occurs in veins formed in the ductile regime parallel to layering and is a H_2O-CO_2 -N_2-salt fluid locally containing minor amounts of CH_4. Although the origin of this fluid is unknown the low salinity (0-15 weight percent NaCl equivalent), low pressure (1-3kbars) and medium temperature (150 to 250 °C) character of the fluid suggests it to be related to late stage metamorphic devolatilization during Caledonian uplift of the Dalradian. The second fluid type was formed in the brittle regime as a high salinity (15 to 20 weight percent NaCl equivalent) low temperature (70-140°C) H_2O-salt fluid with calcic composition. It bears much resemblance to Carboniferous calcic brines responsible for economic base-metal precipitation with widespread occurrence in south west Scotland and Northern Ireland.

VI. References

Anderson, R., Graham, C. M., Boyce, A. J. & Fallick, A. E. (2004): Metamorphic and basin fluids in quartz-carbonate-sulphide veins in the SW Scottish Highlands: a stable isotope and fluid inclusion study. *Geofluids*, Vol. **4**, pp. 169-185

Baron, M. and Parnell, J. (2005): Fluid evolution in base-metal sulphide mineral deposits in the metamorphic basement rocks of southwest Scotland and Northern Ireland. *Geological Journal*, Vol. **40**, pp. 3-21

Boulard E., Guyot F. and Fiquet G. (2012): The influence on Fe content on Raman spectra and unit cell parameters of magnesite-siderite solid solutions. *Phys Chem Minerals* (2012) Vol. **39**, pp. 39–246

Bodnar R. J., (2003): Introduction to aqeous fluid systems. In I. Samson, A. Anderson, & D. Marshall, eds. Fluid inclusions: Analysis and Interpretation. *Mineral. Assoc. Canada, Short Course,* Vol. **32**, pp. 81-99.

Breeding, C. M., Ague, J. J., Grove, M. & Rupke, A. L. (2004): Isotopic and chemical alteration of zircon by metamorphic fluids : U-Pb age depth-profiling of zircon crystals from Barrow´s garnet zone, northeast Scotland. *American Mineralogist*, Vol. **89**, pp. 106-1077.

Burke, E.A.J. (2001): Raman microspectrometry of fluid inclusions. Lithos Vol. **55**, pp. 139-158.

Bucher, K. & Rodney, G. (2011): Metamorphism of Pelitic Rocks (Metapelites). Petrogenesis of metamorphic rocks

Dempster, T. J. (1985): Garnet zoning and metamorphism of the Barrovian Type Area, Scotland. *Contributions to Mineralogy and Petrology*,Vol. **89**, pp. 30-38

Dempster, T. J., Fallick, A. E. & Whittemore, C. J. (2000): Metamorphic reactions in the biotite zone, eastern Scotland: high thermal gradients, metasomatism and cleavage formation. *Contributions to Mineralogy and Petrology,* Vol. **138**, pp. 348-363

Downs R T (2006): The RRUFF Project: an integrated study of the chemistry, crystallography, Raman and infrared spectroscopy of minerals. *Program and Abstracts of the 19th General Meeting of the International Mineralogical Association in Kobe, Japan*. O03-13

Carpenter, R. H., (1974): Pyrrhotite Isograd in Southeastern Tenesse and Southwestern North Carolina. *University of Georgia, Athens, Department of Geology. Georgia 30601: Geological Society of American Bulletin*, Vol. **85**, pp. 451-456

Craw, D. (1990): Regional fluid and metal mobility in the Dalradian metamorphic belt, Southern Grampian Highlands, Scotland. *Mineral. Deposita* **25**, pp. 281-288

Fall, A., Tattitch, B., Bodnar, R. J., (2010): Combined microthermometric and Raman spectroscopic technique to determine the Salinity of H2O-CO2-NaCl fluid inclusions based on clathrate melting. *Geochimica et Cosmochimica Acta*, Vol. **75,** pp. 951-964.

Ferry, J. M., (1981): Petrology of graphitic sulfide-rich schists from south-central Maine: an example of desulfidation during prograde regional metamorphism. *Arizona State Univeristy, Department of Geology. Arizona: American Mineralogist*, Vol. **66**, pp. 908-930.

Fettes, D. J., MacDonald, R., Fitton, J. G., Stephenson, D & Cooper, M. R. (2011): Geochemical evolution of Dalradian metavolcanic rocks: implications for the break-up of the Rodinia supercontinent. *Journal of the Geological Society, London,* Vol. **168**, pp. 1133-1146

Goldfarb, R. J., Baker, T., Dube, B., Groves, D. I., Hart, C. J. R., & Gosselin, P. (2005): Distribution, character, and genesis of gold deposits in metamorphic terranes: *Economic Geology 100th Anniversary volume,* pp. 407-450

Harte, B and Hudson, N.F.C. (1979): Pelite facies series and the temperatures and pressures of Dalradian Metamorphism in E Scotland. *The Caledonides of the Brittish Isles – reviewed. 1979. Geological Society of London.*

Lusty, P. A. J., Naden, J., Bouch, J. E., & McKervey, J. A. (2007): Gold mineralization associated with low temperature basinal brines in Connemara, western Ireland. In: Andrew, C.J., (ed.) *Digging deeper : proceedings of the ninth biennial Meeting of the Society for Geology Applied to Mineral Deposits, Dublin, Ireland 20th-23rd August 2007.* Dublin, Ireland, Irish Association for Economic Geology, pp. 613-616.

Masters, R. L. & Ague, J. J. (2005): Regional-scale fluid flow and element mobility in Barrow´s metamorphic zones, Stonehaven, Scotland. *Contributions to Mineralogy and Petrology*, Vol. **150**, pp. 1-18

Oakes, C. S., Bodnar, R. J., & Simonson J. M. (1990): The system NaCl-$CaCl_2$-H_2O: The ice liquidus at 1 atm total pressure*. *Geochimica et Cosmochimica Acta,* **Vol. 54**, pp. 603-610

Oliver, G. J. H., Wilde, S. A. & Wan, Y (2008): Geochronology and Geodynamics of Scottish Granitoids From the Late Neoproterozoic Break-Up of Rodinia to Palaeozoic Collision*. Journal of the Geological Society, London,* Vol. **165**, pp. 661-674

Osadchii, E.G. and Gorbaty, Y.E. (2010): Raman spectra and unit cell parameters of sphalerite solid solutions ($Fe_xZn_{1-x}S$). *Geochimica et Cosmochimica Acta,* Vol. **74**, pp. 568-573

Parnell, J., Earls, G., Wilkinson, J. J., Hutton, D. H. W., Boyce, A. J., Fallick, A. E., Ellam, R. M., Gleeson, S. A., Moles, N. R., Carey, P. F., & Legg, I. (2000): Regional Fluid Flow and Gold Mineralization in the Dalradian of the Sperrin Mountains, Norhtern Ireland. *Economic Geology,* Vol. **95**, pp. 1389-1416

Peulicke, E. (2012): A description of sulfide paragenesis in Glen Esk metamorphic sequence, Scotland. *Stockholm University Bsc*.

Phillips. G. N., Powell. R., (2010): Formation of gold deposits: a metamorphic devolatilization model. *Journal of metamorphic geology, 2010*, Vol. **28**, pp. 689-718

Pitcairn, I. K., Warwick, P. E., Milton, J. A. & Teagle, D. A. H. (2006b): Method for ultra-low level analysis of gold in rocks. *Anal. Chem*. Vol. **78**, pp. 1290-1295

Pitcairn, I. K., Teagle, D. A. H., Craw, D., Olivo, G. R., Kerrich, R. & Brewer, T. S. (2006): Sources of Metals and Fluids in Orogenic Gold Deposits: Insights from the Otago and Alpine schists, New Zealand.

Pitcairn, I. K., Olivo, G. R., Teagle, D. A. H. and Craw, D. (2010): Sulfide evolution during prograde metamorphism of the Otago and Alpine schists, New Zealand. *The Canadian Mineralogist*, Vol. **48**, pp. 1267-1295

Roedder E. (1984): The fluids in salt. *Am. Mineral,* Vol. **69**, pp. 413-439

Roedder E. (1984): Fluid inclusions. *Reviews in mineralogy, Mineralogical society of America*, Vol. **12**

Shepherd, T. j., A.H., Alderton, D. H. M., (1985): A practical Guide to Fluid Inclusion Studies.

Tomkins, A., Pitcairn, I. K., & Evans, K. (2012): Global sulphur cycle and impact on metallogenesis. Talk at 34th International Geological Congress (IGC): Australia 2012.

Van der Kerkhof, A., Thiery R., (2001): Carbonic inclusions. *Lithos Vol.* **55**, pp. 49-68.

Vorhies, S. H. & Ague, J. J. (2011): Pressure-temerature evolution and thermal regimes in the Barrovian zones, Scotland. *Journal of the Geological Society, London,* Vol. **168**, pp. 1147-1166

Yardley, B. W. D. & Baltazis, E. (1985) Retrogression of staurolite schists and the sources of infiltrating fluids during metamorphism. *Contributions to mineralogy and petrology*, Vol. **89**, pp. 59-68

Internet books:

The Geology of Scotland. 4th Edition. Nigel H. Trewin. Published in 2012 by the Geological Society.

Retrieved 2012-11-14

Geological history of Britain and Ireland. 2nd Edition. Nigel Woodcock and Rob Strachan. 2010.

Retrieved 2012-11-14

VII. Appendix

i. SEM scanning tables

Stonehaven

CHLORITE ZONE						
Sample	ST1	Total mineral (sq. µm)	% of total Sulfide	ST3	Total mineral (sq. µm)	% of total Sulfide
	Pelite			Psammite		
Total Sulfide Area (sq. µm)	25382,62185			501928,3165		
Total Area Scanned (sq. µm)	9,78E+07			1,48E+08		
% sulfide	0,03%			0,34%		
Pyrite	8192,523088	8192,523088	32,28%		467862,5334	93,21%
Pyrrhotite					14018,69739	2,79%
Chalcopyrite	17190,09877	17190,09877	67,72%		15673,17603	3,12%
Sphalerite					1658,282297	0,33%
Galena					1454,166496	0,29%
Cobaltite					223,1327807	0,04%
Gersdorffite					265,60408	0,05%
Arsenian Pyrite					772,724036	0,15%
Py/Py+Po			-			0,970908397

BIOTITE ZONE			
Sample	ST10	Total mineral (sq. µm)	% of total Sulfide
	Pelite		
Total Sulfide Area	1293250,873		
Total Area Scanned	1,23E+08		
% sulfide	1,05%		
Pyrite		1266369,49	97,92%
Pyrrhotite		2549,566544	0,20%
Chalcopyrite		24228,48979	1,87%
Sphalerite			
Galena		98,88920832	0,01%
Cobaltite			
Gersdorffite			
Arsenian Pyrite		4,437336206	0,00%
Py/Py+Po			0,997990757

GARNET ZONE						
Sample	ST30	Total mineral (sq. µm)	% of total Sulfide	ST32	Total mineral (sq. µm)	% of total Sulfide
	Psammite			Pelite		
Total Sulfide Area	100694,5686			872097,9872		
Total Area Scanned	7,31E+06			8,36E+07		
% sulfide	1,38%			1,04%		
Pyrite		70852,21551	70,36%		850500,3822	97,52%
Pyrrhotite		2178,098109	2,16%		19277,53121	2,21%
Chalcopyrite		6862,023303	6,81%		818,3648318	0,09%
Sphalerite		18,38325	0,02%			
Galena						
Cobaltite		44,37336111	0,04%			
Gersdorffite						
Arsenian Pyrite						
Breakdown material		7559,952668	7,51%			
Cobaltpentlandite		0,633905172	0,00%			
Pentlandite		13178,88844	13,09%		1501,708987	0,17%
Py/Py+Po			0,970175424			0,97783626

STAUROLITE ZONE						
Sample	ST39	Total mineral (sq. µm)	% of total Sulfide	ST42	Total mineral (sq. µm)	% of total Sulfide
Total Sulfide Area	1099884,173			194372,1062		
Total Area Scanned	3,08E+08			2,13E+08		
% sulfide	0,36%			0,09%		
Pyrite		1013444,918	92,14%		161858,7441	83,27%
Pyrrhotite		84622,48264	7,69%		22720,87571	11,69%
Chalcopyrite		216,7955308	0,02%		9286,000298	4,78%
Sphalerite					42,47129631	0,02%
Galena		23,45449114	0,00%		107,1290933	0,06%
Cobaltite						
Gersdorffite						
Arsenian Pyrite						
Breakdown material						
Cobaltpentlandite					48,17639697	0,02%
Pentlandite		995,2311227	0,09%		305,539776	0,00%
Coboltoan Pyrite		581,2910423	0,05%		3,169499755	0,00%
Py/Py+Po			0,922935074			0,876904743

SILLIMANITE ZONE			
Sample	ST50	Total mineral (sq. µm)	% of total Sulfide
	Pelite		
Total Sulfide Area	39246,0138		
Total Area Scanned	1,39E+08		
% sulfide	0,03%		
Pyrite		17386,60795	99,36%
Pyrrhotite			
Chalcopyrite		234,5429825	0,60%
Sphalerite			
Galena			
Cobaltite			
Gersdorffite			
Arsenian Pyrite			
Breakdown material			
Cobaltpentlandite			
Pentlandite			
Coboltoan Pyrite		18,3830986	0,05%
Py/Py+Po			1

Table 7. *Sulfide abundances calculated for samples from Stonehaven. Abundances are given in square micrometers and percent of total sulfides for each type sulfide present. In thin sections which contained both pyrite and pyrrhotite the relative proportions of the two minerals were calculated to identify potential transition trends.*

Loch Lomond

CHLORITE ZONE						
Sample	LL19B	Total mineral (sq. µm)	% of total Sulfide	LL25	Total mineral (sq. µm)	% of total Sulfide
Total Sulfide Area (sq. µm)	485936,2901			198885,4761		
Total Area Scanned (sq. µm)	2,02E+08			2,58E+08		
% sulfide	0,24%			0,08%		
Pyrite		40744,55416	8,38%		168976,1748	84,96%
Pyrrhotite		373053,2899	76,77%		5199,247363	2,61%
Chalcopyrite		1333,091595	0,27%		6409,99631	3,22%
Sphalerite					5157,409898	2,59%
Galena		8,240699291	0,00%		1367,956117	0,69%
Cobaltite					2055,103663	1,03%
Gersdorffite					2721,966362	1,37%
Arsenian Pyrite		22,18649852	0,00%		1023,748402	0,51%
Breakdown material						
Cobaltpentlandite		1128,975809	0,23%		0,633899927	0,00%
Pentlandite		69589,53434	14,32%		5961,195246	3,00%
Coboltoan Pyrite		56,41709423	0,01%		12,04409909	0,01%
Py/Py+Po			0,996439263		0,447854099	

BIOTITE ZONE						
Sample	LL1	Total mineral (sq. µm)	% of total Sulfide	LL10	Total mineral (sq. µm)	% of total Sulfide
Total Sulfide Area (sq. µm)	799867,6447			231298,0474		
Total Area Scanned (sq. µm)	1,25E+08			2,28E+07		
% sulfide	0,64%			1,02%		
Pyrite		3355,8663	0,42%		746,1002477	0,32%
Pyrrhotite		754881,0326	94,38%		199589,7382	86,29%
Chalcopyrite		33973,23435	4,25%		1476,986858	0,64%
Sphalerite		2105,815646	0,26%			
Galena		107,762989	0,01%		107,7629912	0,05%
Cobaltite		275,1125752	0,03%			
Gersdorffite						
Arsenian Pyrite		19,01699853	0,00%			
Breakdown material						
Cobaltpentlandite		2591,382987	0,32%		3912,430496	1,69%
Pentlandite		2558,420207	0,32%		25442,84207	11,00%
Coboltoan Pyrite					22,18649781	0,01%
Py/Py+Po			0,956933447		0,992654245	

GARNET ZONE						
Sample	LL32	Total mineral (sq. µm)	% of total Sulfide	LL34	Total mineral (sq. µm)	% of total Sulfide
Total Sulfide Area (sq. µm)	29470,00862			232989,3099		
Total Area Scanned (sq. µm)	1,08E+08			1,19E+08		
% sulfide	0,03%			0,20%		
Pyrite		25448,54738	86,35%		-	-
Pyrrhotite		3288,672897	11,16%		-	-
Chalcopyrite		13,94579875	0,05%		14479,66207	6,21%
Sphalerite		503,3165578	1,71%		1,267810345	0,00%
Galena					119,8080759	0,05%
Cobaltite						
Gersdorffite						
Arsenian Pyrite						
Breakdown material						
Cobaltpentlandite					6002,448092	2,58%
Pentlandite		215,5259818	0,73%		25308,66405	10,86%
Coboltoan Pyrite					28,52573299	0,01%
Py/Py+Po			0,995777351		-	

Table 8. *Sulfide abundances calculated for samples from Loch Lomond. Abundances are given in square micrometers and percent of total sulfides for each sulfide present. In thin sections which contained both pyrite and pyrrhotite the relative proportions of the two minerals were calculated to identify potential transition trends.*